2008-03-25

Impact of Mass Mixing on the Lateral Resistance of Driven-Pile Foundations

Mark Alan Herbst
Brigham Young University - Provo

IMPACT OF MASS MIXING ON THE LATERAL RESISTANCE OF DRIVEN-PILE FOUNDATIONS

by

Mark A. Herbst

A thesis submitted to the faculty of

Brigham Young University

in partial fulfillment of the requirements for the degree of

Master of Science

Department of Civil and Environmental Engineering

Brigham Young University

August 2008

BRIGHAM YOUNG UNIVERSITY

GRADUATE COMMITTEE APPROVAL

of a thesis submitted by

Mark A. Herbst

This thesis has been read by each member of the following graduate committee and by majority vote has been found to be satisfactory.

Date	Kyle M. Rollins, Chair
Date	Travis M. Gerber
Date	Fernando S. Fonseca

BRIGHAM YOUNG UNIVERSITY

As chair of the candidate's graduate committee, I have read the thesis of Mark A. Herbst in its final form and have found that (1) its format, citations, and bibliographical style are consistent and acceptable and fulfill university and department style requirements; (2) its illustrative materials including figures, tables, and charts are in place; and (3) the final manuscript is satisfactory to the graduate committee and is ready for submission to the university library.

Date

Kyle M. Rollins
Chair, Graduate Committee

Accepted for the Department

E. James Nelson
Graduate Coordinator

Accepted for the College

Alan R. Parkinson
Dean, Ira A. Fulton College of Engineering and Technology

ABSTRACT

IMPACT OF MASS MIXING ON THE LATERAL RESISTANCE

OF DRIVEN PILE FOUNDATIONS

Mark A. Herbst

Department of Civil and Environmental Engineering

Master of Science

Although it has been established that in-situ soil mixing has improved the bearing capacity of soils, additional research is needed to better understand the effect of soil mixing on lateral resistance of pile caps. To do this, in-situ soil mixing was used to strengthen weak clay adjacent to a pile cap of a driven pile foundation. The mass stabilization method or mass mixing was used to treat an 11 ft wide, 4 ft thick, and 10 ft deep zone consisting of an average 475 psf clay that was adjacent to a 9-pile group in 3x3 pile configuration capped with a 9 ft x 9 ft x 2.5 ft, 5000 psi concrete cap. The mass mixing involved 220 cubic ft of in-situ soil and was mixed with an additional 220 cubic ft of jet grout spoils producing a mixing ratio of 1 to 1. All of the mass mixing took place after construction of the pile caps. Laboratory

testing of the mass mix slurry showed an unconfined compressive strength of 20,160 psf or 140 psi. Lateral load testing of the pile foundation was then undertaken. The results of this testing were compared with similar testing performed on the same foundation with native soil conditions. The lateral resistance of the native soil was 282 kips at a pile cap displacement of 1.5 inches, and the total lateral resistance of the pile foundation treated with mass mixing was increased by 62% or 170 kips. Of the 170 kips, 90% to 100% can be attributed to the increased passive force on the face of the mass mixed zone and shear on the sides and bottom denoting that the mass mixed zone behaved as a rigid block.

ACKNOWLEDGMENTS

I wish to thank my Professor Dr. Kyle M. Rollins for giving me the opportunity to work on such an exciting project, and for all of his technical assistance and support. I also thank my thesis committee members of Dr. Travis M. Gerber and Dr. Fernando S. Fonseca who gave much of their time to help me answer the many questions I had in regards to this thesis. I also couldn't have done this without the assistance of my fellow students, Matt Adsero and Nate Lemme. My wife, Kyra, was also instrumental in helping me complete this work with her time, patients, and endless encouragement. Also, I need to mention David Anderson, Dustin Minor, and Luke Heiner who from a construction and testing standpoint, made the whole thing happen. Also I would like to thank the many organizations that donated time, materials, and funds particularly, but not limited to, the NCHRP, Hayward Baker, Build Inc, Wadsworth Brothers, and U-DOT.

TABLE OF CONTENTS

LIST OF TABLES

LIST OF FIGURES

1 Introduction

The aging infrastructure of United States Interstate system has recently been under some scrutiny, with many bridge structures being deemed structurally unsound. Many of the bridge structures associated with the interstate system were designed and built many years before seismicity and the associated parameters were taken into consideration for bridge design. These bridges are in need of being retrofitted to meet current seismic code specifications. In the past, structural components were added to the foundations to improve lateral resistance, which improves the foundations performance in the event of an earthquake. Recently, strengthening the soft soil surrounding the piles and pile cap, in lieu of structural retrofits, has been a suggested alternative to increase the lateral resistance of driven pile foundations at reduced cost.

Mass mixing, a soil strengthening technique, which mixes cement with in situ soil to produce a large volume of soil-cement, has been used in numerous projects to increase the strength of soft soils. Most of these applications, however, were employed to increase the axial bearing capacity of the treated soils prior to embankment construction. In these applications significant increases in both strength and stiffness have been observed. This procedure allowed embankments to be constructed over soft soils without slope stability failure and with reduced settlement.

The application of mass mixing to increase the lateral strength of soils surrounding driven pile foundations has not previously been verified or quantified although it seems particularly well suited to the problem. The lateral resistance of deep foundations is primarily developed within 5 to 10 pile diameters of the ground surface. For typical piles with diameters of 1 to 2 ft, this corresponds to a total depth of 10 to 20 ft. Fortunately, this is also the depth range which current mass mixing systems are designed to treat. Therefore, mass mixing offers the potential of significantly increasing lateral pile foundation resistance without the need for expensive structural retrofit In addition, increased strength produced by mass mixing could also increase the passive resistance acting against bridge abutments and pile caps, which would further increase the lateral resistance of a bridge foundation system.

1.1 Project Objectives

The objectives of our research were four-fold.

- Evaluate the increase in lateral pile group resistance due to mass mixing
- Evaluate the increase in lateral passive resistance due to mass mixing
- Compare cost and effectiveness of soil improvement relative to additional structural elements
- Produce a well-document case history of field performance for calibration of computer models so that additional parametric studies can be performed

The research for this project was one component of a much larger research project which is funded by the National Cooperative Highway Research Program (NCHRP). The NCHRP has outlined specific tasks that it would like to ultimately accomplish through this investigation. The above list represents four of the specific tasks that were to be accomplished through this research.

This report will focus only on the increased lateral resistance to pile group foundations through mass mixing treatment of the soft soil surrounding the foundation; however, mass mixing was not the only soil improvement technique implemented during this phase of research. Pile foundations were also tested after the soft soil surrounding the foundations was treated with various geometries of compacted fill, jet grouting, flowable fill, and geopiers. Reports of the results associated with these particular soil treatments can be found in the related thesis work of Lemme (2008), Adsero (2008), and others.

1.2 Scope of Investigation

Four identical full-scale foundations, placed thirty feet apart, were designed, constructed and tested during this phase of research. Each foundation consisted of nine piles, in a 3 x 3 configuration, driven to a depth of approximately 40 ft below grade. Prior to driving, the piles were also instrumented with strain gages at predetermined depths. Inclinometer and shape accelerometer array casings, which extended the length of the driven piles, were also placed in selected middle row piles. A 9.25 ft square reinforced concrete pile cap which extended from the ground surface to 2.5 feet below grade, was constructed on top of the piles. A reinforced

concrete corbel was attached to the concrete pile cap to create a load transfer surface during testing of the foundation systems. A hydraulic actuator was placed between two foundations which were being tested. Steel pipe extensions were attached to each end of the actuator to span the distance between the actuator and foundation. The extensions were then attached to the corbel to enable lateral load transfer from the actuators to the pile caps.

The foundations were first tested under native soil conditions. One test was performed with soil directly behind the pile cap; the second test was performed with the soil directly behind the pile cap excavated to the depth of the pile cap. The results of these two tests were used to determine the total and passive force acting on the foundation when it is loaded laterally under native soil conditions. The shape arrays, strain gages, and inclinometers were also used to determine the deflections and moments in the piles with respect to depth below grade. After these tests were completed, mass mixing was used to create a 4 ft wide zone of soil-cement extending from the ground surface to a depth of 10 ft below the ground surface on one side of the pile cap. Subsequently, lateral load tests were performed on the same foundation both with soil-cement directly in front of the pile cap and after excavating the soil-cement in front of the pile cap to eliminate any passive force contribution. The results of these tests were then compared with the results obtained when the foundation was loaded under native soil conditions to determine the degree of improvement to both lateral pile resistance and passive resistance on the pile cap itself.

2 Literature Review

The soil improvement method selected for lateral testing and that is discussed in this report is a process called soil mixing, particularly mass mixing. There are two main methods of soil mixing that are currently used today, deep soil mixing and mass stabilization or mass mixing. Deep soil mixing involves blending a cementitious material into the soil through a hollow rotating shaft to form strengthened soil columns. This applications is particularly useful for deep soil treatments, hence the name deep soil mixing. However, the deep soil mixing process is rather strenuous for shallow depths, so mass stabilization or mass mixing was invented to treat shallow depths and surface areas. Instead of making soil columns, mass mixing blends the cementitious material directly into the soil and can cover large areas in a short amount of time. Since the lateral resistance of deep foundations is primarily developed within 5 to 10 pile diameters of the ground surface, mass mixing was chosen for the investigation to see how soil mixing can indeed improve the lateral strength of deep foundations in weak cohesive soils. A more in depth review of deep soil mixing and mass mixing is presented in this section.

2.1 Deep Soil Mixing

Excellent accounts of the historical development, evolution and growth of deep soil mixing (DSM) technologies are provided by Bruce et. Al. (1998), Terashi and Juran (2000) and Terashi (2003). The deep soil mixing method encompasses a group of technologies where cementitious material (usually cement or lime) is introduced and blended into the soil through a hollow rotating shaft or shafts equipped with cutting tools and mixing paddles or augers. The materials may be injected under pressure in either slurry (wet) or dry form. Figure 2-1 shows a typical rig used for the dry mixing method with a schematic diagram of the mixing process. The process leads to vertical stabilized columns of about 3 ft (1 m) diameter. Multiple augers are often used in the wet methods. For dry methods (used beneath the water table or in high moisture content clays ($w_n \geq$ liquid limit), typically 220 to 660 lbs (100 to 300 kg) of cementitious material is injected per cubic meter of soil, while for wet methods, 220 to 1100 lbs (100 to 500 kg) is injected. The strength gain of the soil depends on the physical properties of the soil and the quantity of cementitious material injected. Typically, unconfined compressive strength values of 72 to 725 psi (0.5 to 5 Mpa) are achieved in treated granular soils and 29 to 290 psi (0.2-2 Mpa) in cohesive soils.

The versatility of the construction technique allows columns to overlap to form blocks, walls or lattice configurations, as shown in Figure 2-2. The choice of pattern depends on the specific application as illustrated in Figure 2-3. Structural walls are typically used for resisting lateral earth pressures in construction of deep excavations while solid blocks may be used to strengthen large volumes of weak

soil. Lattice or cellular structures may be used to support lightly loaded structures or to control embankment stability.

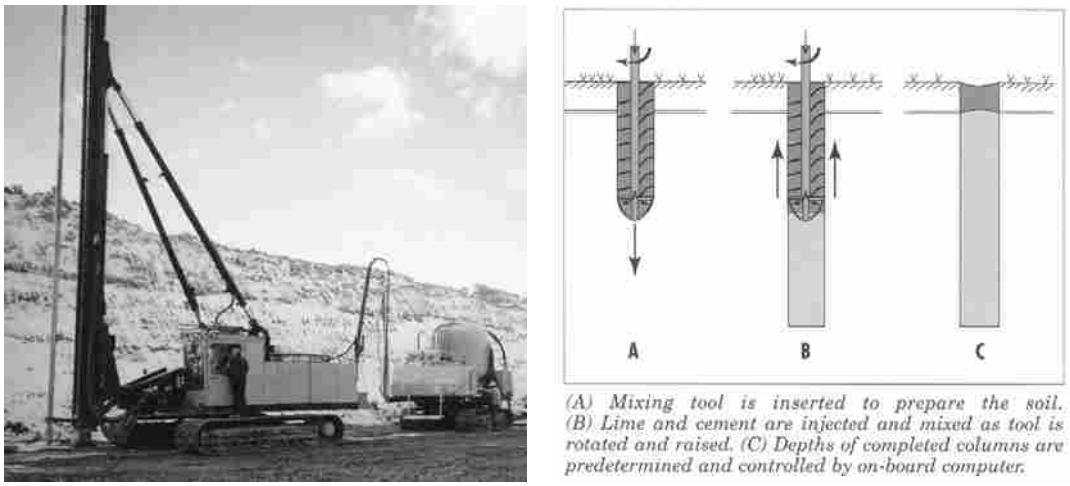

(A) Mixing tool is inserted to prepare the soil. (B) Lime and cement are injected and mixed as tool is rotated and raised. (C) Depths of completed columns are predetermined and controlled by on-board computer.

Figure 2-1 - Dry Method Column Installation.

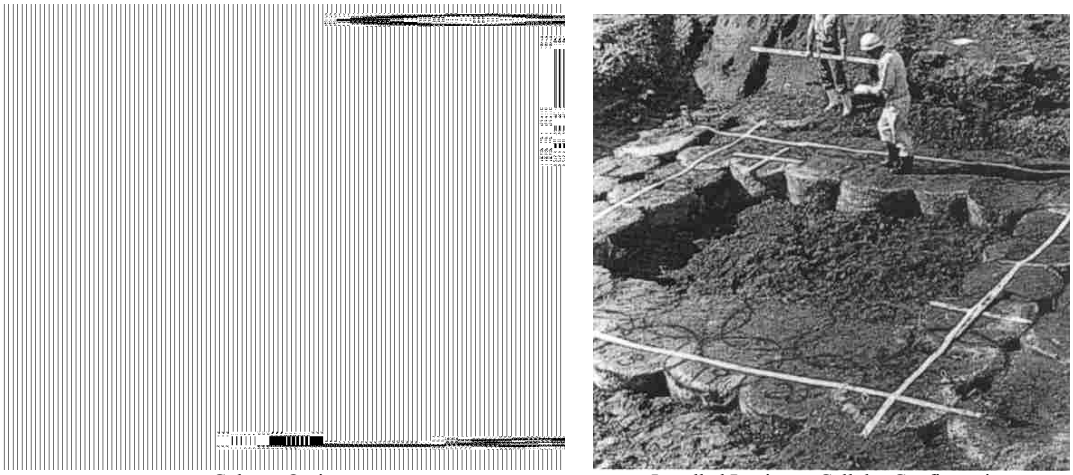

Column Options | Installed Lattice or Cellular Configuration

Figure 2-2 - Deep Mixing Column Patterns (after Porbaha et. al. 1999).

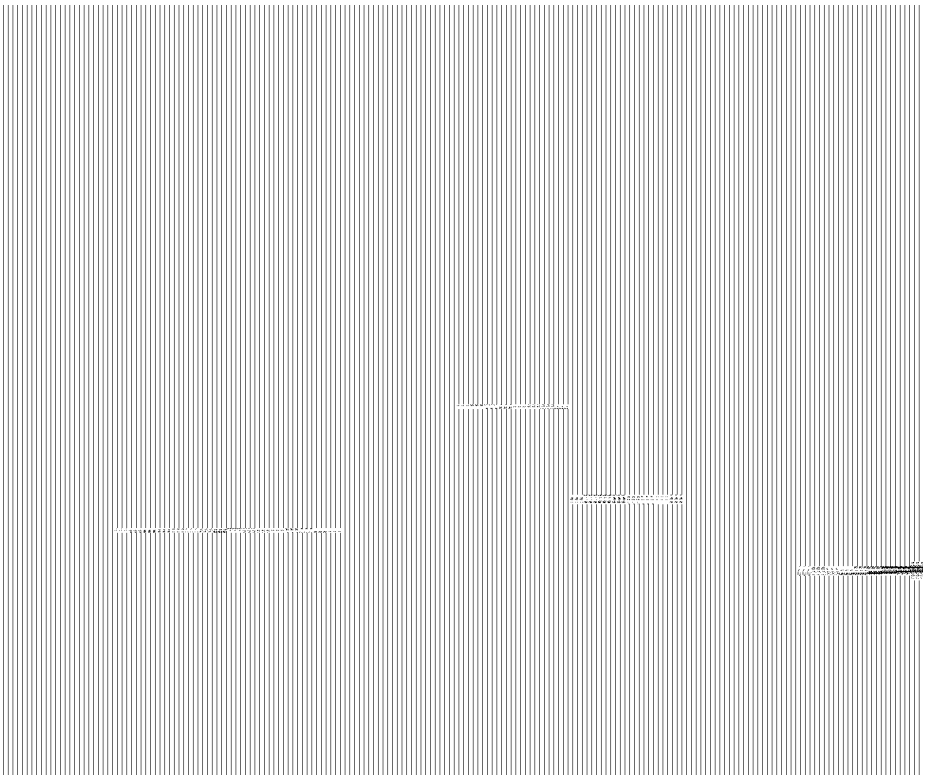

Figure 2-3 - Deep Mixing Applications in Japan (after Terashi and Juran, 2000).

Two deep mixing projects in Oakland, California (Yang, 2003) illustrate the versatility of the technology in mitigating earthquake stability problems associated with either soft clays or liquefiable sands and also illustrate the potential for applications to pile projects. The two projects are illustrated schematically in Figure 2-4.

The first project is the construction of a mechanically stabilized earth (MSE) wall for a roadway over-crossing at the Oakland Airport. Foundation soils were comprised of loose sandy fill and soft clays. Triple shaft equipment using the wet method of cement deep soil mixing was used to stabilize foundation soils to provide wall stability under static and earthquake loading. Acceptance criteria for unconfined compressive strength required an average of 145 psi (1 MPa) at 28 days.

The second project required the stabilization of a 65 ft (20m) high cut slope in soft clays under a proposed container wharf at the Port of Oakland. A DSM buttress system was proposed to provide seismic stability by minimizing potential lateral spread. The buttress consisted of a rectangular grid of DSM walls formed using overlapping 3 ft (1m) diameter columns spaced at 2 ft (0.6m) centers. The grid consisted of longitudinal walls 33 ft (10m) apart and transverse walls 10 ft (3m) apart, allowing piles to be driven at the center of cells. Over 34,000 yd^3 (26,000 m^3) of DSM ground stabilization was constructed over a period of five months. Test specimens for unconfined compressive strengths were retrieved by a triple barrel coring system, and had acceptance criteria of 167 psi (1.15 MPa) at 28 days.

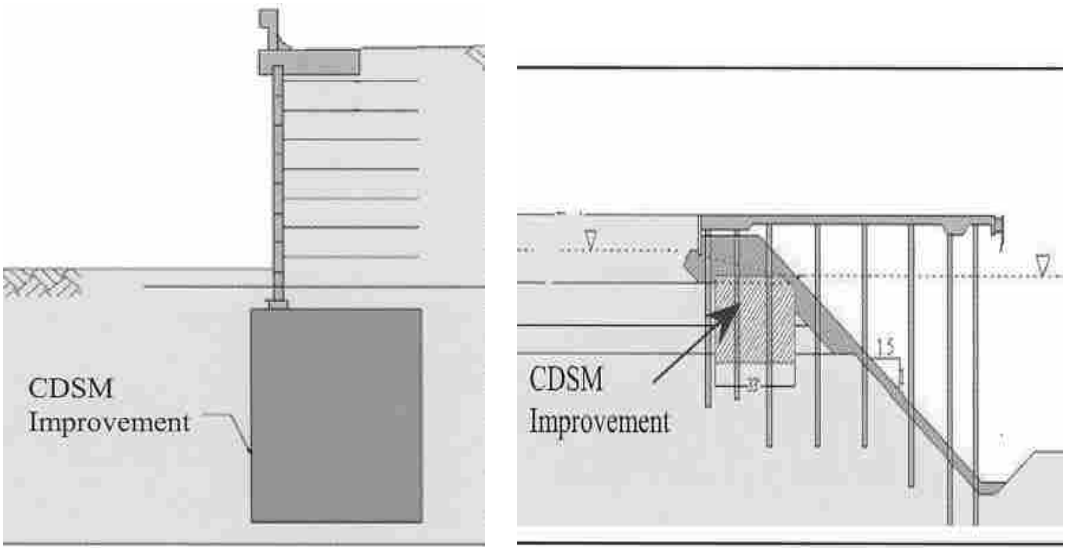

MSE Wall Construction – Oakland Airport

Cut-Slope Stabilization - Port of Oakland Container Wharf

Figure 2-4 - Deep Soil Mixing Projects, Oakland, California (after Yang, 2003).

2.2 Mass Stabilization (Mass Mixing)

In addition to deep soil mixing, a relatively new ground improvement technique called mass stabilization has also started to appear in the United States. Mass stabilization was first introduced in Finland over 20 years ago, and has since been used in projects in over 40 different countries throughout the world. In this ground improvement technique, the soil is stabilized in-situ by mixing dry or wet binder throughout the entire volume of the treated soil layer to a depth of up to about 15 ft (4.6 m). In contrast to typical total volume ground improvement techniques, this soil improvement is done without excavation or replacement of in-situ soil. The binding agent is generally a mixture of lime and cement, but can also include industrial by-products such as fly ash and blast furnace slag. Extensive research is continuing to be done on the effects of various cement add mixtures on the properties of the stabilized soil. Originally, mass stabilization was used in conjunction with deep soil-mixed stabilized columns as described in the previous section; however, this is much less efficient at shallow depths. Figure 2-5 shows two of the common applications of mass stabilization.

The illustration in Figure 2-5 shows mass stabilization being used to reduce the settlement and increase the bearing capacity of the soil underneath an earthen embankment. Mass stabilization can also be used to prevent liquefaction, improve deformation properties of soft soil, increase the dynamic stiffness of soil, and to remediate contaminated soil.

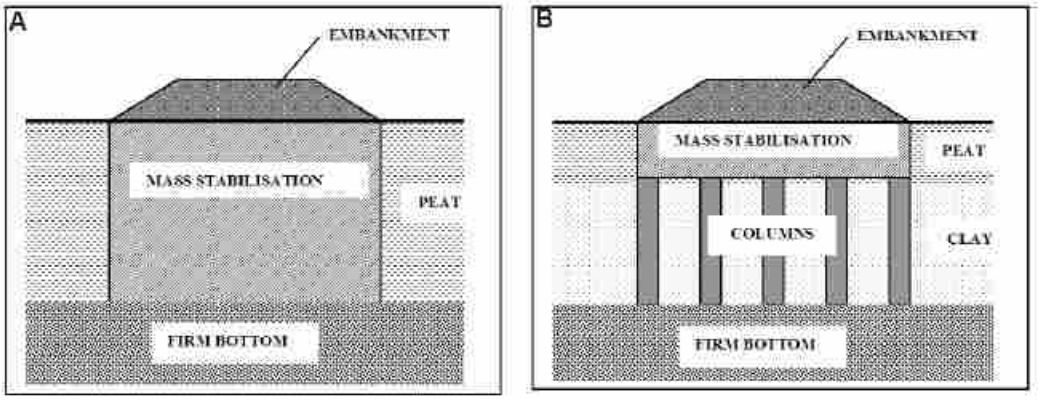

Figure 2-5 - (A) Mass stabilization of a large volume and (B) combined mass and column stabilization (ALLU website 2007).

Currently, there are two primary mass stabilization methods that can be chosen from, namely, *stabilization in layers* and *stabilization by blocks*. The method chosen depends on the type of soil being stabilized, and the nature of the soil improvement project. With stabilization in layers, the soil is simultaneously mixed and moved towards the excavator as illustrated in Figure 2-6. Once the mixed soil has been built up to the proper depth in front of the excavator, the excavator moves forward on top of the completed mass mix and the process is repeated. With this method, the treatment area is not limited to the length of the power mixer, which is the extension tool attached at the excavator as shown in Figure 2-6. This method can only be used with soils that are strong enough to bear the weight of the excavator immediately after being mixed.

The second method known as *stabilization in blocks* is implemented when the soil being treated is not strong enough to bear the weight of the excavator immediately after being mixed. In this approach, 12 to 24 yd^2 (10 to 20 m^2) areas are treated one at a time. If needed, a predetermined amount of sand is placed on the soil before treatment, so it can be added to the soil during the mixing process. In this

stabilization method the depth of treatment is limited by the length of the power mix. Once the soil has been treated, it is overlain with a geotextile reinforcement after which a 3 to 6 ft (1 to 2 m) layer of gravel is preloaded onto the geotextile. This process is repeated down the entire length of the treatment area and the excavator remains on top of the untreated zone along the side of the treated zones as illustrated in Figure 2-7.

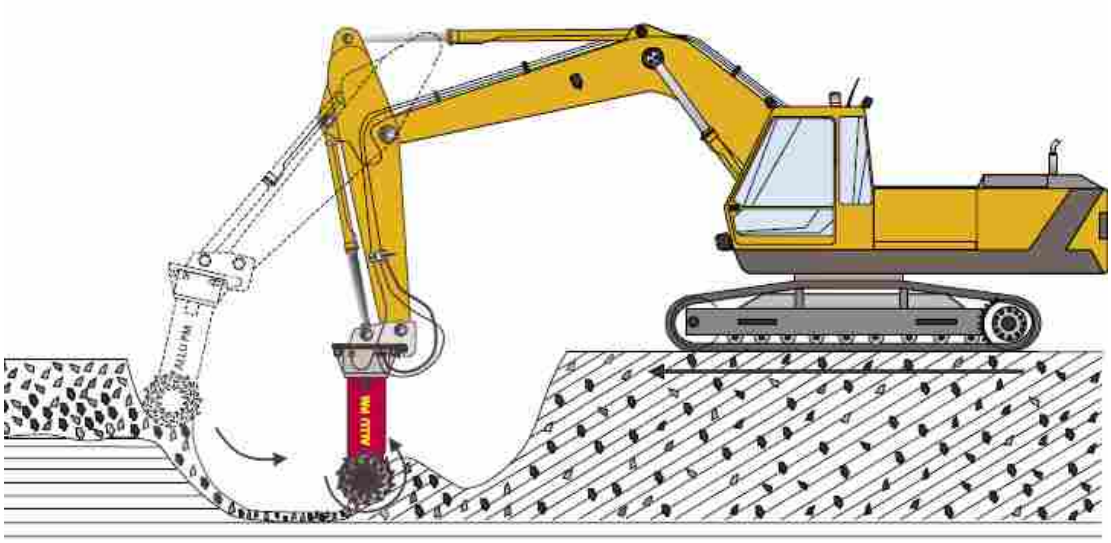

Figure 2-6 - Mass stabilization in layers method (ALLU website 2007).

Generally an extensive investigation of site specific soil characteristics must be performed before a specific design approach is selected. This investigation process involves obtaining samples of all of the major soils in the area and performing various environmental and engineering based soil tests. The chemical/environmental tests include determining the pH, cation exchange capacity, sulfide content, carbonate content, and type and total concentrations of metals and ions (EuroSoilStab 2000). Knowing these chemical properties of the soil will help in

determining the type of binder that would be best suited for the soil. The engineering soil properties that must be determined include the undrained shear strength, compressibility, and permeability of the soil before and after treatment. Based on the chemical and engineering properties of the soil, multiple soil samples are mixed with various types and quantities of binders, cured for 7, 14, 28, and 90 days, and then tested to determine the undrained shear strength, permeability, and leaching behavior of the treated soil. Through this process, the strength of treated soil, rate of soil strength gain, quantity and price of the binding agent, and other important soil properties can be optimized. The laboratory prepared stabilized earth samples will generally have an unconfined compressive strength of 7 to 10 ksf (0.3 to 0.5 MPa); however, due to the inability to homogenously mix the in-situ soil, the strength of improved soils generally ranges from 1 to 3 ksf (0.05 to 0.14 MPa). It is important to note that this is the general strength gain that has been recorded for peaty or extremely soft-clay Scandinavian soils. General practice has been to find binder combinations that will yield strengths of 3 to 5 times that of design specifications to account for this decrease in strength from the laboratory to the field. Additionally, the amount of binder that is necessary to achieve the indicated strength gains will generally vary from 6.2 to 15.5 lb/ft^3 (100 to 250 kg/m^3). The binder accounts for 50% to 70% of the total cost of the stabilization project; thus, this process of determining the optimum amount of binder is very critical. Table 2-1 provides a detailed description of the typical binding agents that work well for different soils. The findings show that a cement plus lime binder is slightly better than just cement when it is mixed in a clay, but both work well in silts and average in organic soils.

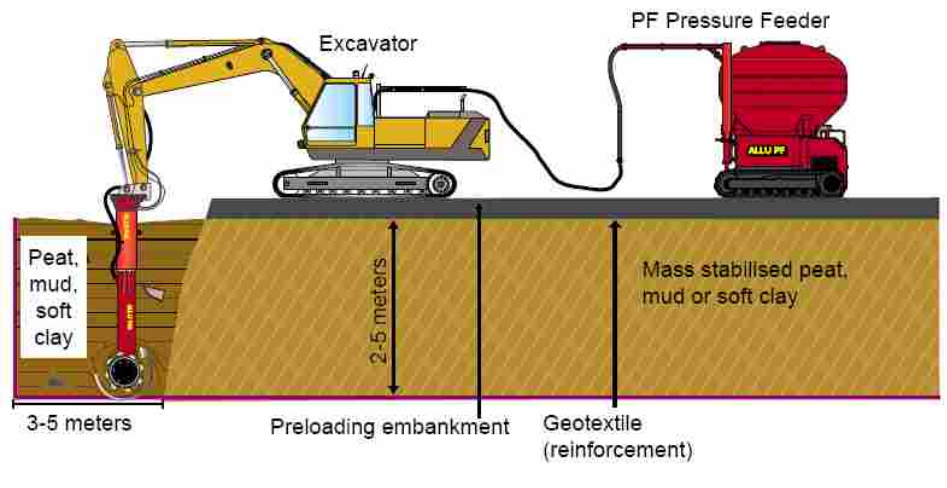

Figure 2-7 - Schematic illustration and photograph of mass stabilization by blocks method (ALLU website 2007).

One of the best binders for all soil conditions was a mixture of lime plus gypsum plus and cement.

The chart in Figure 2-8 gives the strength gain in terms of unconfined compressive strength (UCS) that was achieved when a volume of clay was stabilized in Kivikko, Finland. The expected strength gains are highly variable and depend on the natural water content and unique soil properties of each location, but this chart

shows the correlation between the amount of binder and the typical strength gain that can be expected in clay.

Table 2-1 - Performance of typical binding agents used for various soil types (EuroSoilStab 2000).

Binder	Silt Organic content 0-2 %	Clay Organic content 2-30 %	Organic Soils, e.g. Gyttja Organic Clay Organic content 2-30 %	Peat Organic content 50-100 %
Cement	xx	x	x	xx
Cement+gypsum	x	x	xx	xx
Cement+furnace slag	xx	xx	xx	xxx
Lime+Cement	xx	xx	x	-
Lime+gypsum	xx	xx	xx	-
Lime+slag	x	x	x	-
Lime+gypsum+slag	xx	xx	xx	-
Lime+gypsum+cement	xx	xx	xx	-
Lime	-	xx	-	-

xxx	very good binder in many cases
xx	good binder in many cases
x	good binder in some cases
-	not suitable

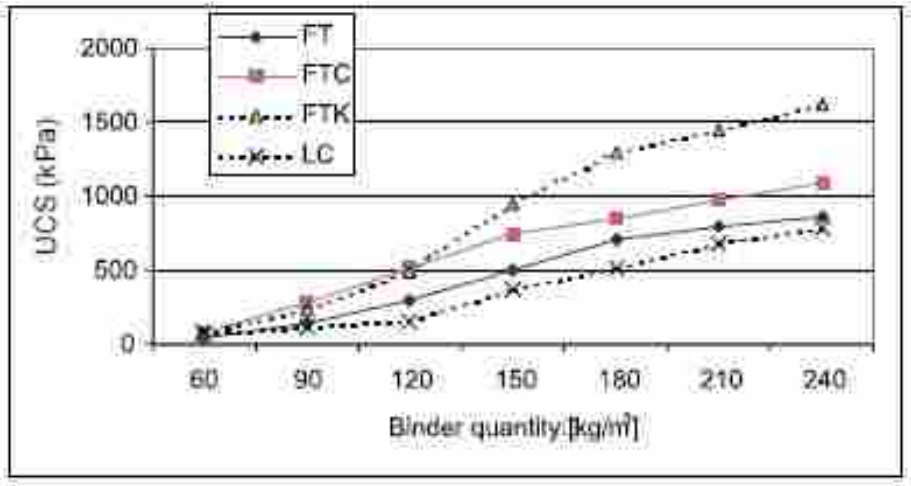

Binder symbols: Numbers indicate the proportion of different binders that include: C = cement, M =blast furnace slag from Sweden, V = a Swedish fly ash, H = a Finnish fly ash, F = Finnstabia-gypsum, T = a secondary hydrated lime with at least 50 % Ca(OH)2, L = lime (CaO), K = blast furnace slag from Finland.

Figure 2-8 - Strength gain in clay samples due to mass stabilization (EuroSoilStab 2000).

During the process of choosing the correct binder for the project, the type of equipment must also be selected. Currently, the Finnish company ALLU is the only company with the patented equipment to perform this type of ground improvement. The ALLU mass stabilization system consists of three pieces of equipment; the power mixer, the pressure binder feeder, and the data acquisition control system. The power mixer comes in three sizes, with the maximum size being able to stabilize soil to a depth of 18 ft (5.5 m). The power mixer can be attached to a large conventional excavator. The motor for the mixing drums is hydraulically driven. The pressure binder feeder is attached to the power mixer and pressure feeds the binder to the nozzles at the end of the power mix. The binder can be fed in dry or slurry form and can be applied to the treated soil prior to mixing or continuously throughout the mixing process. Graphics of the pressure feeder and power mix can be seen in Figure 2-7 explaining the three different methods of mass stabilization. Once the binder and equipment have been selected, the mass stabilization process can begin following one of the two methods described in the pervious section.

2.2.1 Quality Control

During construction, there are also a number of quality control measures that are taken to help guarantee that the treated soil will meet design specifications for strength or other engineering properties. The most common step is to mix test blocks of soil on site and then test the blocks prior to the start of large scale operations. If the blocks meet the design standards, then stabilization can begin. The stabilized earth is continuously tested throughout the stabilization process, and for a specified

time after stabilization has been completed to ensure the soil continues to meet the design requirements.

2.2.2 Advantages of Mass Stabilization

The mass stabilization approach allows a large volume of soil to be efficiently treated in the upper 18 ft (5.5 m) of the profile where soil improvement is most important for laterally loaded piles. The method is also relatively flexible to site conditions and can be performed relatively quickly. In addition, the procedure does not cause settlement or swelling in adjacent structures. The method allows the utilization of existing materials ranging from peats and organic soils to soft clays and does not generate any spoils. Finally, since the procedure is performed in-situ, it typically does not require any excavation, excavation support, or importation of engineered fill.

2.2.3 Disadvantages of Mass Stabilization

Since the method is relatively new to the United States, there is presently a lack of equipment and trained personnel; however, this difficulty will be eliminated as time goes on. The method generally requires more detailed geotechnical investigations as well as laboratory testing with a variety of cement or cement/lime combinations to determine the required treatment specifications. In addition, field testing is necessary to evaluate the improvement because field mixing will not be as efficient as that in the laboratory tests.

3 Geotechnical Site Characterization

The following chapter will describe the soil conditions of the site used for testing. The site was located north of Salt Lake City at the interchange of Redwood Road and I-215 on a Utah Department of Transportation (UDOT) right-of-way. An aerial view of the site is found in Figure 3-1 . The top 4 feet of the site was littered with huge pieces of asphalt, and was excavated from the entire test site. All of the geotechnical field investigations took place before the excavation, and the results from these investigations have been modified to refer to the soil conditions below the excavation.

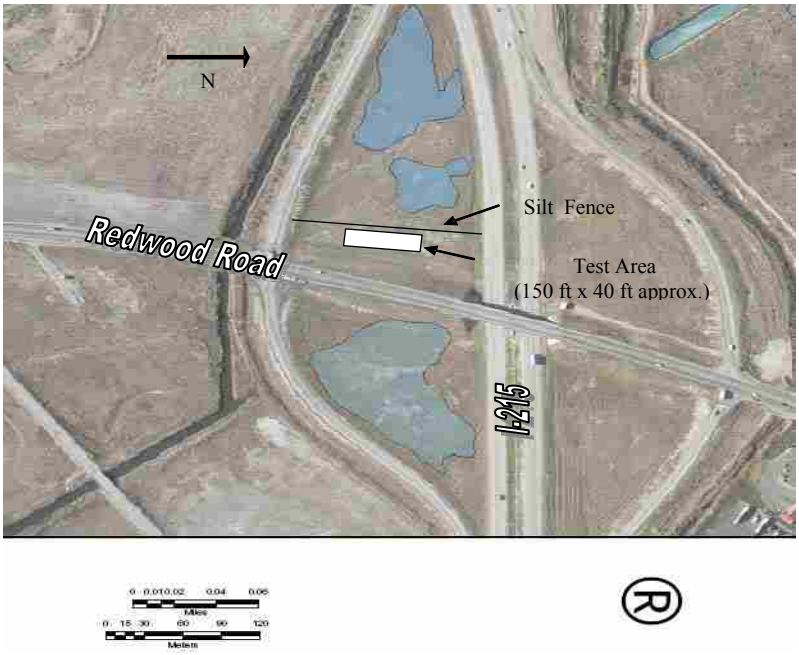

Figure 3-1 - Aerial View of the Test Area

3.1 Field Investigations

Geotechnical site conditions were evaluated using field and laboratory testing. Field testing included one drilled hole with undisturbed sampling, four cone penetration test (CPT) soundings, and shear wave velocity testing. Laboratory testing included unit weight and moisture content determination, Atterberg limits testing, and undrained shear testing. A generalized soil boring log at the test site is provided in . The depth is referenced to the top of the excavation which was 2.5 feet above the base of the pile cap as shown in the figure. A plan view of the borehole and CPT locations relative to the finished pile caps is shown in Figure 3-2.

3.2 Soil Profile, Classification and Shear Strength

A generalized soil boring log at the test site is provided in Figure 3-3 (a). The depth is referenced to the top of the excavation which was 2.5 feet above the base of the pile cap as shown in the figure. The soil profile consists predominantly of cohesive soils; however, some thin sand layers are located throughout the profile. The cohesive soils typically classify as CL or CH materials with plasticity indices of about 20 as shown in Figure 3-3 (a). In contrast, the soil layer from a depth of 15 to 25 feet consists of interbedded silt (ML) and sand (SM) layers as will be highlighted by the subsequent plots of CPT cone tip resistance.

The liquid limit, plastic limit and natural moisture content are plotted in Figure 3-3 (b) at each depth where Atterberg limit testing was performed. The water table is at a depth of 1.5 feet, which is equivalent to a depth of 5.5 feet below the pre-

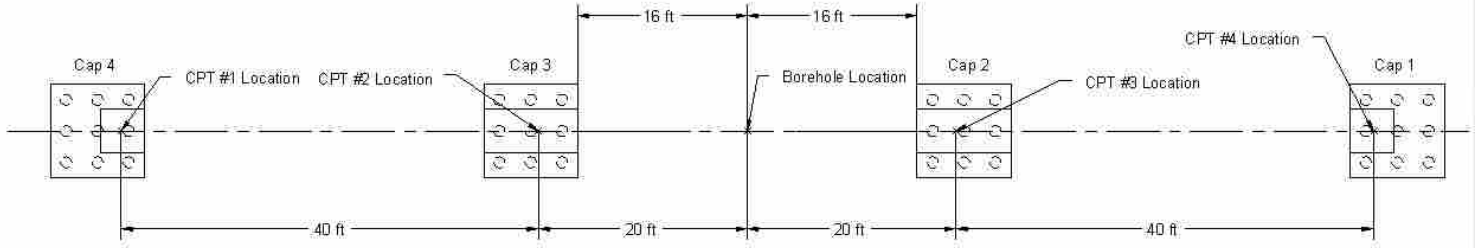

Figure 3-2 - Plan view showing location of boring andCPT soundings relative to completed pile caps.

excavation ground surface. The natural water content is less than the liquid limit near the ground surface suggesting that the soil is overconsolidated. However, the water content is greater than the liquid limit for soil specimens from a depth of 5 to 27 feet. This suggests that these materials may be sensitive. Below a depth of 30 feet the water content is approximately equal to the liquid limit, suggesting that the soils are close to normally consolidated.

The undrained shear strength is plotted as a function of depth in Figure 3-3(c). Undrained shear strength was measured using a miniature vane shear test (Torvane test) on undisturbed samples immediately after they were obtained in the field. In addition, unconfined compression tests were performed on most of the undisturbed samples. Both the Torvane and unconfined compression tests indicate that the undrained shear strength decreases rapidly from the ground surface to a depth of about 6 feet. However, the undrained shear strength from the unconfined compression tests is typically about 30% lower than that from the Torvane tests. After a depth of 6 feet the trend reverses, and the shear strength begins to increase with depth. This profile is typical of a soil profile with a surface crust that has been overconsolidated by desiccation. The unconfined compression tests performed on samples taken at the depths of 27 and 48 feet yielded soil strengths substantially lower than that from the Torvane test. These unconfined compression tests appear to have been conducted on soil with sand lenses, and are not likely to be representative of the in-situ soil. The undrained shear strength was also computed from the cone tip resistance using the following correlation equation

$$s_u = \frac{(q_c - \sigma)}{N_k} \tag{3-1}$$

where q_c is the cone tip resistance, σ is the total vertical stress, and N_k is a variable which was taken to be 15 for this study. The undrained shear strength obtained from the above equation is also plotted versus depth in Figure 3-3(c) and the agreement with the strengths obtained from the Torvane and unconfined compression tests is reasonably good. Nevertheless, there is much greater variability and the drained strength in the interbedded sand layers is ignored. A summary of laboratory test results is provided in Table 3-1.

Table 3-1 - Laboratory test results.

	In-Place		Atterberg Limits					
Depth below Excavated Surface (ft)	Saturated Unit Weight (pcf)	Natural Water Content (%)	Liquid Limit (%)	Plastic Limit (%)	Plastic Index (%)	Unconfined Compressive Strength (psf)	Miniature Vane Shear Strength (Torvane) (psf)	Unified Soil Classification Symbol
1.25	117.6	34.2	39	18	21	1104	-	CL
2.75	117.4	34.4	38	18	20	626	620	CL
5.75	104.6	56	51	21	30	384	320	CH
8.5	112.4	41.5	38	18	20	684	534	CL
11.5	110.8	44.1	38	19	19	741	500	CL
16.5	126.6	24.2	19	18	1	1081	560	ML
26.75	116.9	35	27	14	13	237	780	CL
33.5	124.6	26.1	27	14	13	1306	780	CL
36.75	117.1	34.8	35	17	18	1381	840	CL
41.75	112.0	42.1	46	17	29	1037	520	CL
48	117.2	34.6	33	16	17	297	660	CL

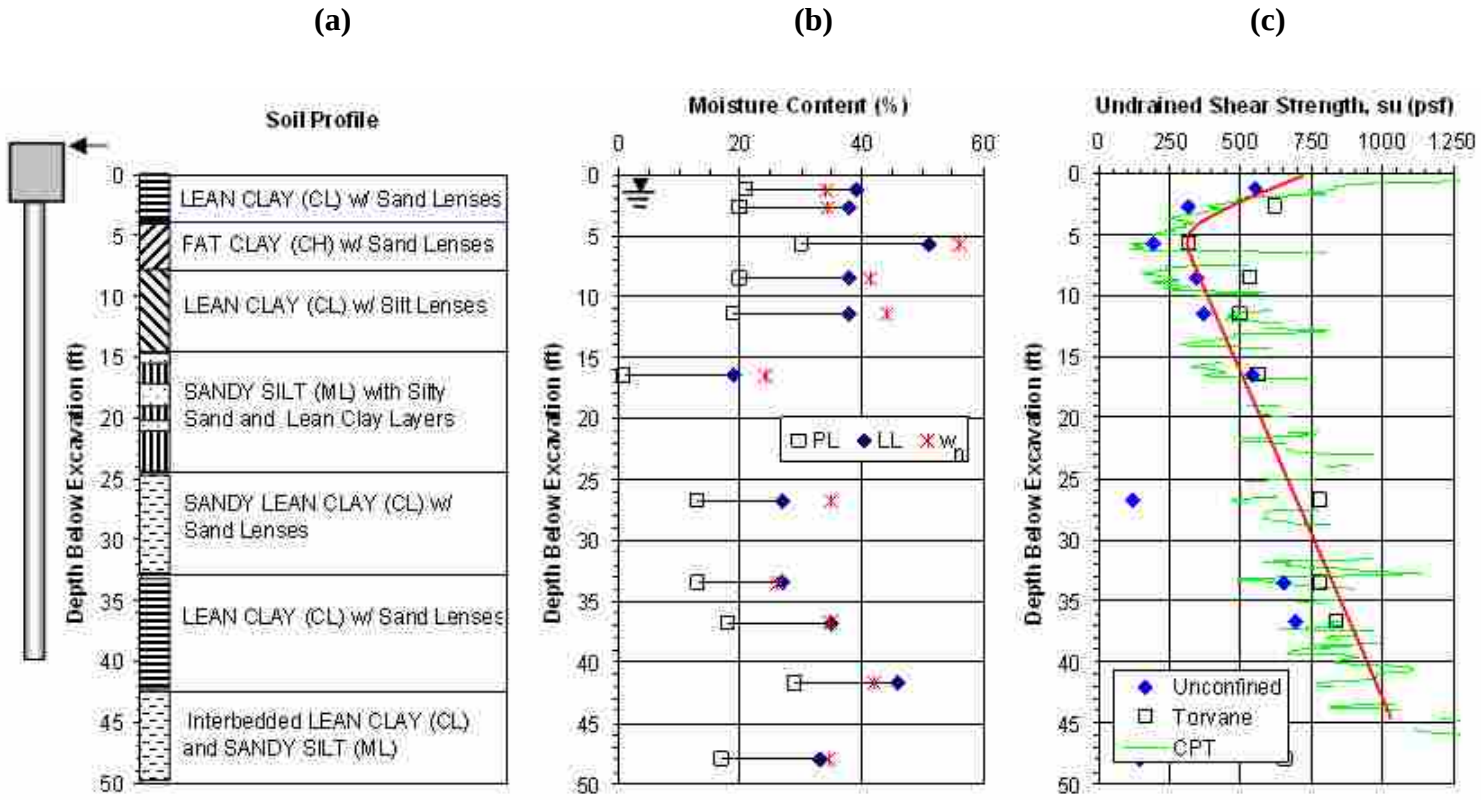

Figure 3-3 Plot of (a) soil profile, (b) Atterberg limits and natural water content versus depth, and (c) undrained shear strength versus depth.

3.3 Cone Penetration and Seismic Cone Testing

Four cone penetration tests (CPT) were performed across the test site. Plots of cone tip resistance, friction ratio, and pore pressure for the centermost test are provided as a function of depth in Figure 3-4. In addition, the interpreted soil profile is also shown. From the ground surface to a depth of about 15 feet the soil profile appears to be relatively consistent with a cone tip resistance of about 6 tsf and a friction ratio of about 1%. However, one thin sand layer is clearly evident between 6 and 8 feet. The cone tip resistance, friction ratio, and pore pressure plots clearly show the interbedded silt and sand layering in the soil profile between 15 and 27 feet below the ground surface.

Figure 3-5 provides plots of the cone tip resistance, friction ratio and pore pressure as a function of depth for all four of the CPT soundings. The measured parameters and layering are generally very consistent for all four sounding which indicates that the lateral pile load tests can be fairly compared from one foundation to the next.

Figure 3-6 provides a plot of the shear wave velocity as a function of depth obtained from the downhole seismic cone testing. The interpreted soil profile and cone tip resistance are also provided in Figure 3-6 for reference. The shear wave velocity in the upper 10 feet of the profile is between 300 and 400 feet/sec. This velocity is relatively low and suggests a low shear strength. Between a depth of 10 to 20 feet the velocity increases to about 550 feet/sec. This increase in velocity is likely associated with the interbedded sand layers in these depths. Below 20 feet, the

velocity drops to a value of around 500 feet/sec and remains relatively constant to a depth of 45 feet.

Knowledge of the average shear wave velocity, standard penetration resistance, and undrained shear strength of the soil to a depth of 100 feet is generally necessary to determine a specific International Building Code (IBC) seismic site classification. However, this is not the case if the site is classified as Site Class E. Any soil profile with more than 10 feet of soil having the following characteristics is classified as a Site Class E.

1. Plasticity index, $PI < 20$
2. Moisture content, $w \geq 40\%$
3. Undrained Shear strength, $S_u < 500$ psf

A close look at Table 3-1 or Figure 3-3 shows that this site meets all three of the above criteria. Therefore, the soil profile information obtained to a depth of 50 feet is sufficient to classify the site as an IBC Site Class E.

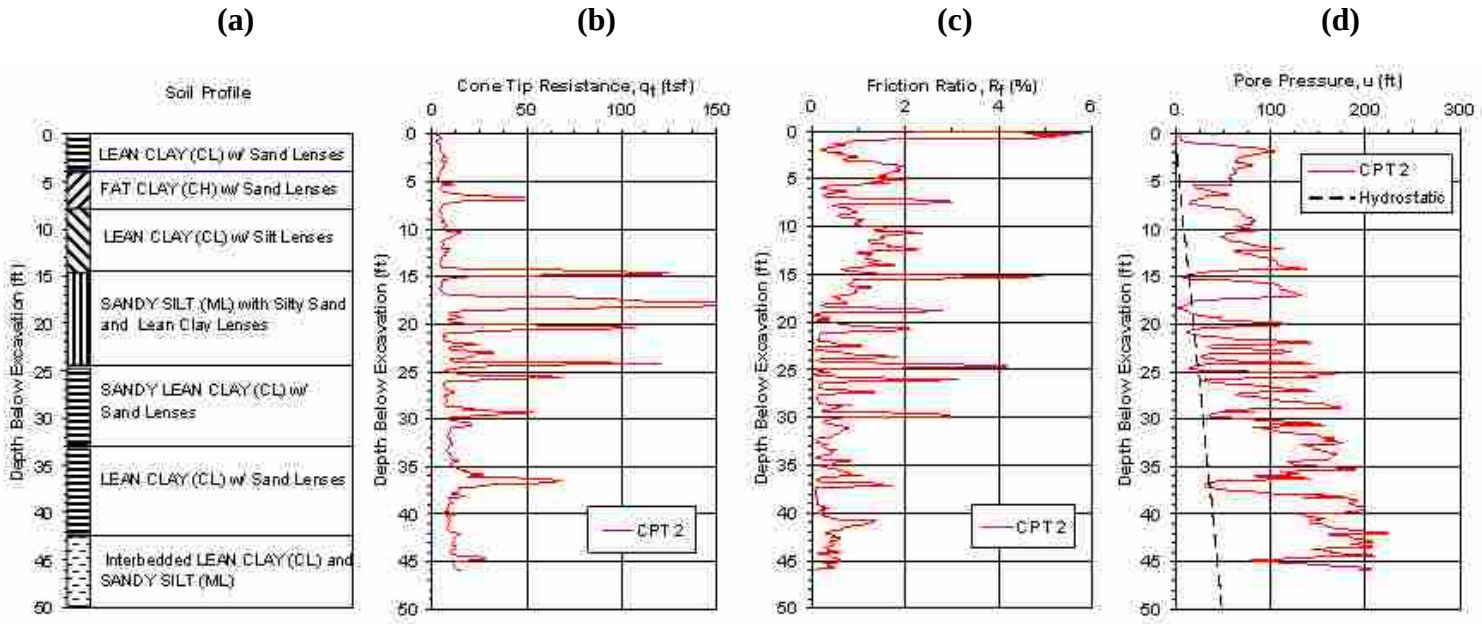

Figure 3-4 – Plot of (a) soil profile, (b) cone tip resistance versus depth, (c) friction ratio versus depth, and (d) pore pressure versus depth curves from cone penetration test (CPT) sounding 2 near the center of the site.

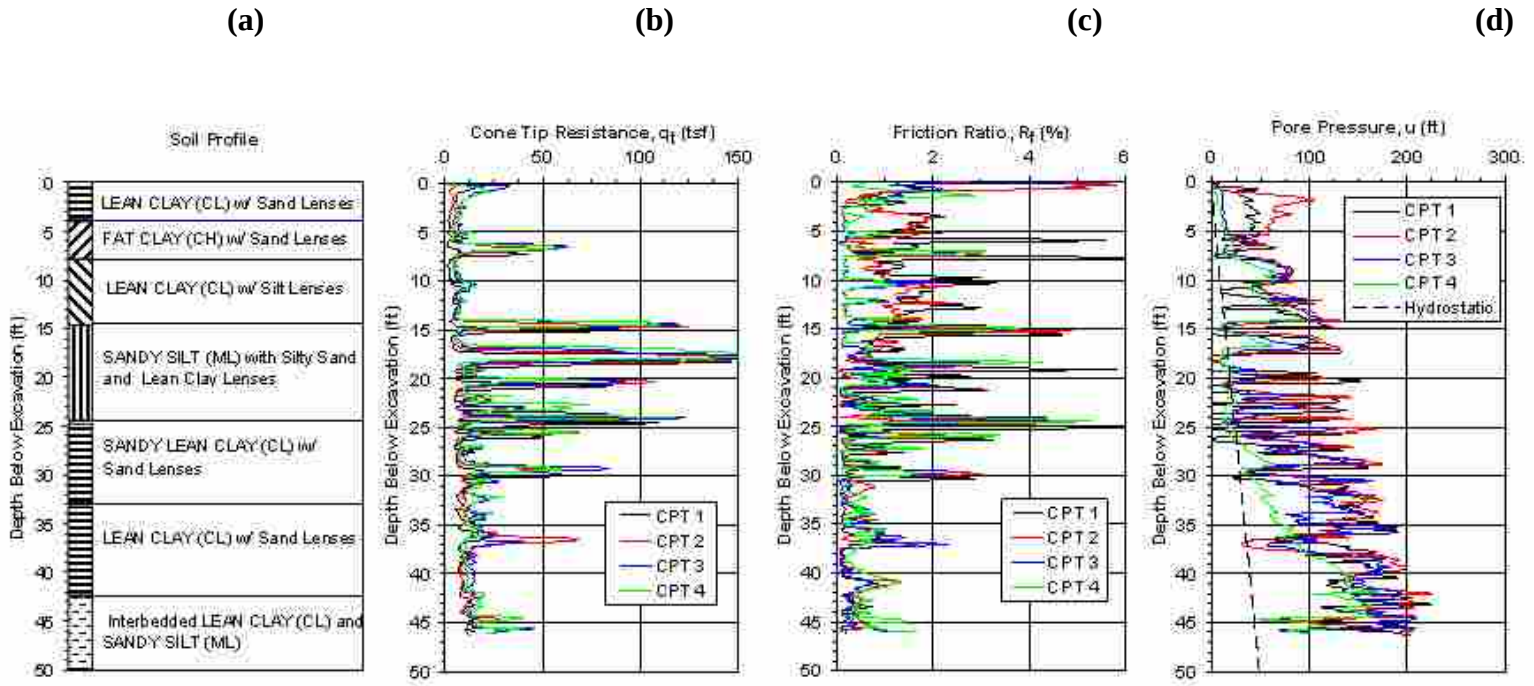

Figure 3-5 - Plot (a) soil profile, (b) cone tip resistance versus depth, (c) friction ratio versus depth and, (d) pore pressure versus depth from all four cone penetration test (CPT) soundings.

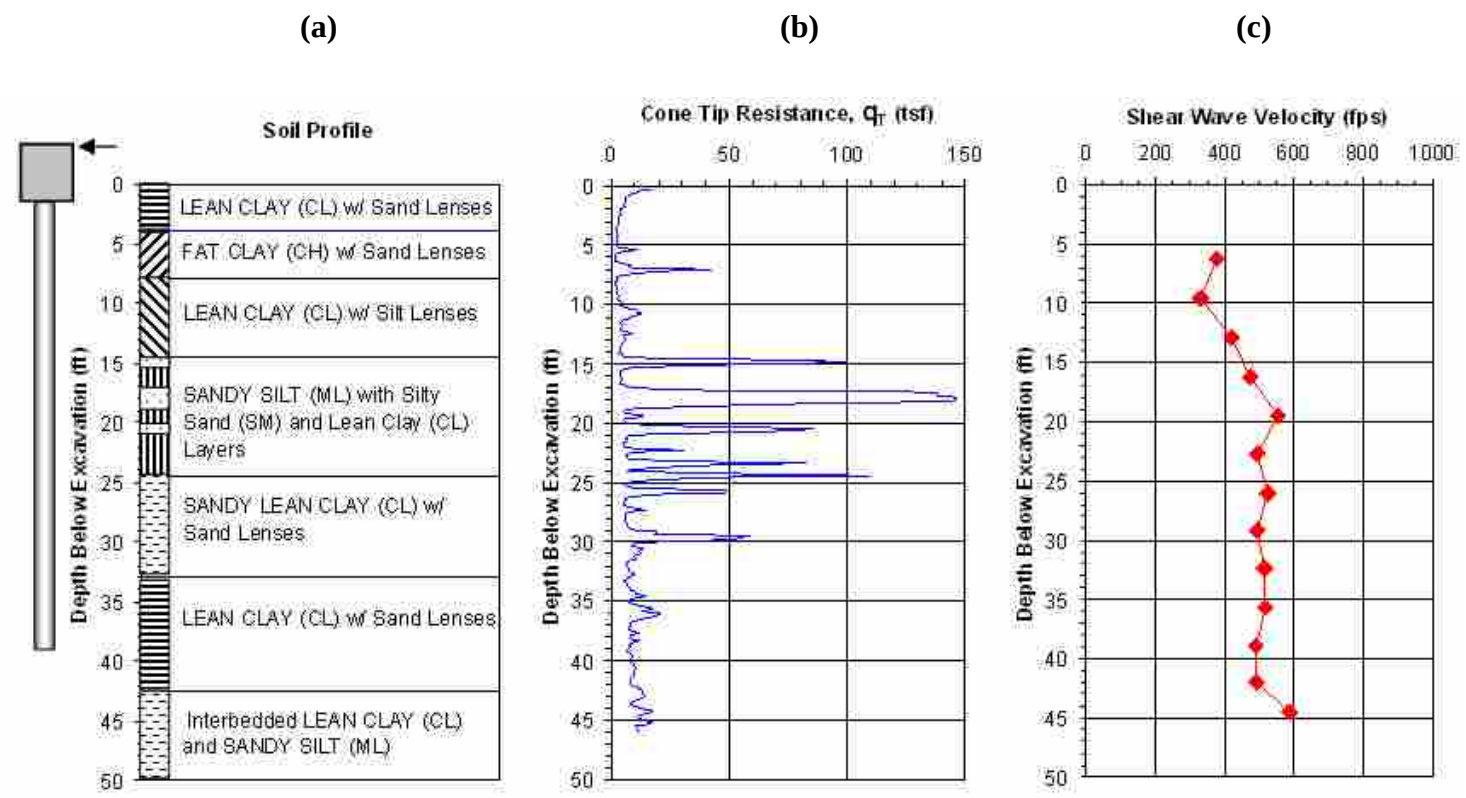

Figure 3-6 Plot of (a) soil profile, (b) cone tip resistance versus depth, and (c) shear wave velocity versus depth from seismic cone testing.

4 Test Layout and Procedure

The following section will detail the construction process for the foundations and define the properties of the materials used to create the foundations. This section will also explain the basic layout of the actuators and pile caps, along with the instrumentation configuration on each of the foundations.

4.1 Construction, Layout, and Materials

Once the site had been excavated to the proper elevation of 4.5 feet below the original grade, the four pile groups were driven. An overall plan view of the four pile group locations is shown in Figure 3-2. As shown in Figure 4-1, each pile group consisted of nine test piles which were driven in a 3 x 3 orientation with a nominal center to center spacing of 3 feet in both directions. The tests piles were 12.75 inch OD pipe piles with a 0.375 inch wall thickness and they were driven closed-ended with a hydraulic hammer to a depth of approximately 45 feet below the excavated ground surface on June 13-15, 2007. The test piles had a beveled end which allowed a 1.5 inch thick plate to be welded flush with the edge of the pile at the bottom. The steel conformed to ASTM A252 Grade 2 specifications and had a yield strength of 58,700 psi based on the 0.2% offset criteria. The moment of inertia of the pile itself was 279 in^4; however, angle irons were welded on opposite sides of

the two to three test pile piles within each group, as discussed subsequently, which increased the moment of inertia to 342 in^4.

The center piles of each row were instrumented with strain gages prior to installation (see Figure 4-1). (Note: For caps 2 and 4, the middle pile of the center row was not instrumented with strain gages). The strain gages were placed at pre-determined depths of 2, 6, 11, and 13.5 feet below the tops of the piles. Strain gages were placed along the north and south sides of the piles in the direction of loading. The strain gage depths were determined through computer modeling to be the most critical depths in developing bending moment curves for the laterally loaded piles. Figure 4-2 is a photo of an installed pile group.

The piles were driven so that they would extend 2 ft into the base of the pile cap. In some cases this was not accomplished so the piles were cut off to this elevation. A steel reinforcing cage was installed at the top of each test pile to connect the test piles to the pile cap. The reinforcing cage consisted of 6 - #8 reinforcing bars which were confined within a #4 bar spiral with a diameter of 8 inches and a pitch of 6 inches. The reinforcing cage extended 2.25 feet above the base of the cap and 8.75 feet below the base. The steel pipe pile was filled with concrete which had an average unconfined compressive strength of 5150 psi based on tests of four specimens. A drawing showing the cross-section for the test piles is provided in Figure 4-3. Once the piles were filled, construction of the pile cap was then commenced.

Figure 4-4 shows the plan and profile drawings of pile caps 1 and 2. Pile caps 1 and 2 (the two northern most pile caps) were constructed by excavating 2.5

feet into the virgin clay. The concrete was poured directly against vertical soil faces on the front and back sides of each pile cap. This construction procedure made it possible to evaluate passive force against the front and back faces of the pile caps. In contrast, plywood forms were used along the sides of all of the caps and were braced laterally against the adjacent soil faces. This construction procedure created a gap between the cap sidewall and the soil so that side friction would be eliminated.

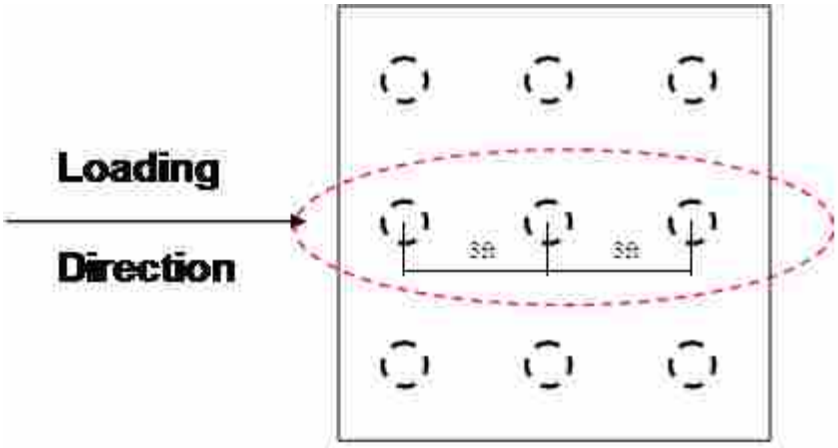

Figure 4-1 - Driven 3x3 pile group all 3ft on center in both directions (piles instrumented with strain gages circled in red).

Pile cap 3 was constructed in a similar manner, except that flowable fill was installed under the pile cap to a depth of 7 feet below the top of the finished cap, 9 feet wide, and 13.5 feet in the direction of loading before piles were driven. Flowable fill was also installed on the north side of the cap to the same depth as that installed under the cap and then, after cap installation, up the side at a width of 4.5 feet from the pile cap to the level of the top of the cap. Pile cap 4 was constructed in the same way as cap 3, except that compacted fill was installed prior to pile driving. The compacted fill was installed to a depth of 3 feet below the bottom of the pile cap

Figure 4-2 - Driven pile layout prior to cap construction.

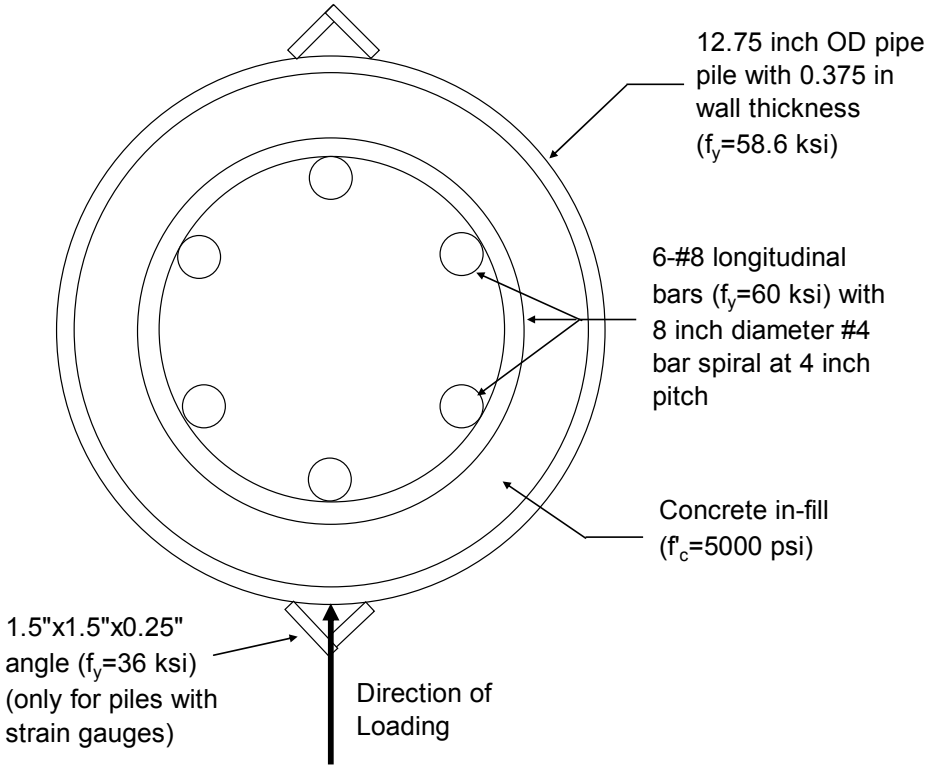

Figure 4-3 - Cross-section of piles within the pile groups.

with a width of 9 feet transverse to the load direction and a length of 14 feet in the direction of loading. Compacted fill was also installed along the north side of the cap to the level of the cap.

Steel reinforcing mats were placed in the top and bottom of each cap with a three inch concrete cover. The top reinforcing mat in the pile caps was designed with #7 bars at 10 inch spacing in both directions, with a decrease in spacing to 6 inches in the transverse direction under the short corbel on caps 1 and 4. The bottom mats were designed with #9 bars at 6.5 inch spacing longitudinally and #7 bars at 10 inch spacing transverse to the load direction. Plan view drawings of the top and bottom reinforcing mats for piles caps 1, 2, 3, and 4 are provided in Figure 4-5 and Figure 4-6.

A corbel was constructed on each cap to allow the actuator to apply load above the ground surface without affecting the soil around the pile cap. The corbel extended the full length of the pile cap for caps 2 and 3 to allow the actuators to be attached to both sides of the caps. Alternatively, the corbel only extended about half of the pile cap length in cap 1 and 4 as only one sided was needed for the actuator attachment. This is shown in Figure 4-4 which illustrates the corbel configuration on top of caps 1 and 2. The corbel was designed using the traditional ACI design method found in section 11.9 of the ACI code. The corbel was reinforced with #5 bar hoops and #9 bars as the main reinforcement as shown in Figure 4-7 and Figure 4-8. Also included in Figure 4-9 is a cross sectional view of the corbel steel looking at the interface where the actuator connects to the corbel. Design calculations and more detailed steel reinforcement drawings are provided in Appendix A.

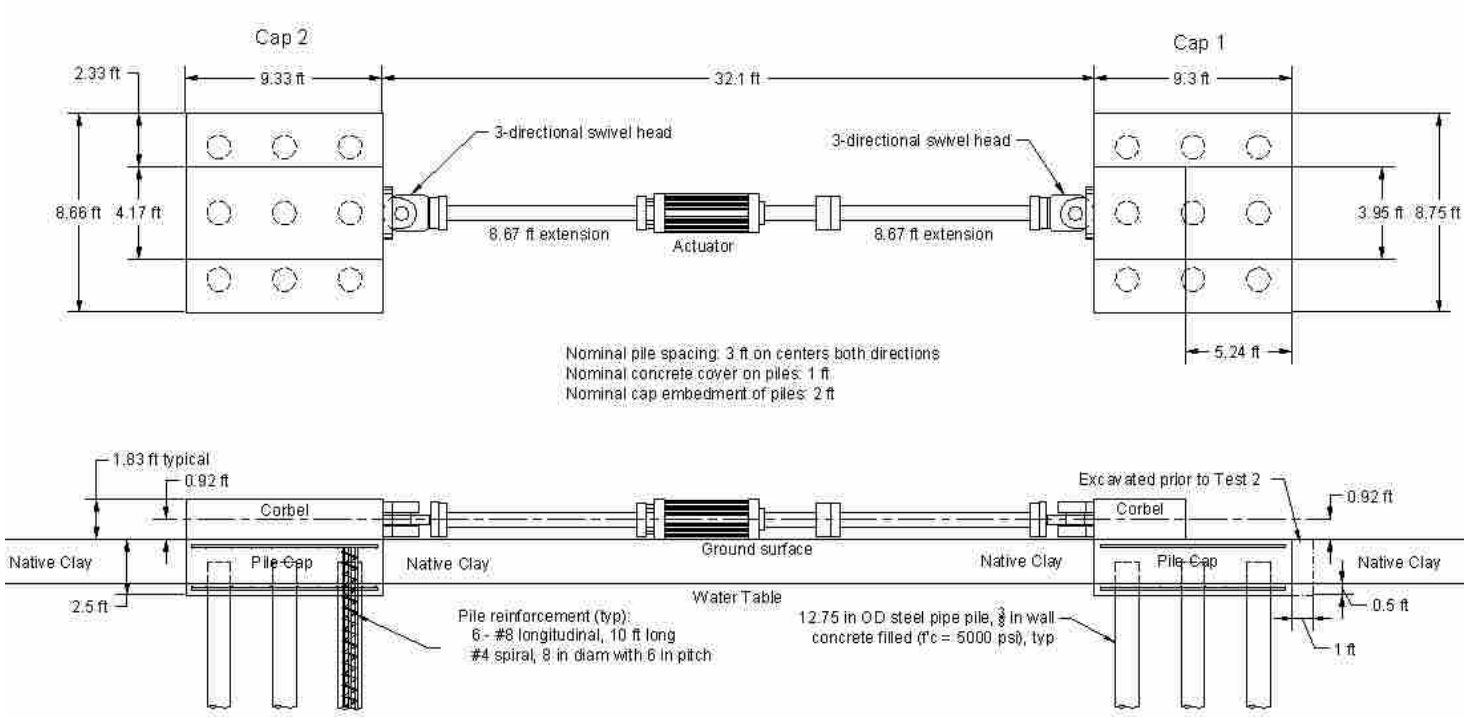

Figure 4-4 Plan and profile drawings of pile caps 1 and 2 during Test 1 when the pile groups were pulled together by the actuator. During Test 2 the soil adjacent to the pile cap was excavated to the base of the cap and the pile caps were pushed apart by the actuator.

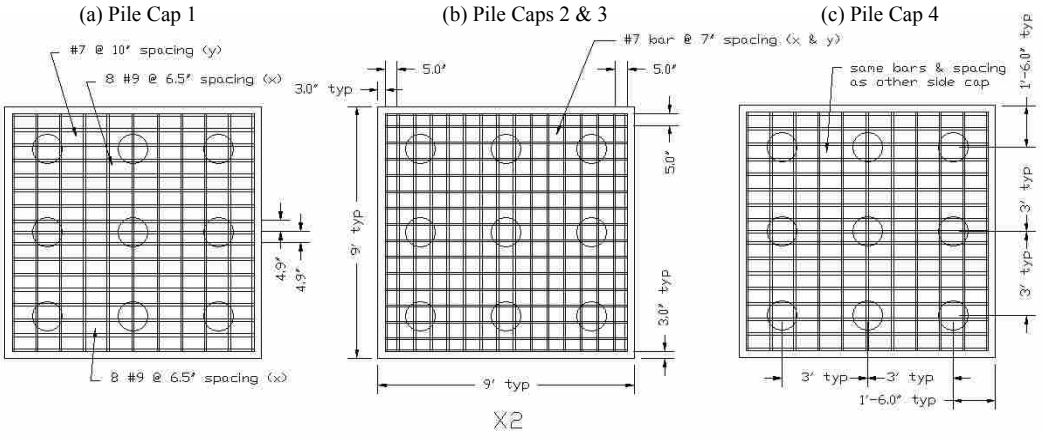

Figure 4-5 - Layout of bottom reinforcing mat for the test pile groups.

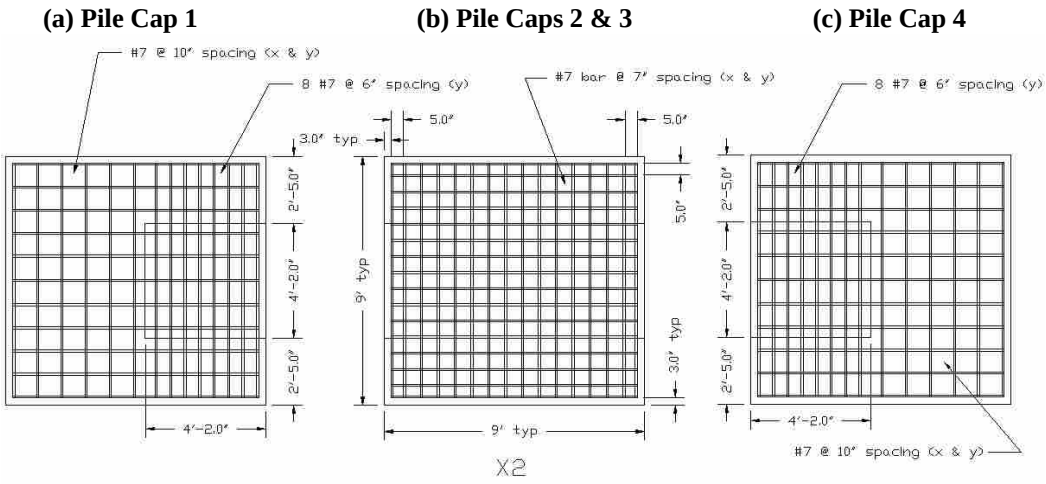

Figure 4-6 - Layout of top reinforcing mat for the test pile groups.

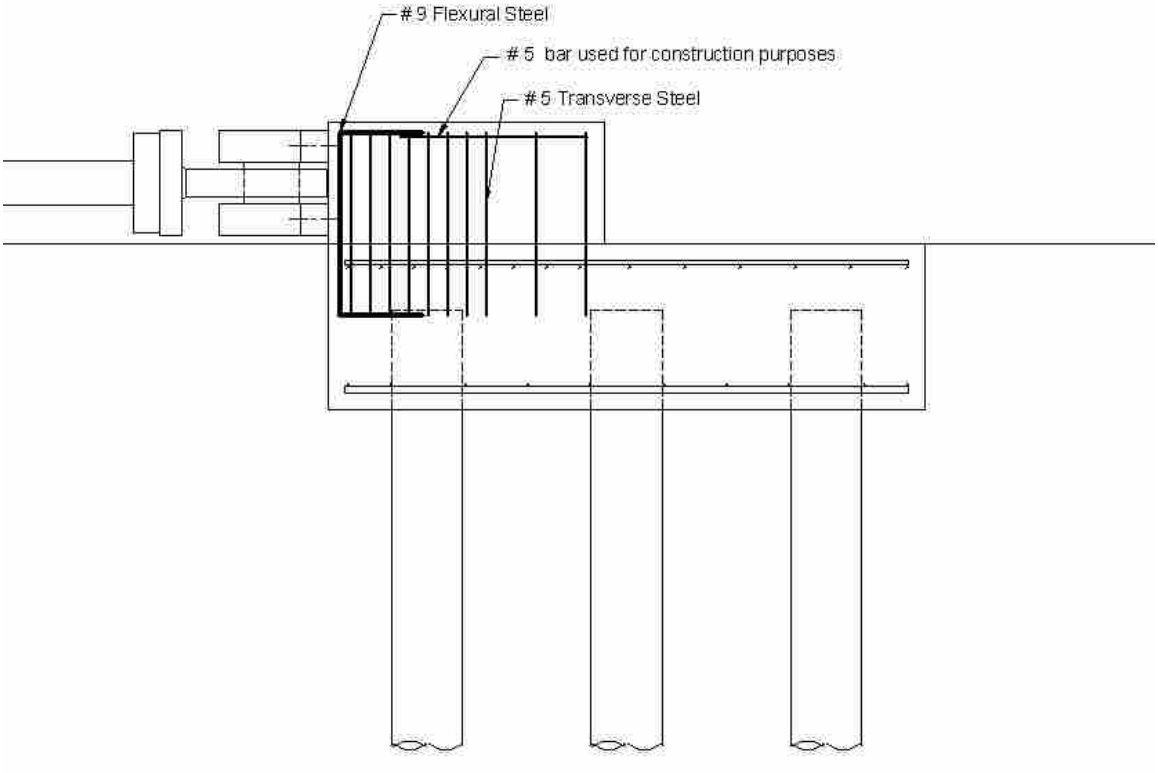

Figure 4-7 – Corbel steel layout for caps 1 and 4.

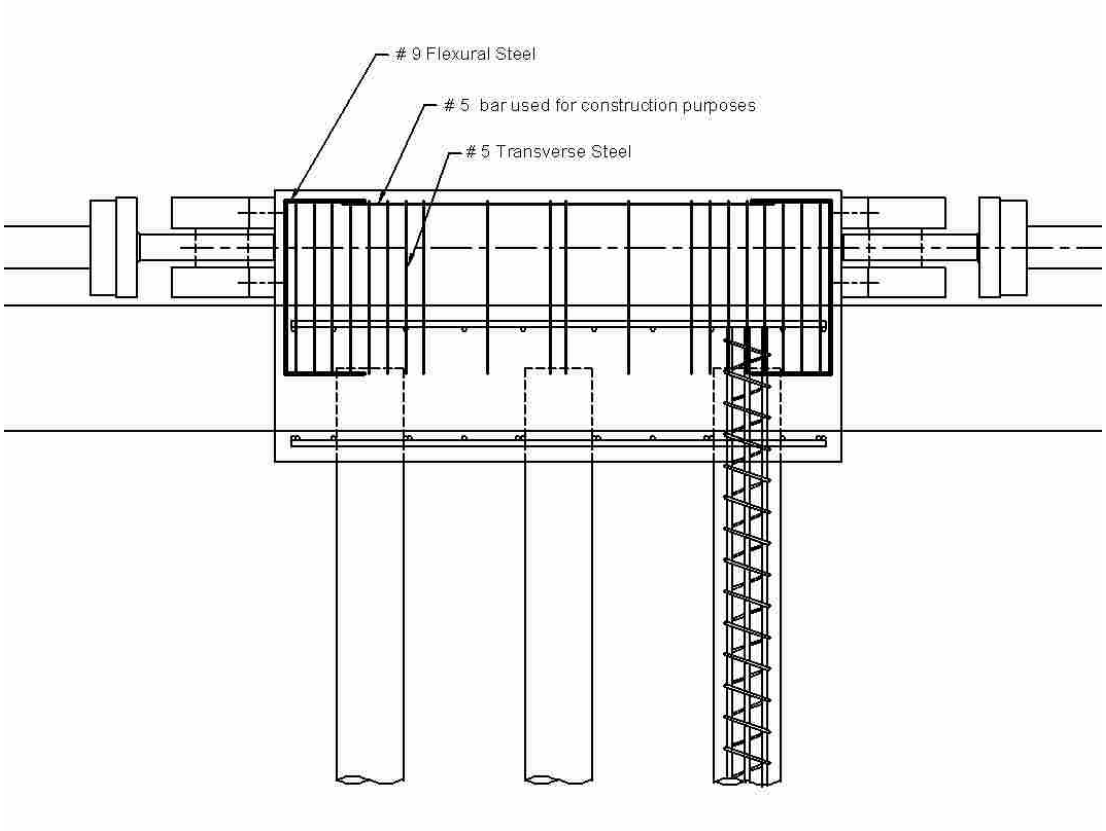

Figure 4-8 – Corbel steel layout for caps 2 and 3.

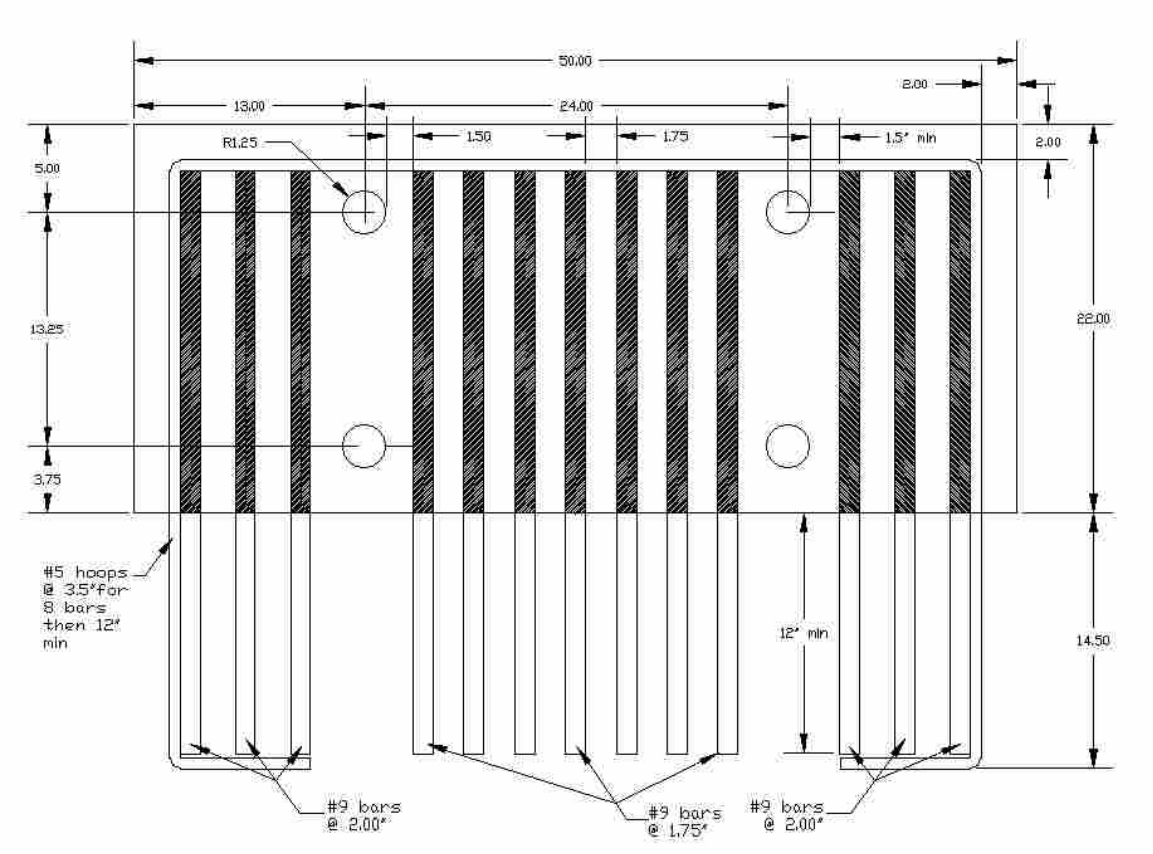

Figure 4-9 – View of corbel steel looking at the actuator connection interface.

4.2 Actuator Layout

Most of the tests performed involved reacting one pile group against another, through applying a lateral load with an MTS actuator with the load centered at a height of 0.92 (11 inches) above the top of the pile cap. Each of the actuators had a capacity of about 600 kips in compression and 450 kips in tension. The pile groups were spaced approximately 32 feet apart edge to edge. This spacing was considered to be large enough to ensure that the volumes of affected soil created by the displacement of each foundation would not significantly interfere with each other. The actuators were fitted

with two 8.67-ft extension pieces each made of 8.5 inch outside diameter 69 ksi steel pipe with a wall thickness of 0.75 inches in order to span the distance between the two foundations. 18x18 inch plates 5 inches thick of 36 ksi were welded to the ends of the extensions to connect the extensions to the actuators and the pile caps. The actuators were attached to each corbel using steel tie-rods which extended through PVC sleeves in the corbel and were bolted to the back face of the corbel. The tie-rods were pre-stressed to minimize displacement of the steel during the load tests. A three-dimensional swivel head was located at each end of the actuator to provide a zero moment or "pinned" connection. Each swivel could accommodate ± 5º of pile cap rotation about a horizontal line (pitch) and ± 15º of pile cap rotation about a vertical line (yaw). A photo the actuators and extensions positioned between the two piles caps in the field is provided in Figure 4-9.

Figure 4-10 - Photo of actuator setup between caps 1 & 2.

4.3 Instrumentation

Six types of instrumentation were used during the tests, namely: strain gages, inclinometers, shape accelerometer arrays, string potentiometers, actuator pressure transducer for load measurements, and surface grids to evaluate heave/settlement or crack patterns. As noted previously, the middle piles were instrumented with waterproof electrical resistance type strain gages (Texas Measurements Group model WFLA-6-120-*LT) at depths of 2, 6, 11, and 13.5 feet below the top of the pile. Angle irons (as shown in Figure 4-4) were welded on opposite sides of the instrumented piles to a depth of 20 ft to protect the strain gauges during pile driving.

The strain gauge depths were selected to provide the maximum negative and positive moments along the pile. For a "fixed-head" or "restrained-head" pile the maximum negative moment is expected to occur at the pile-pile cap interface. Preliminary LPILE analyses suggested that the maximum positive moment would likely occur between 11 and 13 feet below the top of the piles. The depths of the strain gages will vary due to the different driving depth of each individual pile. However, the individual driving depth of each pile was carefully recorded so the actual depths of the strain gages could be obtained. Also, some of the strain gages were damaged in the installation process and, therefore, some instrumented piles will not have data for all strain gage depths.

In addition to the strain gages, the north and south middle piles of each pile group were instrumented with inclinometer tubes. These tubes were placed in the center of the piles before they were filled with concrete and ran the entire depth of the pile. After the

concrete was poured and cured, the inclinometer tubes served as a means of obtaining the pile and pile cap deflections during testing. Inclinometer measurements were typically performed before testing and then again once the final displacement increment had been reached. Using a standard inclinometer and corresponding data mate, the slope in the pile was recorded at 2 foot depth intervals. This procedure made it possible to develop displacement versus depth curves at selected intervals and determine the deflected shape of the pile at the start of each test. Inclinometer readings typically provide displacement measurements with an accuracy of 0.05 inches per 50 readings.

Next to the inclinometer tubes a 1 inch outside diameter PVC pipe was also placed before the concrete pour. These tubes were fitted with a new measuring technology called a shape accelerometer array manufactured by Measurand, Inc. In addition to the middle north and south piles, the center piles were also equipped with the shape arrays. Each shape array consisted of a 25-ft long flexible waterproof cable which had triaxial micro-electrical-mechanical (mems) type accelerometers embedded at 1 ft intervals. By double integrating the accelerations at each level throughout time, the shape arrays provided real-time displacement versus depth profiles at 1 ft intervals throughout the entire testing period relative to the initial deflected shape. The shape arrays were designed to provide displacements with accuracy similar to that from an inclinometer. To provide accurate measurements from the shape arrays, a tight fit between the 1 inch PVC pipe and the array must be maintained. To accomplish this, webbing of various thicknesses was inserted along the length of the shape array minimizing any gaps between the array and the PVC pipe. The shape arrays measured

displacements in both the X and Y directions. For consistency the X direction was chosen as the direction of loading. Occasionally, due to the difficulty of installing the shape arrays, the nodes of the shape arrays would twist or rotate as they were installed thus resulting in the X direction not aligning with the direction of loading. Since it can be assumed that the greatest displacements would be in the direction of loading, to adjust for these instances a square root of the sum of the squares approach was used defining an X1-direction which was the total displacement in the direction of loading as shown in equation 4-1.

$$X1(direction) = \sqrt{X(direction)^2 + Y(direction)^2} \quad \textbf{(4-1)}$$

Lateral pile cap displacement was measured using two string potentiometers (string pots) attached to the pile cap at the elevation of the loading point (0.92 ft above the top of the cap) on the east and west sides of the actuator attachment point. Lateral pile cap displacement was also measured on the back side of each corbel with two string potentiometers attached 0.167 ft (2 inches) and 1.75 ft (21 inches) above the top of the pile cap directly in line with the load direction. Finally, vertical pile cap displacement was measured at two points along the length of each pile cap to evaluate pile cap rotation. Each potentiometer was attached to an independent reference beam supported at a distance of about 6 ft from the side of the pile cap. The diagram in Figure 4-11 shows the locations of the string pots used in the various tests.

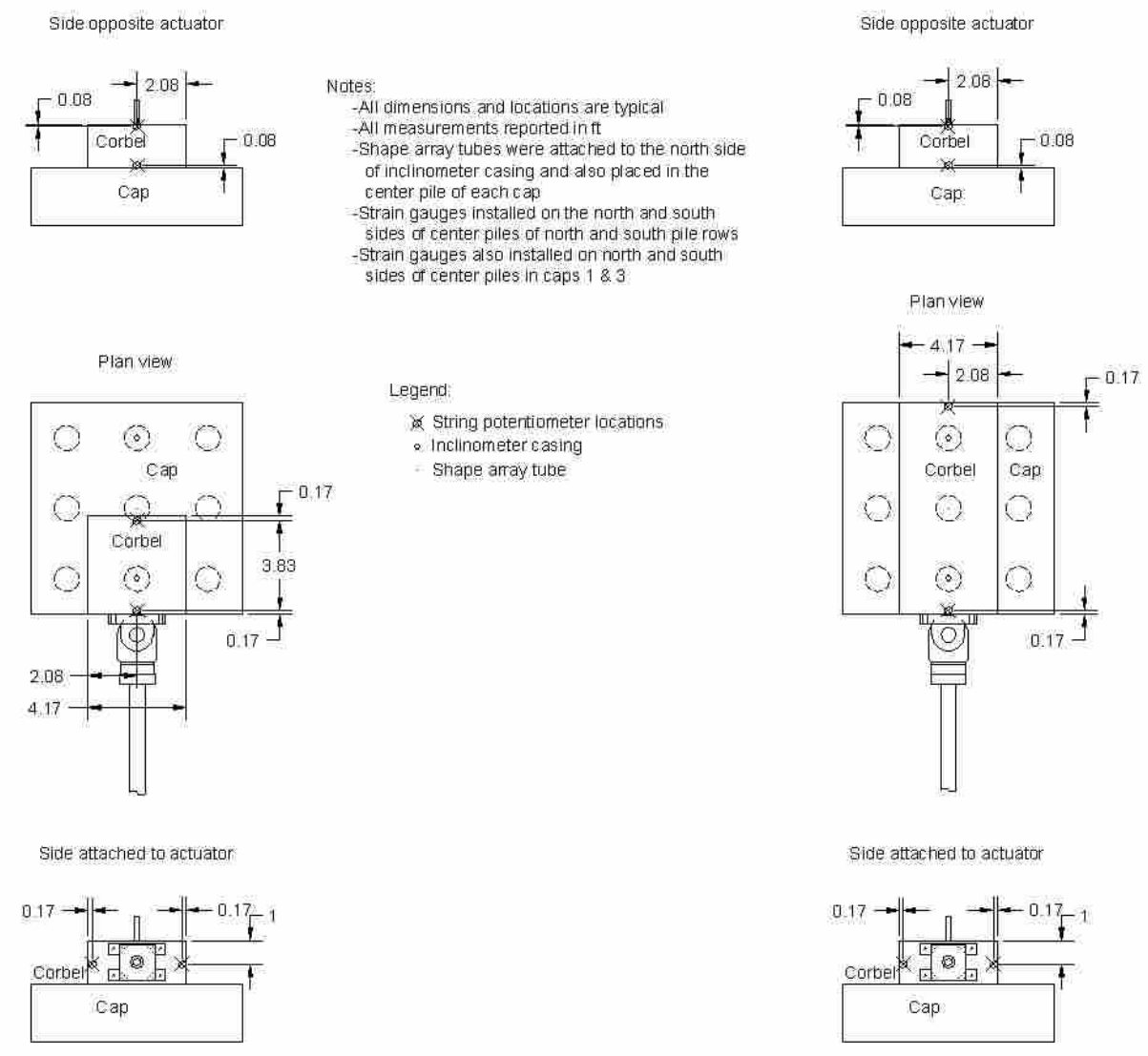

Figure 4-11 - Typical instrumentation layout.

Applied load was measured by pressure transducers on the actuator which were calibrated in the laboratory prior to testing in the field. Load data were recorded using the actuator control computer and software.

Surface grids were painted on the surface area behind the cap being tested. The grid was 12 feet wide by 10 feet long and had grid lines every 2 feet. The grids were surveyed before the test and at the maximum deflection during the test. The grid was also used to map the shear planes that developed during lateral loading.

4.4 Test Procedure

This section describes the general lateral load test procedure used for this series of tests: If there are variations to an individual test it will be noted in their individual section.

Lateral pile group load testing was conducted from July 16 to August 29, 2007. The piles had been in the ground for about one month prior to the first test. Load was applied to the pile caps using the actuator which was powered by a portable pump with a 60 gallon/minute capacity. The pump unit was powered by a portable diesel generator. The lateral load tests were carried out with a displacement control approach with pile cap displacement increments of approximately 0.125, 0.25, 0.50, 0.75, 1.0, and 1.5 inches. During this process the actuator extended or contracted at a rate of about 1.5 inches/minute. In addition, at each increment 10 cycles with a peak displacement amplitude of about ±0.05 inches were applied with a frequency of approximately 1 Hz to evaluate dynamic response of the pile cap. After this small displacement cycling at each increment, the pile group was pulled back to the initial starting point prior to loading to the next higher displacement increment. Typically, the testing procedure was paused at the end of the 1.5 inch (final) test increment cyclic portion and held for 20 to 30 minutes

while inclinometer measurements were made before ramping back down to zero displacement.

A schematic testing layout for the tests 1, 2, 9 and 15 included in this report is shown in Figure 4-14, Figure 4-15, Figure 4-16, and Figure 4-17, respectively. The first consisted of a lateral pull into the virgin clay. The second was a lateral push into the virgin clay, but with the passive force removed by a 1 foot wide excavation to the depth of the cap. The third test was a lateral pull into a mass mixed treated soil. Finally, the fourth test had a 1 foot wide excavation of the mass mix to the depth of the cap and was laterally pulled again to obtain the passive results of the mass mix. The virgin clay tests 1 and 2 act as a baseline for measuring the mass mix soil improvements in tests 9 and 15.

4.5 Mass Mixing Soil Treatment Procedure

After the completion of tests 1 and 2, the area around pile caps 1 and 2 was treated using jet grouting and mass mixing. The area treated with mass mixing was at the south end of cap 1 as shown in Figure 4-16. Plan and profile drawings of the pile caps 1 and 2 after soil improvement are shown in Figure 4-18 and Figure 4-19. The native soil was excavated to a depth of 5 feet below the top of the cap using a 43 inch wide bucket creating a trench spanning the width of pile cap 1 (8.66 feet) and extending about 1.5 to 2 ft beyond the edge of the cap as shown in Figure 4-19. The total excavation width was about 4 feet. The excavation was then filled to the top of the cap with jet grout spoils. Afterwards, the remaining intact soil from 5 to 10 feet below the top of the cap was progressively excavated with the excavator bucket and mixed with the jet grout spoils.

Mixing was accomplished by repeatedly stirring the native soil and grout spoil until the consistency of the mixture became relatively homogeneous and no large blocks were obvious in the mixture. This process required approximately 10 to 15 minutes of mixing and provided a 1 to 1 ratio of soil to grout spoil mixture. Photographs of the mixing process are provided in Figure 4-12. A photograph of the finished mass mixed zone is also provided in Figure 4-13, in which the final dimensions of 11 feet long and 4 feet thick can be seen.

The cement content of the resulting mixed soil zone requires some effort to estimate. The original jet grout used in the jet grouting procedure was designed to have a specific gravity of approximately 1.52, which is the equivalent of a 1 to 1 water to cement ratio by weight using normal type I cement. For the treated area, the cement content per volume of jet grout would theoretically be about 26 pcf based off a 4 foot diameter jet grout column at a pull rate of 9.85 in/sec. If that grout weight were to remain consistent for the jet grout spoils, then the mass mixing procedure would have reduced that cement content by half when mixing it in a 1 to 1 ratio by volume with the intact soil. So, the cement content of the mass mix would be approximately 13 pcf. However, there are several unknown factors that could affect the actual cement content. intact soil. So, the cement content of the mass mix would be approximately 13 pcf. However, there are several unknown factors that could affect the actual cement content. For example, the slurry was basically the tailings of the jet grouting procedure. During the procedure it would be expected that various amounts of clay would have mixed with the slurry thus decreasing the cement content. Also, in the mass mixing process a

Figure 4-12 – The process of mixing the insitu soil with the jet grout spoils.

Figure 4-13 – Photograph of the finished mass mixed zone.

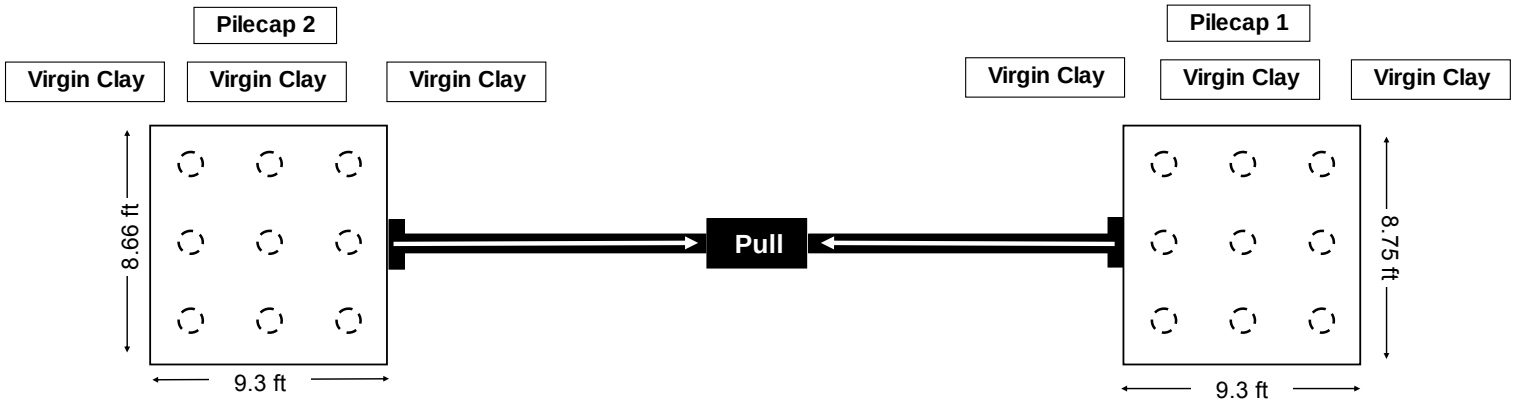

Figure 4-14 – Test 1 lateral push into virgin clay.

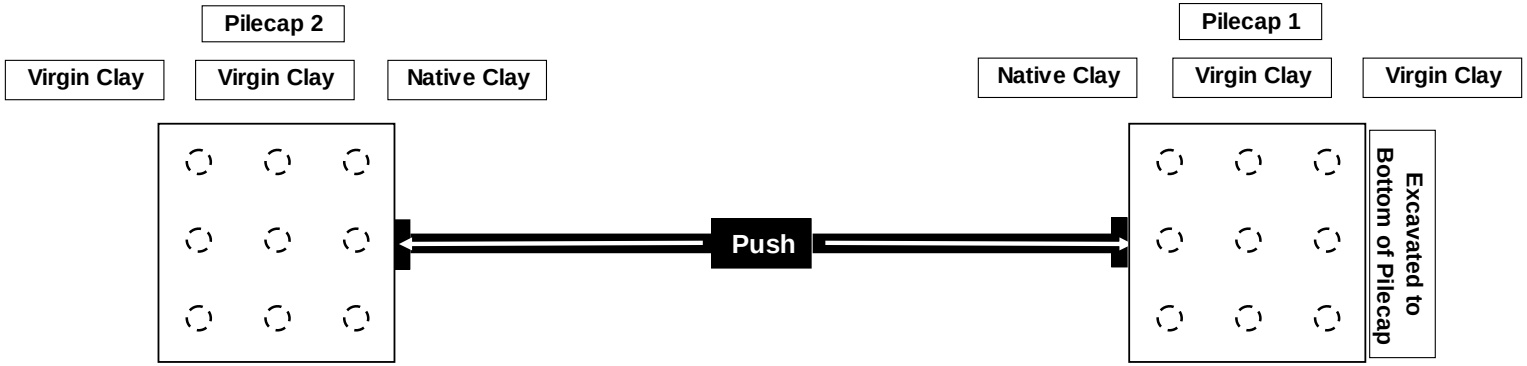

Figure 4-15 – Test 2 lateral push into virgin clay with soil excavated adjacent to cap 1 to eliminate passive pressure on the cap.

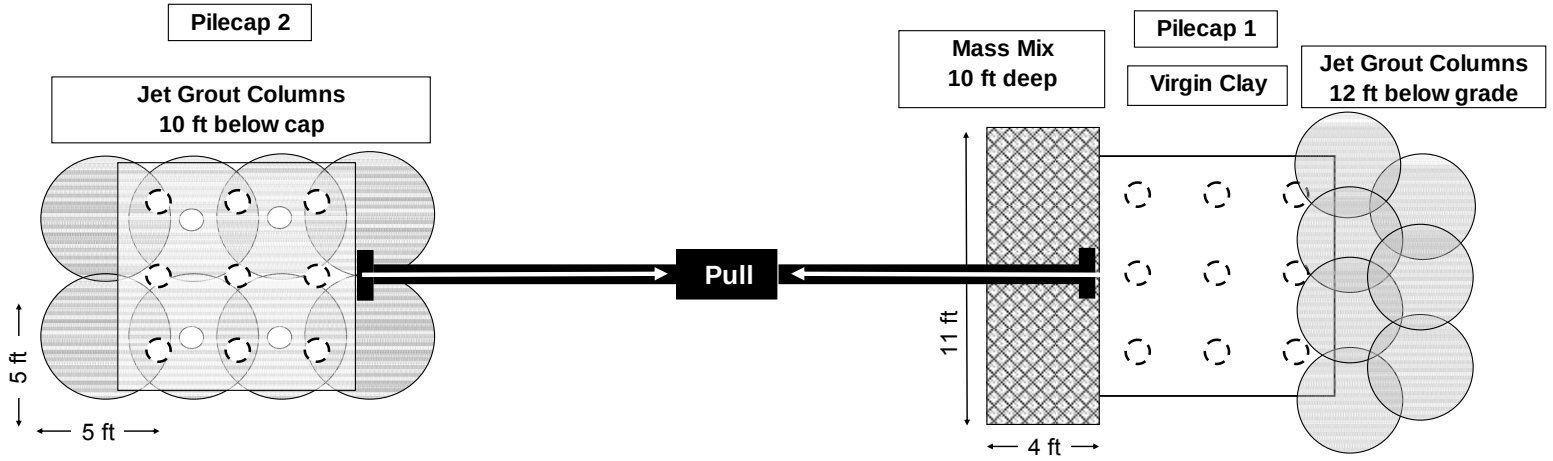

Figure 4-16 – Test 9 lateral pull into zone of soil improved by mass mixing.

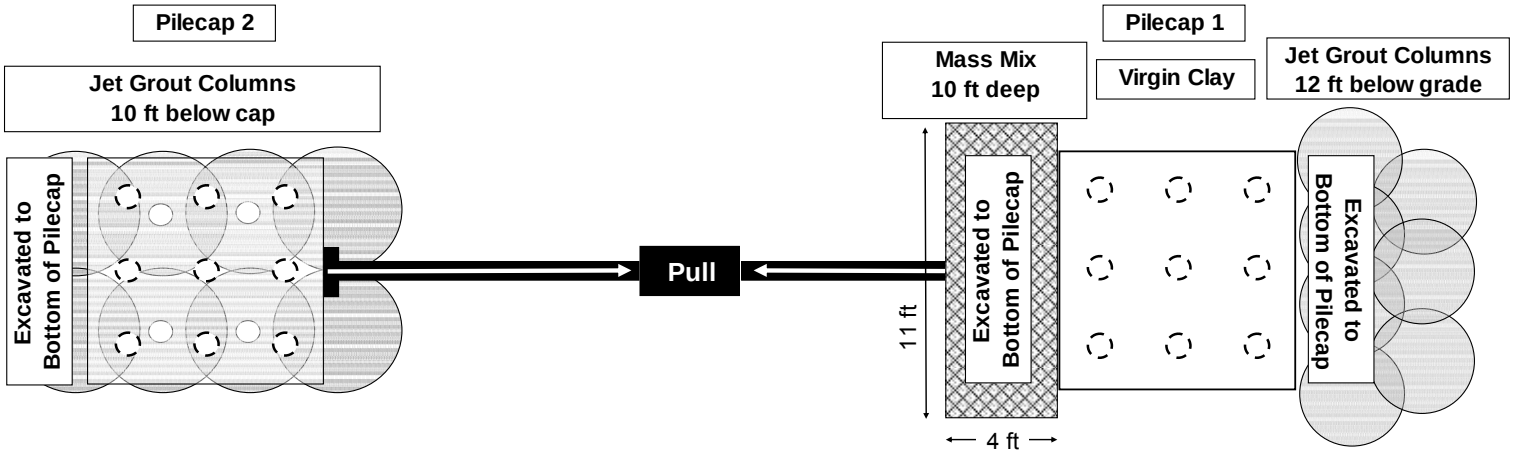

Figure 4-17 – Test 15 lateral pull into zone of mass mixing after excavating soil adjacent to cap 1 to eliminate passive pressure on the cap.

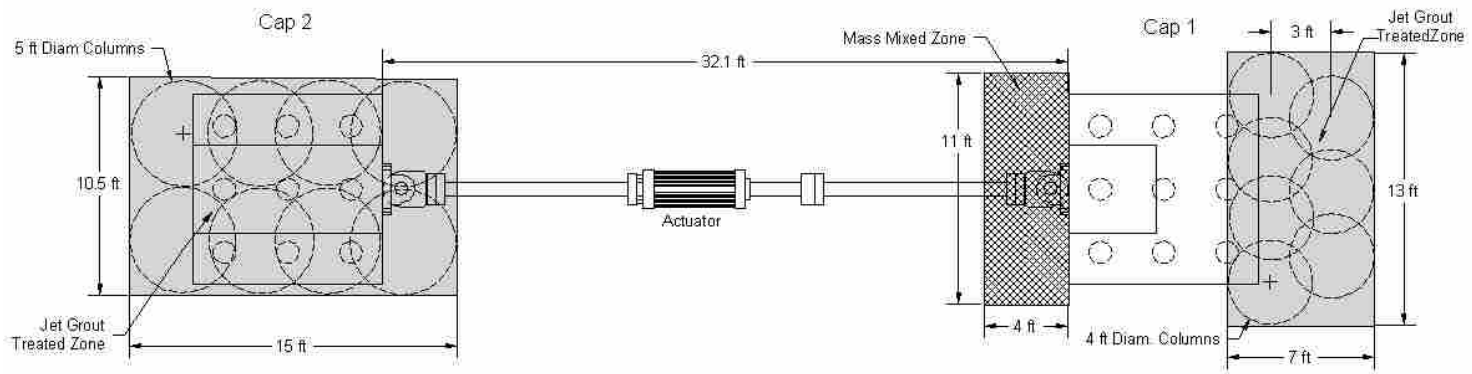

Figure 4-18 – Plan views of cap 2 (left) and cap 1 (right) after mass mixing and jet grouting soil improvements. (Dimensions in feet)

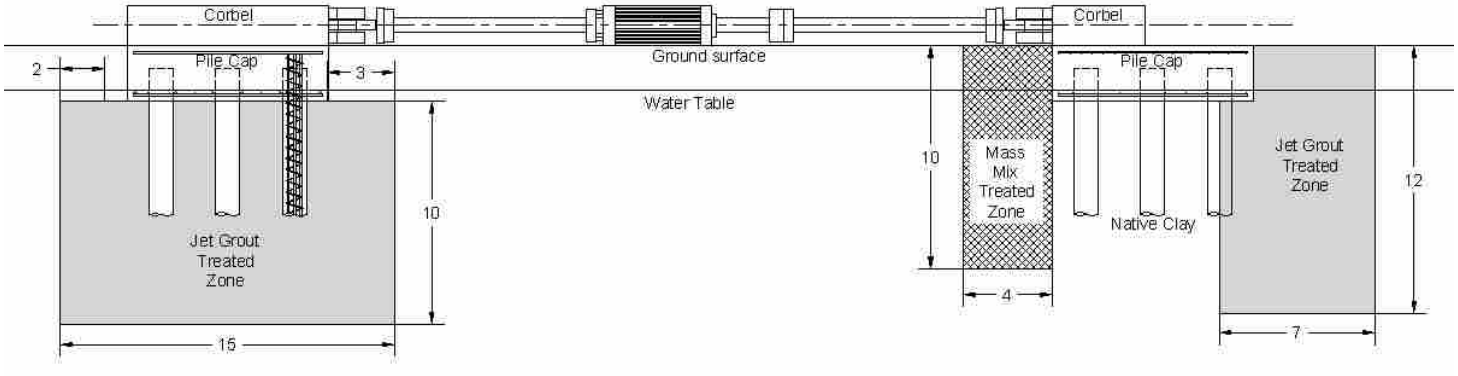

Figure 4-19 - Profile views of cap 2 (left) and cap 1 (right) after mass mixing and jet grouting soil improvements. (Dimensions in feet)

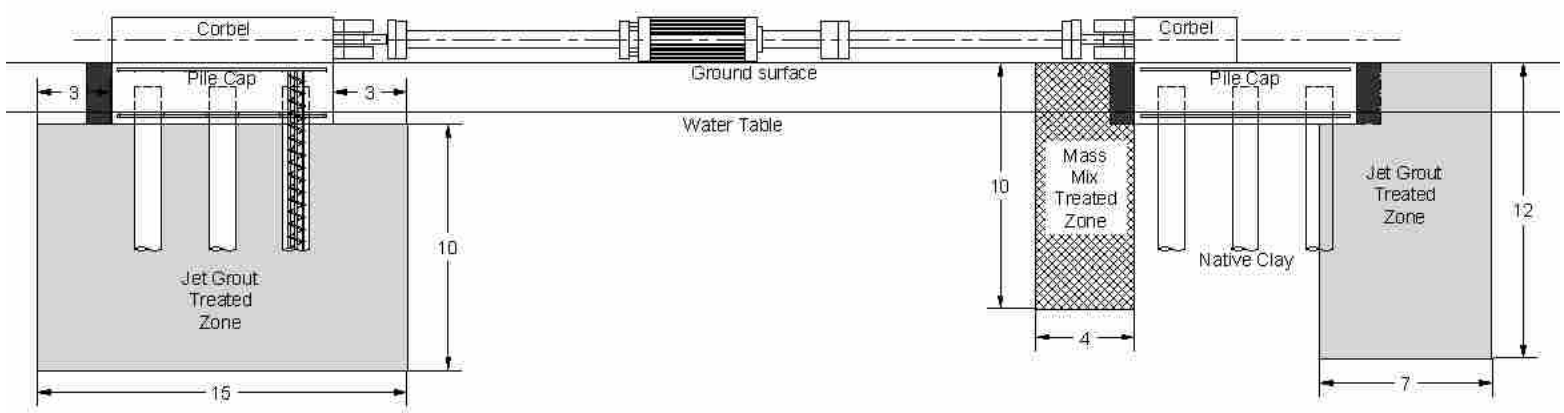

Figure 4-20 - Profile views of cap 2 (left) and cap 1 (right) after 1 foot wide excavations to the bottom of the cap on the south side of cap 2 and on both sides of cap 1. The excavations were made in preparation for test 15 to eliminate the passive resistance of the soil behind the cap. (Dimensions in feet)

homogeneous mixture was attempted, but it is possible that the mixing wasn't perfect allowing greater cement content in areas than in others. These factors could potentially decrease the cement content, but would be unlikely to increase it.

Directly after the mixing was completed, primary test samples for the mass mix were collected by inserting a PVC pipe into the mixture and extracting the soil cement mixture. The mixture was then placed in test cylinders for curing. Unconfined compression tests were then preformed in accordance with ASTM standards. However, when the unconfined compression tests were preformed at 7 and 14 days curing time on the primary samples, no appreciable strength was evident.

To investigate the lack of strength, six 3" diameter core samples were extracted and tested after 38 and 63 days of curing. Table 4-1 shows the results of unconfined compression tests on the cored samples. Specimen No. 3 was short in length compared to the diameter, so a correction factor was applied in accordance to ASTM 42-C. The test results in Table 4-2 indicate that one sample tested at 38 days had a strength of 131 psi, while four samples tested at 63 days averaged a strength

Table 4-1 – Unconfined compressive strengths of mass mix cored samples.

Specimen No.	Curing Time (days)	Unconfined Compressive Strength (psi)
1	38	131.30
3	63	130.16
4	63	140.06
5	63	150.40
6	63	137.67

Table 4-2 – Mean and standard deviation results of the unconfined compressive test for the mass mix cored samples.

Batch No.	Curing Time (days)	Mean UCS (psi)	Standard Deviation
1	38	131.30	-
2	63	139.57	8.36

of about 140 psi with a standard deviation of about 8 psi. Based on the compression test results on the cored samples, it was decided that for unknown factors the primary samples were not representative. It can be further assumed, since only a small amount of strength increase is evident between 38 and 63 days, that the strength gain vs time relationship would follow those typical of other cementitious materials which reach 90% or more of ultimate strength in 28 days. If the soil-cement mixture cured at the same rate as concrete alone, then the compressive strength of the mixture at the time of testing would be approximately 126 psi.

To determine if the measured compressive strengths were reasonable relative to the cement content employed, comparisons were made with unconfined compression test results obtained by mass mixing in clay performed with different binders in Finland as shown in Figure 2-8. The 140 psi compressive strength would be the equivalent of 965 KPa and the estimated 13 pcf of cement content is equivalent to about 208 kg/m^3. The measured compressive strength is almost identical to that for a cement binder with gypsum and lime (FTC). Thus the estimated cement content of 13 pcf appears to be reasonable relative to the unconfined compression test results.

5 Test Results

The results of fours tests are discussed and compared in this section. The first consisted of a lateral pull into the virgin clay. The second was a lateral push into the virgin clay, but with the passive force removed by a 1 foot wide excavation to the depth of the cap. The third test was a lateral pull into a mass mixed treated soil. Finally, the fourth test had a 1 foot wide excavation of the mass mix to the depth of the cap and was laterally pulled again to obtain the passive results of the mass mix.

5.1 Virgin Clay Test

The first test was performed on the virgin clay between cap 1 and cap 2, the northern most caps. This particular test involved a lateral pull as shown in Figure 4-14. The objective of this test was to find the lateral strength of the virgin soil for comparison to later soil improvements.

All instrumentation of string potentiometers, shape arrays, inclinometers, actuator pressure transducer, strain gages, and surface grids were in place and initial measurements taken prior to the test. The location of all the instrumentation for caps 1 and 2 is found in chapter 4 Test Layout and Procedure. Strain gages on cap 1 were located on the three middle piles, but only on the south and north piles of cap 2. The

test followed the standard procedure with one exception. On the 1.5 inch increment test, the pile caps were displaced to that target displacement. Once the displacement was reached, the actuator proceeded into the cyclic test, and then ramped back down to zero displacement and was not held for inclinometer readings. In order to obtain the inclinometer readings for the 1.5 inch test increment an additional reload ramp was necessary from which the inclinometer measurements were taken. Finally, since this was the first test the values measured were all zero set to the initial values of this test just prior to commencement.

5.1.1 Load-Displacement Results

Plots of the complete pile cap load versus displacement curves for cap 1 and cap 2 for the test 1 are presented in Figure 5-1 and Figure 5-2. These curves were obtained from the actuator pressure transducer and the string potentiometers attached to their corresponding cap. These plots provide the load path taken during loading, unloading and reloading for each cycle. At the end of each loading cycle it was necessary to apply a tensile force to bring the actuator deflection back to zero. This does not appear to be a result of yielding in the pile based on measured bending moments. The behavior could result from a flow of weak soil into the gap behind the pile during loading or lateral resistance due to side shear on the pile as it moves in the opposite direction. During re-loading, the load is typically less than that obtained during virgin loading and considerably more linear. The peak load during reloading is typically about 90% of the peak load during the initial loading. After the deflection exceeds the maximum previous deflection for a give cycle, the load

increases and the load-deflection curve transitions into what appears to be the virgin curve.

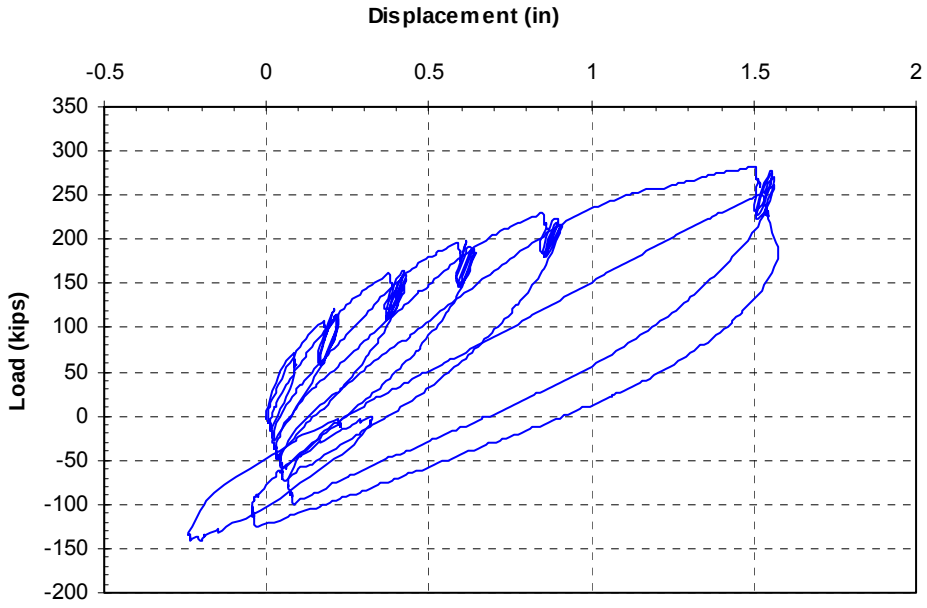

Figure 5-1- Complete load-displacement curve for cap 1 during test 1.

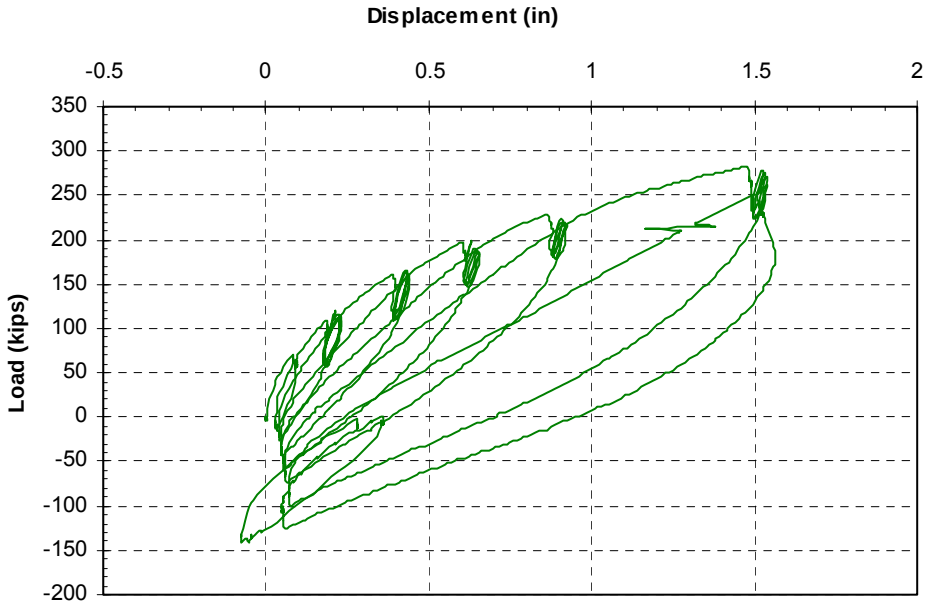

Figure 5-2 – Complete load-displacement curve for cap 2 during test 1.

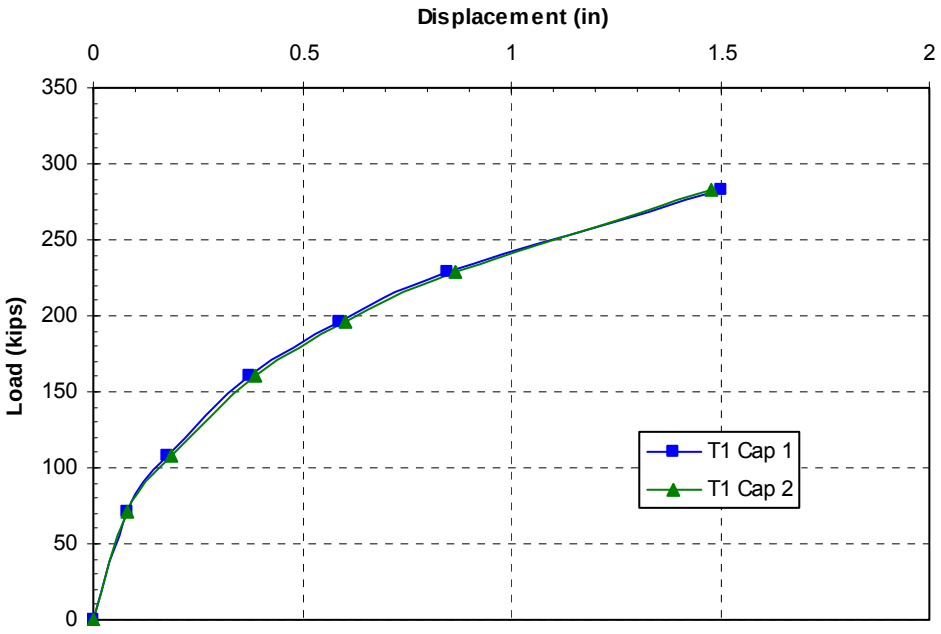

Figure 5-3 – Comparison of peak load-displacement curves for caps 1 and 2 during test 1.

The virgin pile head load vs. displacement curves for each pile group have been developed in Figure 5-3 by plotting the peak values and eliminating the unload and reload segments. Although the actuator was set to push the caps to target displacement increments of 0.125, 0.25, 0.5, 0.75, 1.0, 1.5 inches, small seating movement and distortions in the actuator during load led to somewhat smaller displacements than anticipated. For example, the actual peak displacement increments for cap 1 were 0.08, 0.18, 0.38, 0.59, 0.85, and 1.51 inches respectively. Peak displacement increments for cap 2 were 0.08, 0.19, 0.39, 0.61, 0.87, and 1.48 inches respectively as measured by the corresponding string potentiometers. Because the increments were arbitrarily selected, these small discrepancies are insignificant.

The curves in Figure 5-3 exhibit the conventional hyperbolic shape that would be expected for a pile in soft clay. However, because the peak displacement was limited to 1.5 inches to prevent excessive moments in the pile, the slope of the load versus displacement curve never reached a horizontal asymptote. Nevertheless, the last part of the curve is relatively linear suggesting that the lateral resistance is primarily due to the flextural resistance of the pile. The maximum applied load during the last pull was 282.2 kips and resulted in a displacement of 1.50 inches for cap 1 and 1.48 inches for cap 2. For comparison purposes this load of 282 kips at 1.5 inch displacement will be used for the virgin soil.

Despite the fact that the two pile groups were 32 ft apart and had minor variations in construction details, the two load-displacement curves shown in Figure 5-3 are nearly identical. These results suggest that the soil properties across the site are sufficiently uniform that valid comparisons can be made between the pile caps with various soil improvement techniques relative to the untreated conditions.

5.1.2 Rotation versus Load Results

Pile cap rotation versus load curves based on the string potentiometer and shape array measurements for caps 1 and 2 during test 1 are provided in Figure 5-4 and Figure 5-5 respectively. For cap 1 the curves are fairly consistent up to a load of about 230 kips after which the rotation measured from the string potentiometers begins to increase more rapidly with load. At the final load of 282 kips the rotation measured by the different instrumentation differed by 0.1 degrees whereas they only differed by 0.04 degrees or less before the 230 kip loading.

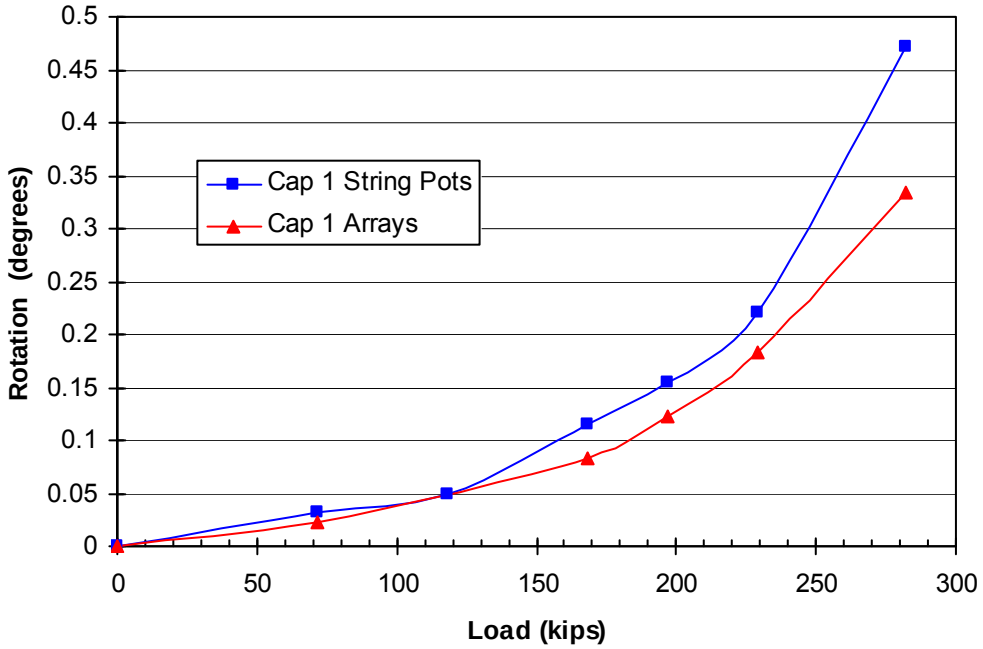

Figure 5-4 - Peak pile cap load versus pile head rotation from the string potentiometers and arrays for cap 1 during test 1.

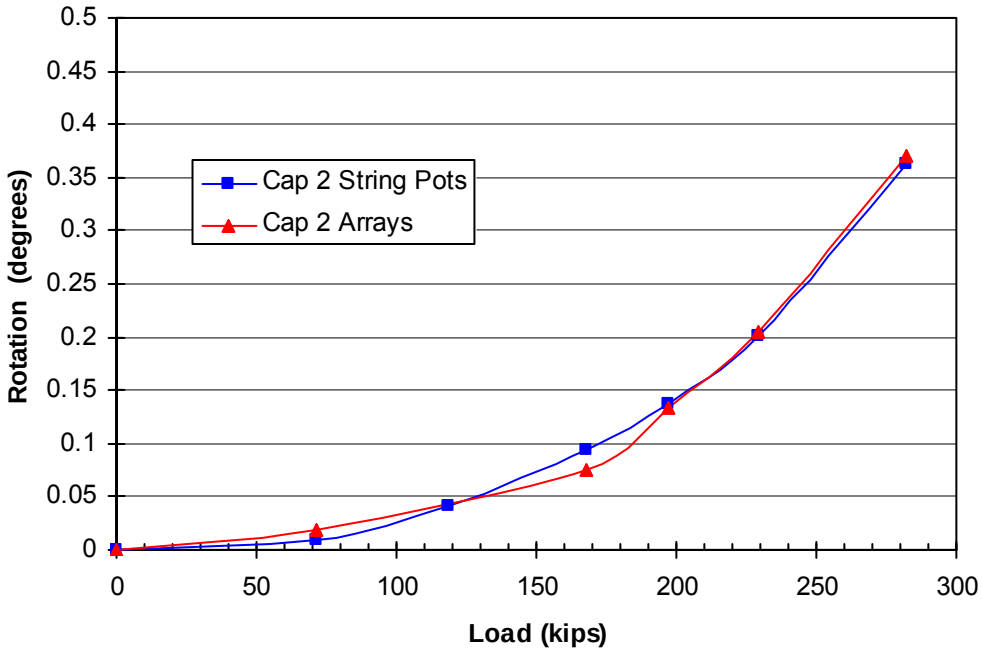

Figure 5-5 - Peak pile cap load versus pile head rotation from the string potentiometers and arrays for cap 2 during test 1.

Cap 2, on the other hand, experiences great agreement between both the string potentiometers and the arrays throughout the test. The curves are fairly linear up to a load of about 170 kips after which the rotation begins to increase more rapidly with load. Measured rotations are fairly consistent for both caps, with the exception of the 282 kip measurement from the string potentiometers on cap 1 which appears to be over estimating the rotation. While pile cap rotation is clearly observed, it is considerably lower than the rotation of the single pile under "free-head" conditions where rotation is significantly greater.

5.1.3 Depth versus Displacement Results

The shape arrays and inclinometers were used to record displacement versus depth profiles in the piles during the tests. The shape arrays recorded continuously during loading and could therefore be used to provide displacement profiles at any point in the test. In contrast, 15 to 20 minutes were required to make inclinometer measurements on the four instrumented piles at a given displacement increment, therefore, inclinometer measurements were only made initially prior to testing and after the final maximum displacement increment to prevent disruption of the testing procedure. To provide an indication of the accuracy of the downhole measurements, displacements from the string potentiometers at the elevation of the applied load are compared to those obtained from the shape arrays at the maximum load for each loading increment. In addition, displacement profiles from the inclinometers were compared to those from the shape arrays during the 1.5 inch hold portion of the test in which inclinometer data were recorded.

Displacement versus depth curves obtained from the shape accelerometer arrays in the piles within pile cap 1 and 2 are provided in Figure 5-6 and Figure 5-7, respectively. The location of the shape arrays relative to the piles in the group and the loading direction are shown by the legends in each figure. The average displacements measured by the string potentiometers at the elevation of the load application for each load increment are also shown in these figures for comparison purposes.

Due to a defective array, the data collected from the south (A-142) array on cap 1 were erroneous. As a result, only the center array (A-104) and the north array (A-106) are used to compare to the string potentiometer and inclinometer data shown subsequently. Additionally, the data from A-106 was adjusted for the X direction not being aligned with the direction of loading using the method discussed in Section 4.3. On cap 2, the south array (A-112) produced erroneous data which will not be presented. Nevertheless, the center array (A-115) and the north array (A-134) provide useful comparisons which are shown in Figure 5-7. Additionally, due to operator error no array data were recorded for the target 0.25 inch displacement increment, therefore this data is missing from the plots in Figure 5-6 and Figure 5-7.

To make an accurate comparison between the arrays and the string potentiometers in Figure 5-6**,** the array data for cap 1 had to be extrapolated to the same depth as the string potentiometers since the arrays terminated at the base of the corbel. To do this, a linear trendline was created using the measured displacements at depths of 1.83 and 2.83 feet below the top of the corbel and extrapolating 0.92 ft upward to the elevation of the load point At these depths it can be assumed that the

array would behave linearly as that portion of the array was enclosed in the concrete pile cap. Using this approach, the pile head displacement obtained from array 106 varied less than 0.05 inch from that measured by the string potentiometer, while the difference in pile head displacement from array 104 and the string potentiometer varied from 0.1 inches at 282 kips to 0.01 inches at 71.5 kips. Thus, array 106 tends to give more accurate results than array 104 when compared to the string potentiometers on cap 1.

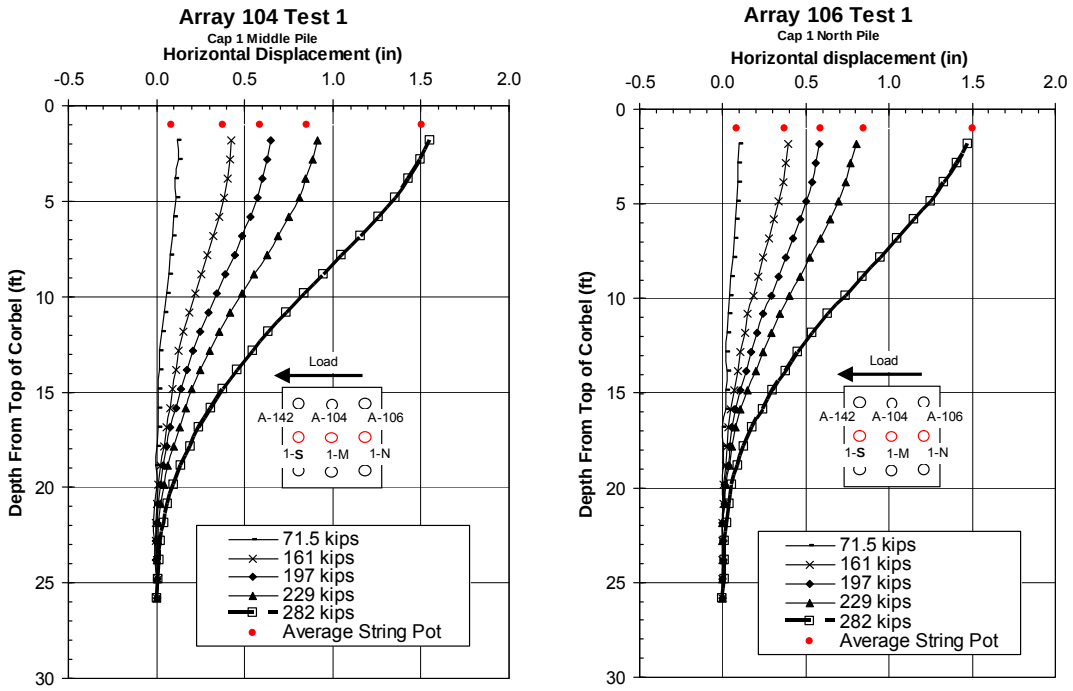

Figure 5-6 – Displacement versus depth curves obtained from shape arrays at several displacement increments for pile cap 1 during test 1. Pile head displacement from string potentiometers are shown for comparison.

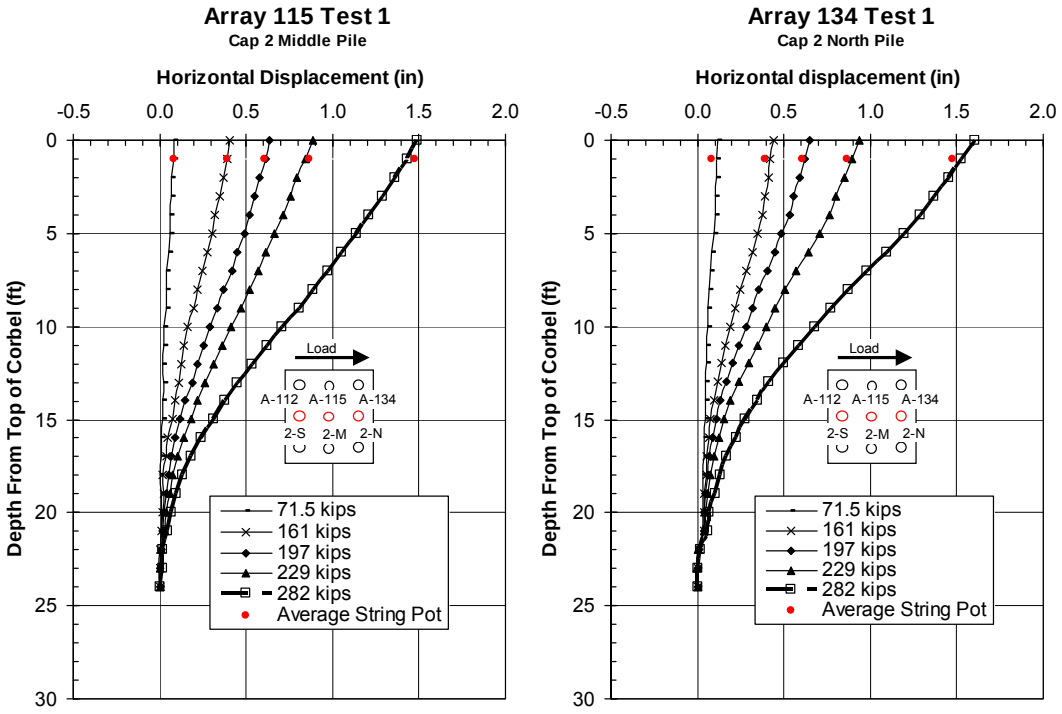

Figure 5-7- Displacement versus depth curves obtained from shape arrays at several displacement increments for pile cap 2 during test 1. Pile head displacement from string potentiometers are shown for comparison.

The displacements from the arrays on cap 2 showed even greater agreement with those from the string potentiometers as seen in Figure 5-7. For example, in the worst case, pile head displacements from Array 115 in the center pile were less than 0.04 inch different than those from the string potentiometers. Array 134 in the north pile also provided close agreement with slightly higher displacements than the string potentiometers and a difference of only 0.04 inch or less.

Figure 5-8 provides comparisons between the displacement versus depth curves obtained from the shape arrays and the two inclinometer pipes in pile cap 1 at the maximum pile head displacement of 1.5 inches. When looking at the inclinometer and array comparison for cap 1, the slopes of the center array (A-104)

and the inclinometers are nearly identical from the top of the corbel until about 17 feet below the top of corbel; however, the displacements at the same depths during that same interval vary from 0.17 to 0.14 inches. On the other hand, displacements from array 106 and the north inclinometer vary by less than 0.05 inch with the greatest discrepancy at a depth of 15 feet below the base of the pile cap.

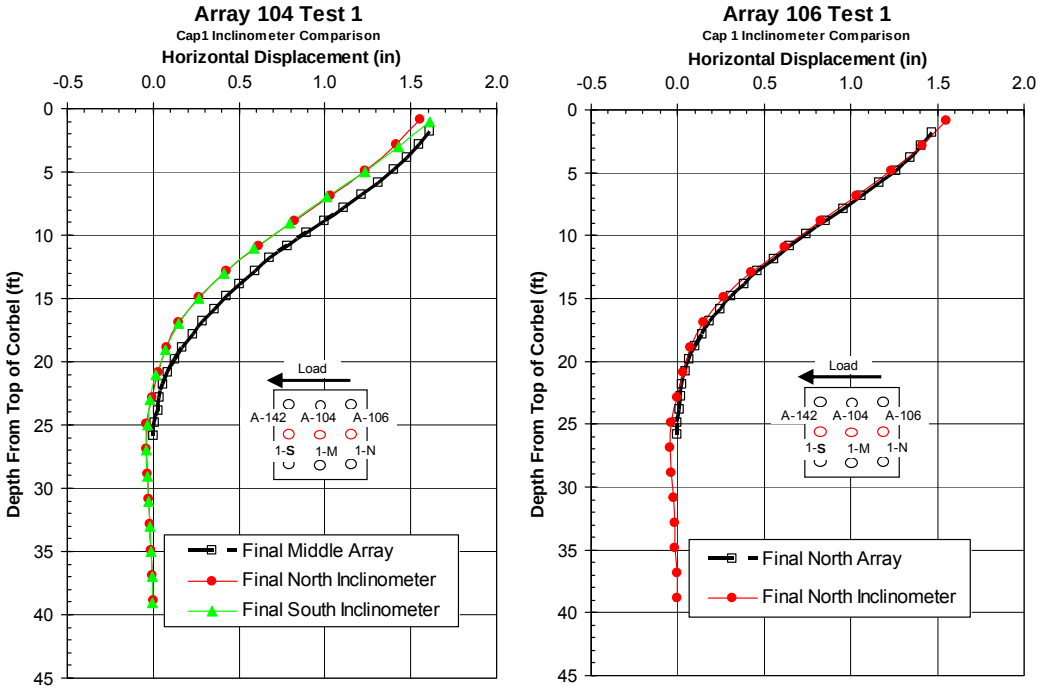

Figure 5-8 – Test 1 inclinometer vs. array comparisons for cap 1 at maximum displacement.

The full reason for the differences in displacements between the center array (A-104) and the inclinometers is to a degree unknown. One reason for the discrepancies could be due to the fact that the arrays were only 24 feet long whereas the inclinometers ran the entire length of the piles. If there was any displacement in the pile deeper than the arrays could measure, the arrays could not account for that since they were set up to reference displacement from the deepest node. As seen in

Figure 5-8, the inclinometers often indicate a negative displacement at depths below the arrays, which could account for some of the discrepancies between the arrays and the inclinometers.

Another reason for discrepancies between the arrays and the inclinometer could be due to the difficulty of getting a tight fit between the shape array and the pipe. If the fit is not tight, the array could move within the PVC pipe housing the array and yield displacements which were different, usually less, than those in the pile. One other consideration for the discrepancies could be the fact that array 104 and the inclinometers are measuring different piles in the cap. This could account for some small discrepancies, but not to the full degree that is shown by array 104 in this test.

Figure 5-9 show the inclinometer and array comparisons for cap 2. Array 115 shows a slope variance with the inclinometers, which could be due to the fact that it is the middle pile being compared to the north and south piles. Array 134 in the north pile shows almost a perfect match with the north inclinometer only varying by 0.04 inches at its greatest discrepancy.

Overall, the two inclinometer profiles for each cap are remarkably similar in each case. The displacement profiles from the shape arrays are also quite consistent with the profiles from the inclinometers. These results provide increased confidence in the accuracy of the profiles. An overview of the results show that the piles start to experience bending at about 23 feet below the top of the corbel. The most significant bending tends to occur between 21 and 16 feet below the top of corbel, which is an indication to the location of the maximum bending moments.

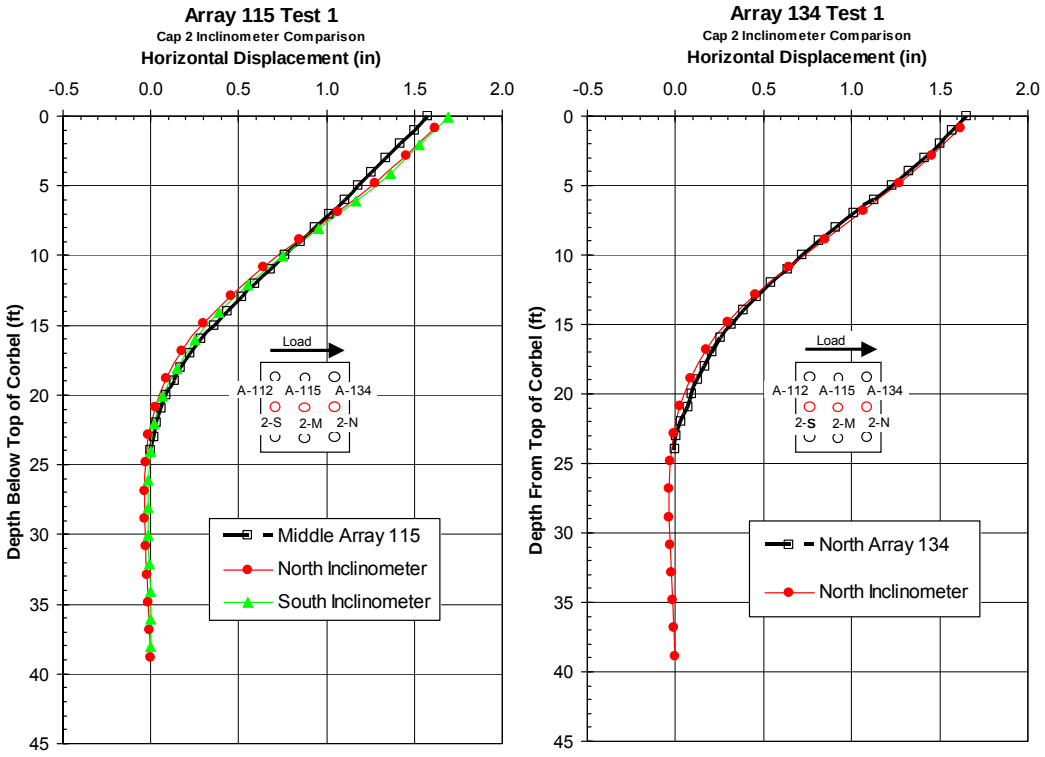

Figure 5-9 - Test 1 inclinometer vs. array comparisons for cap 2 at maximum displacement.

5.1.4 Bending Moment versus Depth

When evaluating the lateral resistance of deep foundations, it is important to know the maximum bending moment and the depth in the pile where it occurs. The bending moment, M, was calculated from the array deflection data using the equation

$$M = EI\frac{\partial^2 y}{\partial x^2} \qquad \textbf{(5-1)}$$

where E is the modulus of elasticity, I is the moment of inertia, and $\partial^2 y / \partial x^2$ is the curvature along the length of the pile. This equation can be approximated numerically using the equation

$$M = \frac{EI(f_{-1} - 2f_0 + f_1)}{h^2} \quad \textbf{(5-2)}$$

where f_{-1} is the horizontal displacement one level above the point of consideration o, f_0 is the displacement at the point of interest, f_1 is the displacement one level below the point of interest, and h is the distance between displacement measurement levels. The moment computed using equation (5-2) is very sensitive to minor variations or errors in the measured displacement versus depth curves. To reduce the influence of minor variances in the measured displacement data on the computed moment, a 5th order polynomial equation was developed based on the measured data to smooth the displacement versus depth curves. The displacements used in equation (5-2) were then based on smoothed values computed with the polynomial equation. While the difference in the displacement values at any depth were generally very small, this procedure produced moment versus depth curves with more realistic shapes.

As indicated previously, the spacing between the array nodes was 12 inches, which corresponds to the interval h. A composite EI of 14.15 x 10^9 lbs-in^2 for the concrete filled pile was used based on the EI of the steel pile and the EI of the concrete used to fill the pile. To calculate the EI of the steel pile, a modulus of elasticity of 29 x 10^6 psi and a moment of inertia of 344 in^4 was used. Similarly for the EI of the concrete, a modulus of elasticity of 4.1 x 10^6 psi based off of the 5100

psi unconfined compressive strength and a moment of inertia of 1018 in^4 was used. Additionally, using equation (5-2) a positive displacement will produce a maximum bending moment directly under the cap which will be negative.

To compliment the bending moments obtained from the arrays, strain gages were also used to derive bending moments. As mentioned before, strain gages were placed at depths of 2, 6, 11, and 13.5 feet below the top of the pile and the top of the piles were driven with approximately 2 feet of stickup. Since piles cannot be driven to precisely to a given elevation, these depths these depths vary to some degree. The bending moments from the stain gages where obtained from the equation

$$M = \frac{EI\varepsilon_{Combined}}{y} \quad \textbf{(5-3)}$$

where EI is the composite modulus of elasticity and moment of inertia for the pile which are the same values used in the array bending moments equation, $\varepsilon_{Combined}$ is the difference in strain obtained from the strain gages located opposite each other at the depth of interest, and y is the diameter of the pile or 12.75 inches.

The notation chosen to describe the sign convention of the moments was that a positive displacement of the cap would result in a negative moment at the bottom of the cap. The datum of these graphs was changed to be measured as the depth below the bottom of the pile cap. This was done because once the piles enter the pile cap the EI changes and becomes difficult to estimate without a large degree of uncertainty. The negative bending moments measured at the interface of the piles and pile cap will have some degree of error due to the changing EI. This error is

minimized to some degree by the fact that the displacements used to derive the bending moments included those that were obtained from within the pile cap. These bending moments were then truncated to the bottom of the pile cap where the EI could be estimated.

Using equations (5-2) and (5-3) with the procedures described above, moment versus depth graphs were obtained. The curves were obtained from the shape arrays and inclinometer readings while the individual points represent moments computed at the locations of the strain gages. The maximum total load associated with each target displacement is also listed in the legend for each figure.

Figure 5-10 shows the moment versus depth curves for the center pile of cap 1. Array 104 and the strain gages measured the maximum positive bending moment between the depths of 9 to 11 feet below the bottom of the pile cap. The maximum positive moment created by the 465 kip load was between 69 and 72 kip-ft. The strain gages for the middle pile correspond with the array by only varying as little at 1 kip-ft and at most only 7 kip-ft for the positive moments. The negative moments measured by the strain gages in Figure 5-10 tend to be higher than the trend derived by the array. However, if the array were to continue on its trend into the pile cap there would still only be a 10 kip-ft difference or less for all the loads except the 465 kip load. At the 465 kip load the moment from the strain gage at the bottom of the cap measured -79 kip-ft, while the trend of the array would be around -59 kip-ft, thus leaving a wide range as to what the actual magnitude of the negative moment might be.

Bending moments for the north pile were also derived and shown in Figure 5-11. The only strain gages on this pile that remained operational for the test were at about the bottom of the pile cap and 4 feet below. The array shows the maximum bending moment occurring between 11 to 13 feet. At the 465 kip load the greatest moment the pile experienced was 73 kip-ft, which is almost identical to the values measured in the middle pile at the same load. The maximum negative moments derived by array 106 tend to be higher than the strain gages if their trend continued to the bottom of the cap. At the 465 kip load the moment from the strain gage at the bottom of the cap measured -69 kip-ft, while the trend of the array would be around -80 kip-ft.

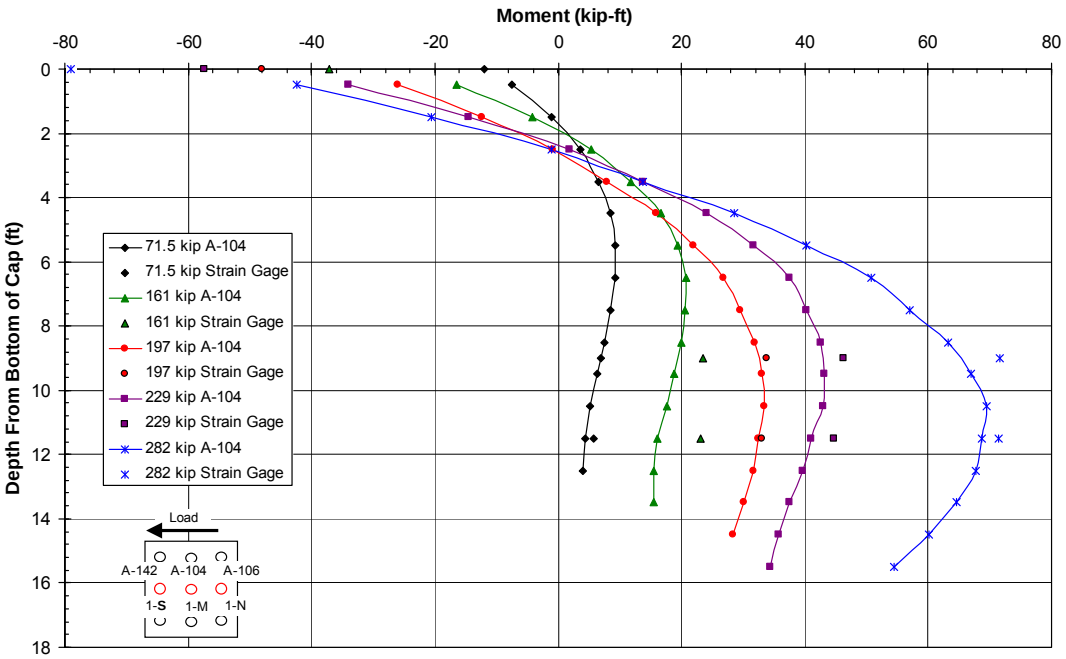

Figure 5-10 – Test 1 cap 1 middle pile bending moment vs. depth as derived from the strain gage and array 104 displacement data.

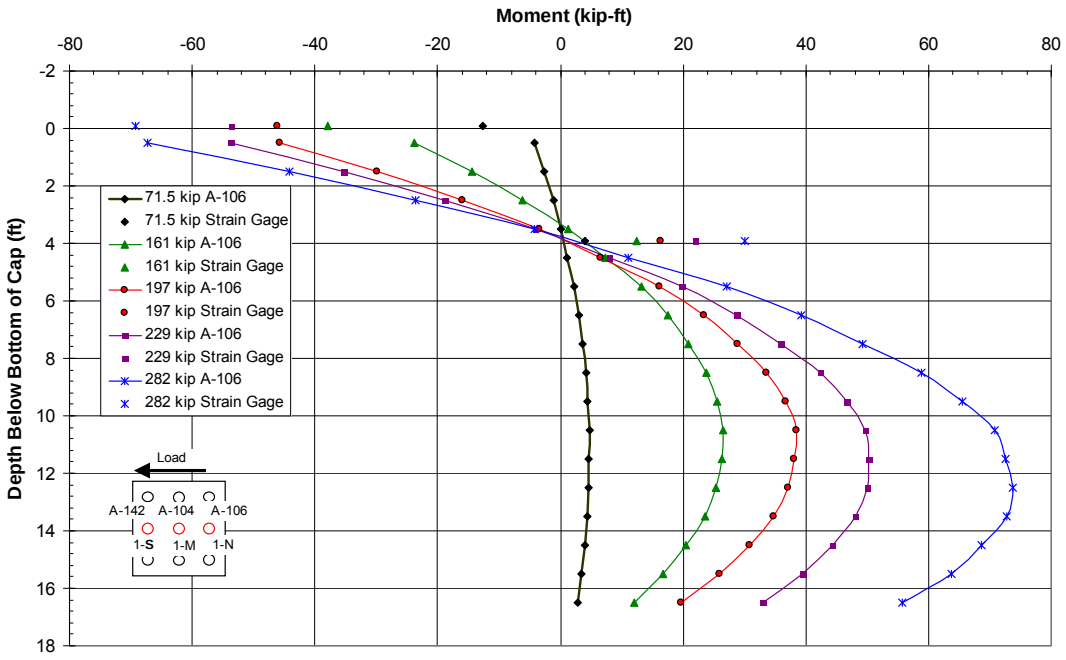

Figure 5-11 – Test 1 cap 1 north pile bending moment vs. depth as derived from the strain gage and array 106 displacement data.

There is a notable discrepancy with the data from the north pile is the bending moments at 4 feet below the cap. The array data tends to converge to zero moment at that depth, but the strain gages still show a significant amount of positive moment. In comparing the bending moments of the middle and north piles of cap 1, both have similar maximum positive moments, but the north piles' moments seem to be about 1.5 feet deeper. The maximum negative moments for the strain gages at the bottom of the cap varied up to 10 kip-ft at the maximum load. The arrays vary from -59 kip-ft from the middle pile to -80 kip-ft from the north pile at maximum load of 282 kips. The discrepancies between the arrays are believed to be due to the different displacements recorded as well as numerical errors resulting from the polynomial fit and subsequent differentiation process, but due to similar slopes, the bending moments still demonstrate similar trends.

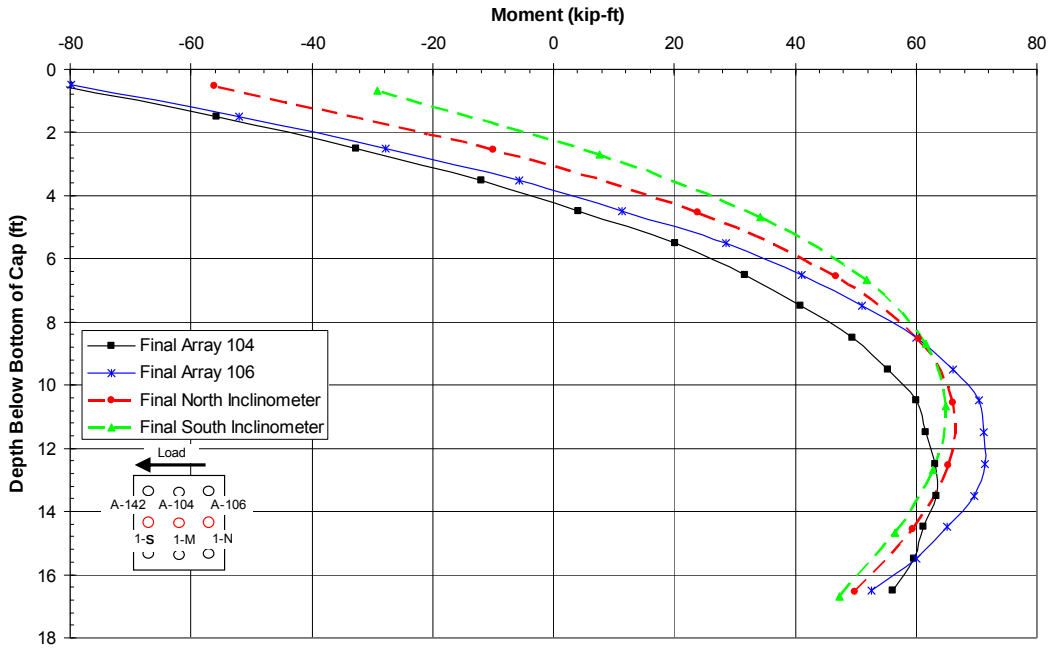

Figure 5-12 – Test 1 cap 1 bending moments vs. depth of the arrays and inclinometers at maximum displacement.

With the arrays being a fairly new technology, it was interesting to see how the moments derived from them compare to the moments derived from the inclinometer data using the same numerical method. The displacements from Figure 5-8 were used to produce Figure 5-12. When looking at the maximum positive moment the inclinometers show a great congruency with only 2 kip-ft difference whereas the arrays differ by about 10 kip-ft. The maximum negative moments are the opposite. The arrays only vary by 2 kip-ft, while the inclinometers vary by 16 kip-ft. The instruments together only varied by 10 kip-ft at 16 feet below the cap, but increasingly deviate further apart as the depth decreases and approaches the cap. This provides some evidence that the method used to derive the bending moments is more accurate at greater depths.

Just as bending moments versus depth graphs were obtained for cap 1, the same analysis was done for cap 2. As mentioned previously, there were no data for the south pile. The middle pile of cap 2 had no strain gages so there is no comparison in Figure 5-13. Maximum positive bending moments in the middle pile appear to occur between 13 and 14 feet below the bottom of the cap, with the greatest moment being 71 kip-ft. The maximum negative moments directly under the cap range from -1 to -33 kip-ft.

The location of maximum positive moments for the north pile of cap 2 in Figure 5-14 occur a little higher than the middle pile ranging between 10.5 and 11.5 feet below the bottom of the cap. The greatest moment in the north pile at the 465 kip load was 69 kip-ft which is comparable to the middle pile. The maximum negative moments for the north pile are a little greater than the middle pile ranging from -5 to -40 kip-ft, nevertheless, they are still considerably lower then what was measured on cap 1. The strain gages in Figure 5-14 tend to be lower than the shape array by about 15 kip-ft, but still denote the general trend derived from the array's displacements.

The displacements from Figure 5-9 were used to produce Figure 5-15, which shows a great comparison of the north array and the inclinometers on cap 2. However, the middle array on cap 2 shows a different trend. When looking at the maximum positive moment the inclinometers and the north array are in good agreement with about a 4 kip-ft difference where as the middle array shows about the same magnitude of bending moment, just differs in the depth of the moment by almost 3 feet. This gives evidence that the discrepancies in measured displacements,

although small, have a great impact on the derived bending moments using the numerical method.

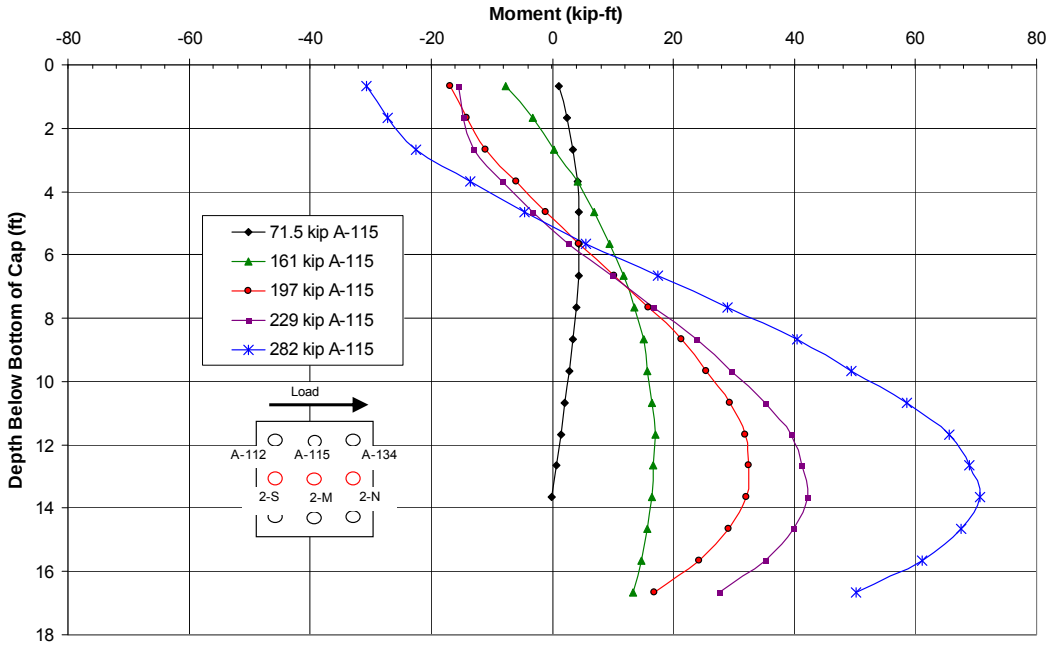

Figure 5-13 - Test 1 cap 2 middle pile bending moment vs. depth as derived from array 115 displacement data.

The maximum negative moments in Figure 5-15 continue to show a degree of similarity with the north array and the inclinometer. Their results span a range of about 20 kip-ft, but are still 10 to 12 kip-ft lower than what was measured on cap 1. Not much can be discerned from the trend of the middle array's negative bending moments as it had to be truncated due to inconsistencies of the numerical method at depths just below the cap.

In the final review of test 1, the behavior of both pile caps in the weak virgin clay was consistent. Both caps displaced close to 1.5 inches at a load of 282 kips. The depth versus displacement comparisons were consistent with the arrays closely

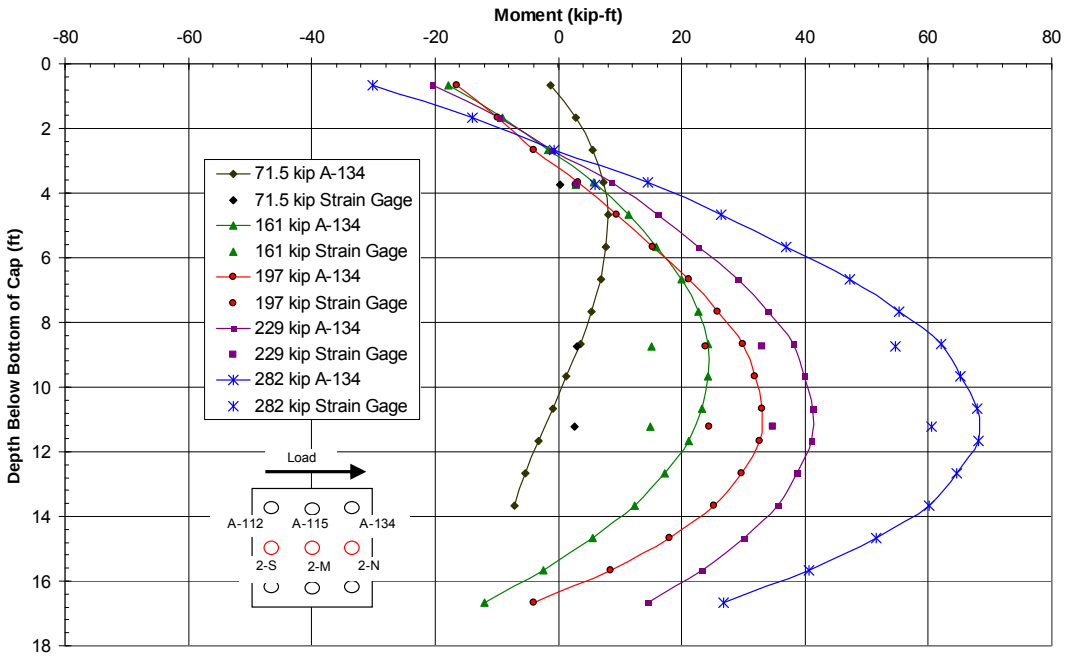

Figure 5-14 - Test 1 cap 2 north pile bending moment vs. depth as derived from strain gage and array 134 displacement data.

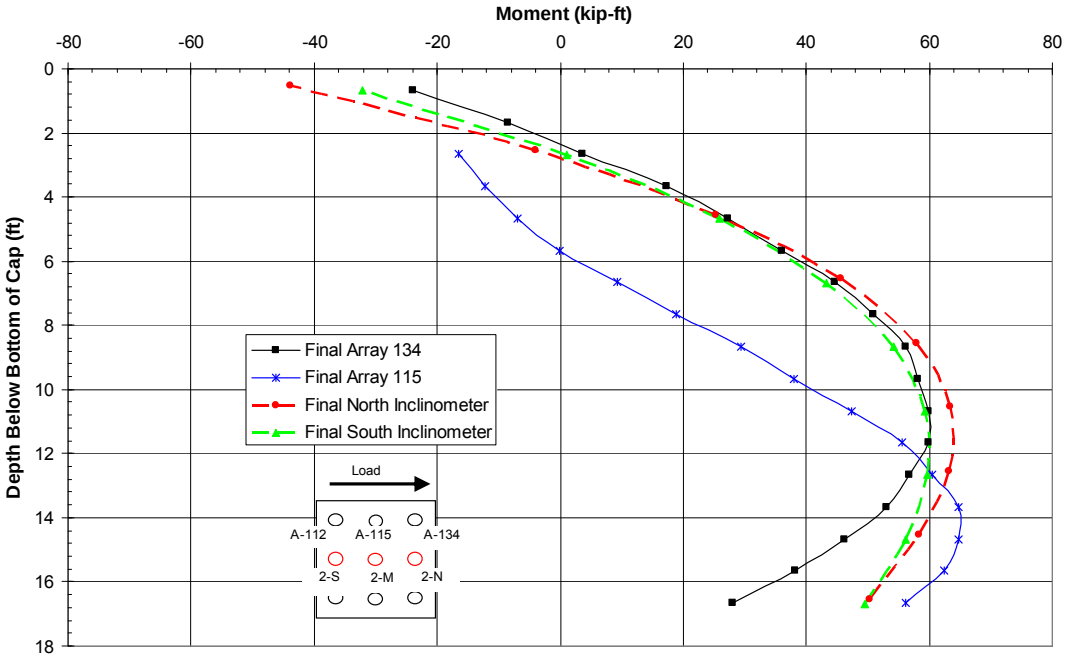

Figure 5-15 - Test 1 cap 2 bending moments vs. depth of the arrays and inclinometers at maximum displacement.

matching the string potentiometers and inclinometers with the exception of the middle array of cap 1. The bending moment results also demonstrate fairly consistent behavior with the exception of the middle array in cap 2. Because the measured behavior on both caps was relatively similar, the following statements can be made regarding the bending moments. The negative bending moment is always greatest at the base of the cap, while the depth to the maximum moment increases from 9 ft to 12 ft below the cap as the pile head displacement increases from 0.5 in to 1.5 inches. Both the maximum negative and positive moments increase as the pile cap displacement increases. The front piles, closest to the load source or actuator, experienced a maximum bending moment at the depths of 10.5 to 11.5 feet below the bottom of the cap, the middle piles 9.5 to 12.5 feet, and the back piles 11 to 13 feet. The difference between the array and strain gage measurements of the maximum positive moments was less than 10 kip-ft. Significant differences were observed for the maximum negative moment from the strain gages and arrays,

5.1.5 Moment versus Load Results

Figure 5-16 and Figure 5-17 provide plots of the maximum positive and negative bending moments versus applied pile cap load, respectively for cap 1 during test 1. Similarly, Figure 5-18 and Figure 5-19 provide plots of the maximum positive and negative bending moments versus applied pile cap load, respectively for cap 2 during test 1. Moment data come from both shape array and strain gauge data when available. Initially, the curves are relatively linear; however, the bending moment tends to increase more rapidly with load at the higher load levels as the soil

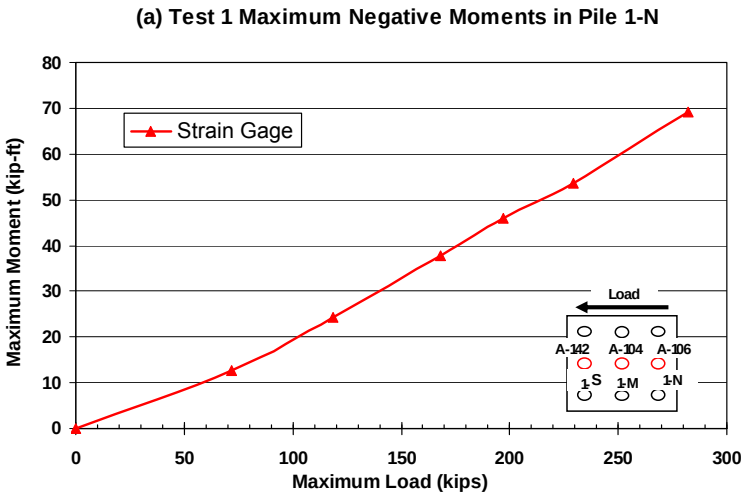

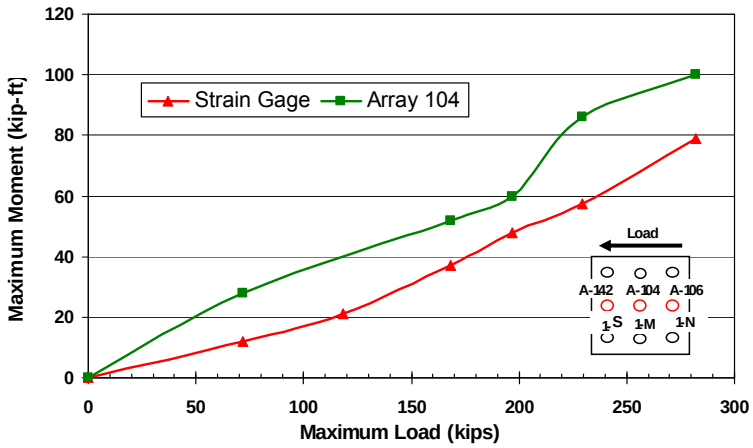

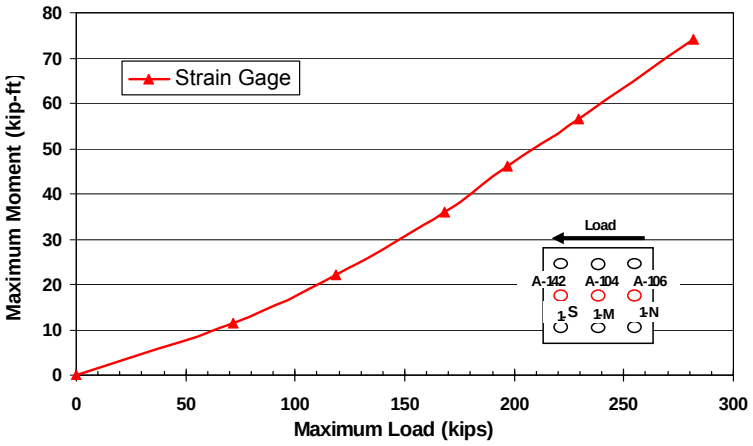

Figure 5-16 - Maximum negative moment (base of cap) versus total pile cap load for piles (a) 1-N, (b) 1-M, and (c) 1-S in cap 1 during test 1.

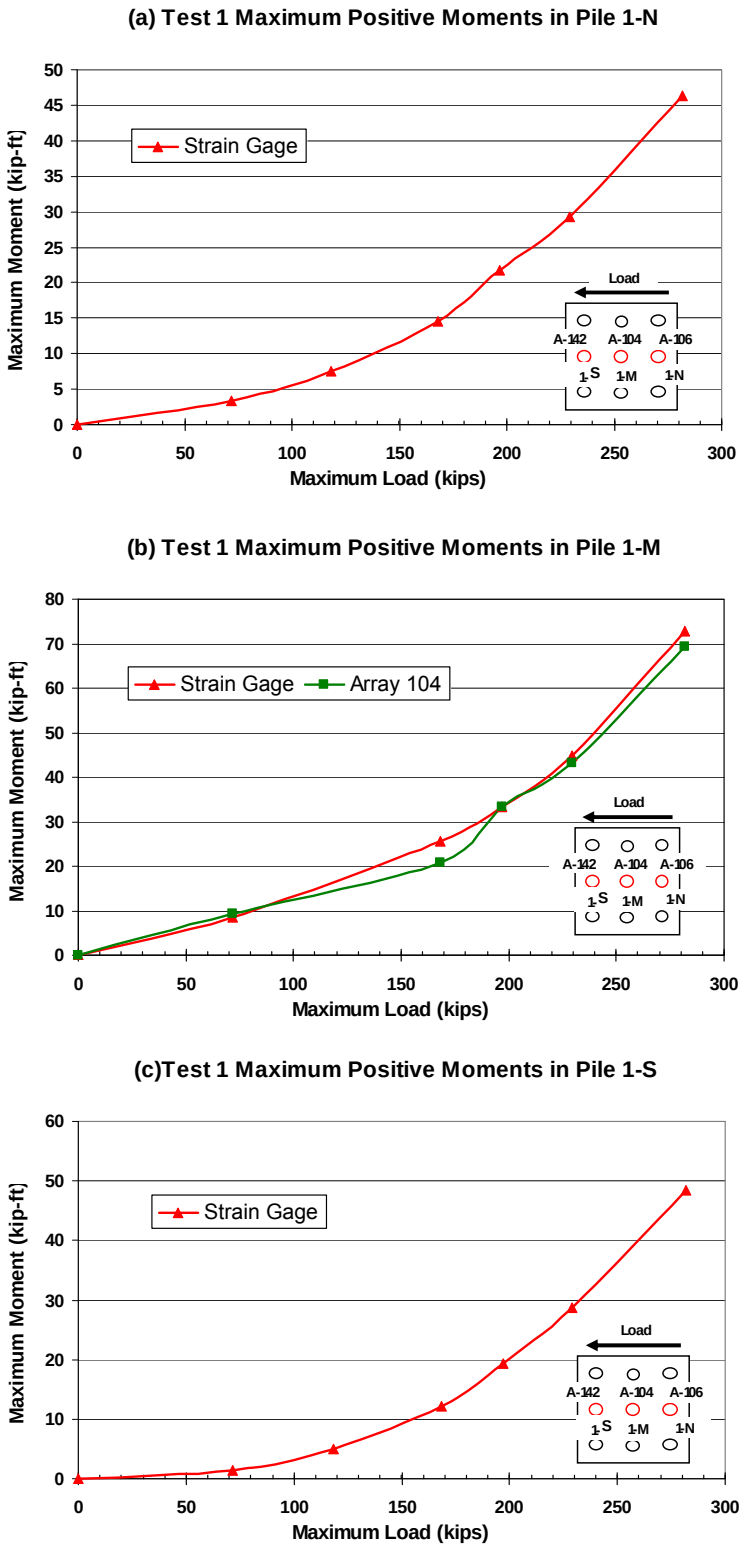

Figure 5-17- Maximum positive moment versus total pile cap load for piles (a) 1-N, (b) 1-M, and (c) 1-S in cap 1 during test 1.

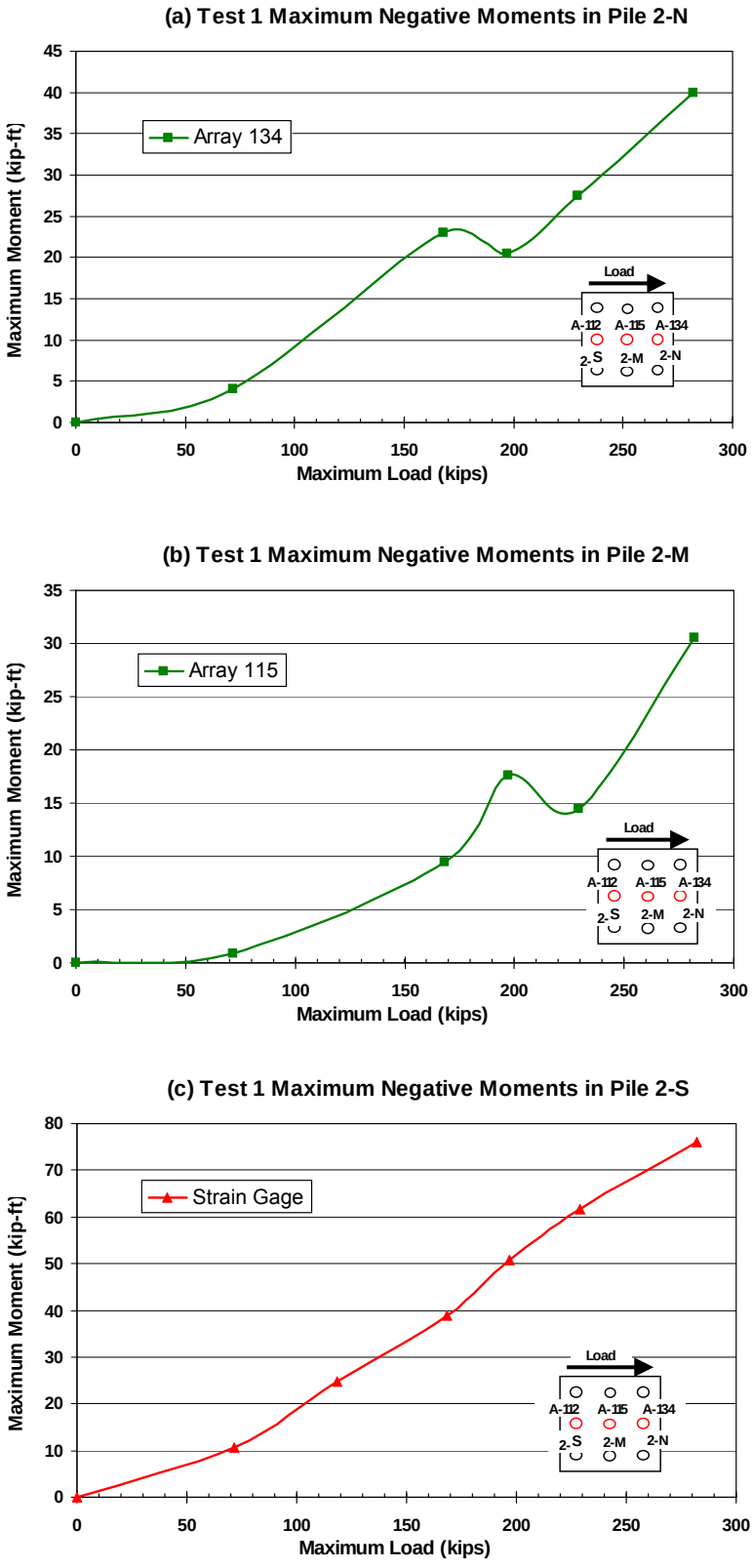

Figure 5-18 - Maximum negative moment versus total pile cap load for piles (a) 2-N, (b) 2-M, and (c) 2-S in cap 2 during test 1.

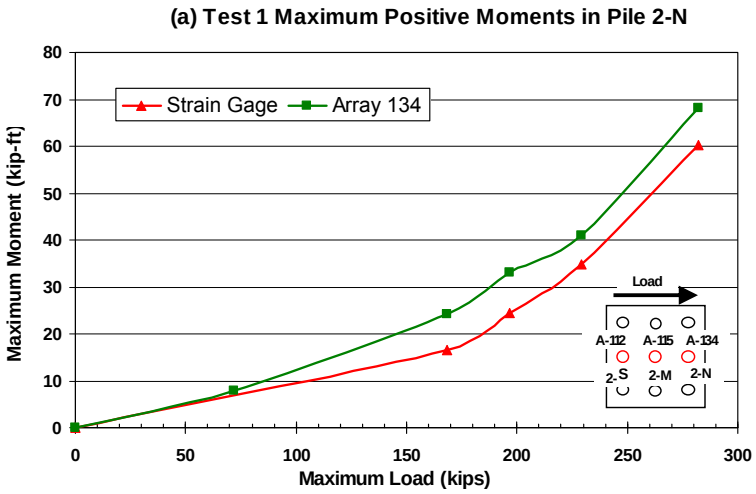

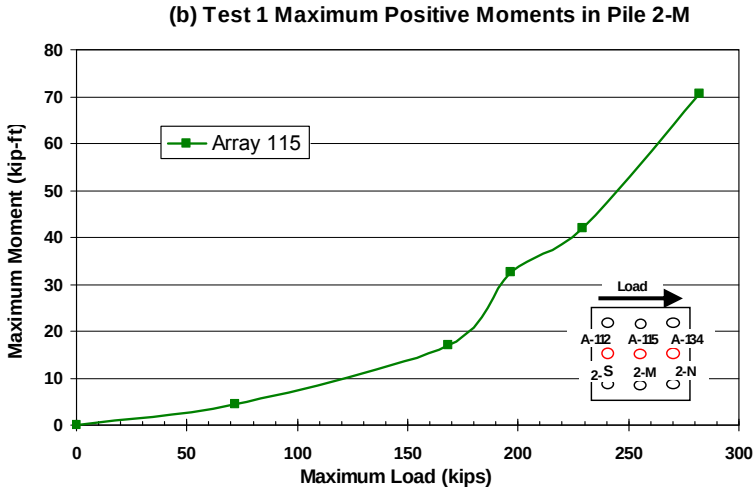

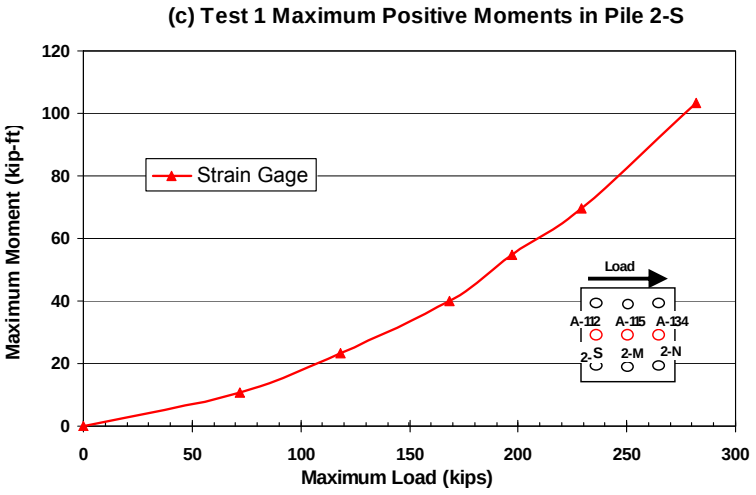

Figure 5-19 - Maximum positive moment versus total pile cap load for piles (a) 2-N, (b) 2-M, and (c) 2-S in cap 2 during test 1.

resistance is overcome. The curves from the strain gauges provide relatively consistent moment versus load curves with little evidence of strong group interaction effects for the displacement levels involved. The agreement between the curves computed by the strain gauges and shape arrays varies.

5.2 Virgin Clay Test without Soil Adjacent to the Pile Cap

After pile caps 1 and 2 were pulled together laterally into the virgin soil, another lateral load test was performed by pushing the two pile caps apart. However, prior to testing, the soil directly behind the pile cap was excavated to the base of the cap to evaluate the decrease in passive resistance. The purpose of this test was to determine how much of the lateral resistance measured in test 1, the virgin soil test, was due to the passive resistance provided by the soil behind the cap. To accomplish this, a one foot wide excavation of the virgin soil along the north face of cap 1 to the depth of the cap was made as shown in Figure 4-15.

The baseline values for the displacements in test 2 were the initial measurements taken prior to test 1. Since test 2 took place after the pile caps had been pulled together in the test 1, there was still some residual displacement once the load was released in the direction of the original displacement. Thus, test 2 started with a negative initial displacement of about 0.3 inches. All instrumentation was in place and identical to that of test 1. The test followed the standard procedure with one exception. Due to the residual gap and initial offset resulting from test 1, the 0.125 inch test increment for test 2 was omitted.

5.2.1 Load-Displacement Results

Figure 5-20 and Figure 5-21 provide the complete pile cap load versus pile head displacement curves for caps 1 and 2, respectively during test 2. Load was obtained from the actuator pressure transducer and displacements from the string potentiometers attached to their corresponding cap. The actuator pushed the caps to target the prescribed increments of 0.25, 0.5, 0.75, 1.0, 1.5 inches, being referenced to cap 1 rather than cap 2, which was stronger. The actual displacements for cap 1 with the residual offset of -0.27 inches were -0.01, 0.26, 0.48, 0.75, and 1.28, inches respectively. The displacements for cap 2 with the residual offset of -0.32 inches were -0.12, 0.06, 0.19, 0.34, and 0.63 inches, respectively, as measured by the corresponding string potentiometers. These displacements are consistent with expectations as cap 1 had no passive soil resistance directly behind it. Because of the reduction in lateral resistance due to the elimination of passive force on the pile cap, cap 1 reached a displacement of 1.28 inches while cap 2 had only displaced 0.63 inches.

During reloading, the slope of the load-displacement curves flattened but exhibited about same shape as the curve for virgin loading. However, at larger displacements there is a change of slope in the re-loading curve indicative of gapping. During reloading, the load at the previous peak displacement typically decreased to between 4% and 10% of the previous peak value. The decrease in lateral resistance was similar for both caps and was also about the same as that observed for test 1. As displacements increase beyond the previous peak displacement, the load-displacement curve appears to rejoin the virgin curve. After

the peak load for a given increment was reached, the actuator pulled the pile caps backward to reach the original actuator position. In most cases, this required some tensile force because of movement of the soft soil into the gap behind the piles created during loading. Because of differences in the lateral resistance in the two caps, there was some residual displacement at the end of each load cycle even though the actuator returned to its original position.

Figure 5-22 provides the maximum load-displacement curves for caps 1 and 2 during test 2. The legend distinguishes each test by the notation T1 for test 1 and T2 for test 2. This comparison definitely shows the softer behavior of cap 1 where the passive force behind cap 1 had been removed. Figure 5-23 provides a comparison between the load-displacement curves for caps 1 and 2 during tests 1 and 2. The load-displacement curves for test 2 have been shifted right 0.15 inch to account for the apparent flow of the soft clay into the gap between the soil and pile cap that occurred when displacing the pile cap in the opposite direction. When this minor adjustment in displacement is made, the curve for cap 2 matches the curves for caps 1 and 2 during test 1 at larger displacements as would be expected. A comparison of load-displacement curves for cap 1 with and without passive soil force acting on the pile cap can then be made. Assuming zero passive force at zero displacement and then obtaining the difference between the load-displacement curves for cap 1 with and without passive force at displacements for 0.25, 0.5, 0.75, 1.0, and 1.5, inches Figure 5-24 was obtained. Thus, based on the curves in Figure 5-23, the passive force versus displacement curve shown in Figure 5-24 has been

developed which indicates that the full passive force of approximately 50 kips was essentially developed by a displacement of about 0.75 inches.

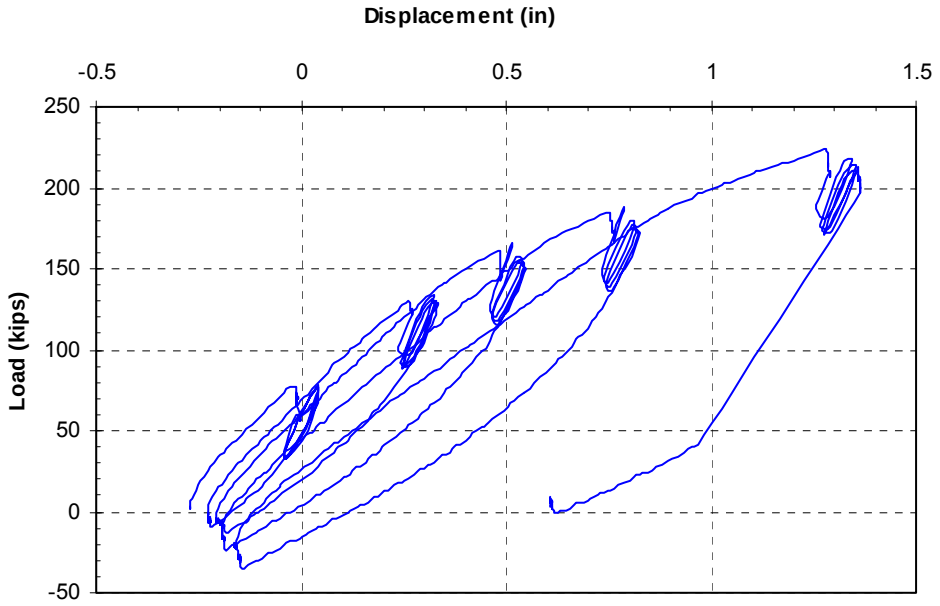

Figure 5-20 - Complete pile cap load versus pile head displacement curve for cap 1 during test 2.

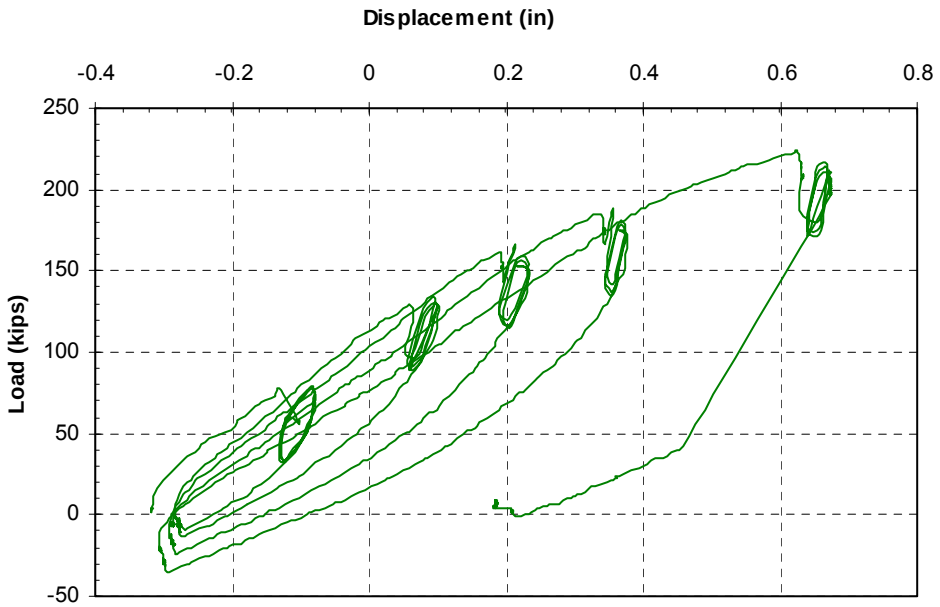

Figure 5-21 - Complete pile cap load versus pile head displacement curve for cap 2 during test 2.

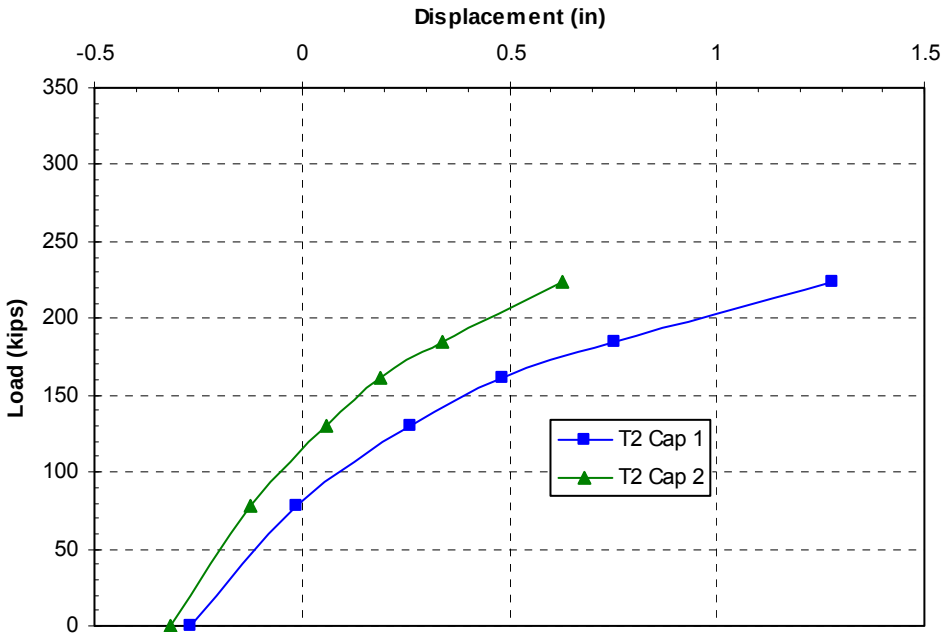

Figure 5-22 - Peak pile cap load versus pile head displacement curves for caps 1 and 2 during test 2.

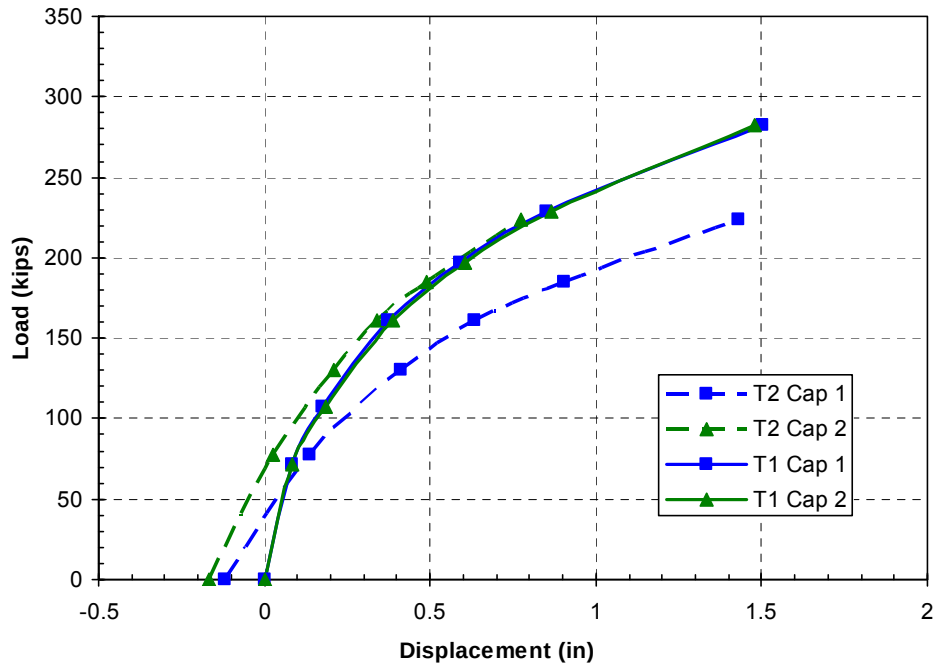

Figure 5-23 - Comparison of peak pile cap load versus pile head displacement curves for caps 1 and 2 during tests 1 and 2.

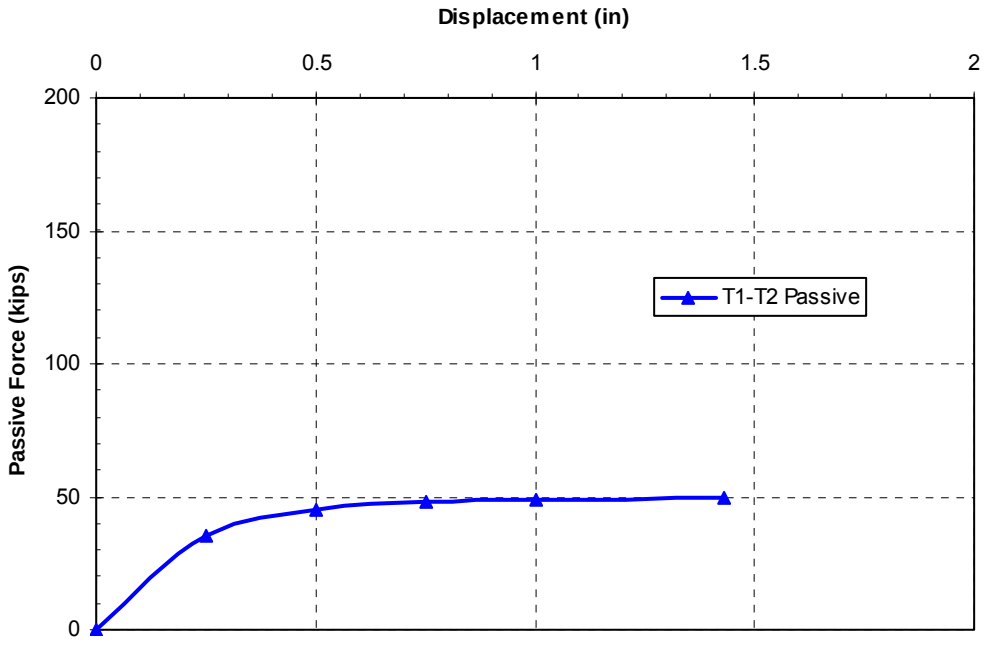

Figure 5-24 –Development of passive force for virgin clay around cap 1.

5.2.2 Rotation versus Load Results

Pile head load versus rotation curves obtained from string potentiometer and shape array measurements for the pile caps 1 and 2 during test 2 are provided in Figure 5-25 and Figure 5-26, respectively. Because of the initial negative offset, the pile caps had a slight negative rotation at the start of the test. As load increased, the rotation shifted to a positive value. Rotation of pile cap 1, where passive force was absent, exceeds that of pile cap 2 at higher load levels as would be expected. The total rotation measured on pile cap 1 was about 0.3 degrees. This is significantly greater than the rotations observed on both caps during test 1, which measured about 0.17 degrees at the same load. This also was expected as pile cap 1 of test 2 had the passive force directly behind the cap removed.

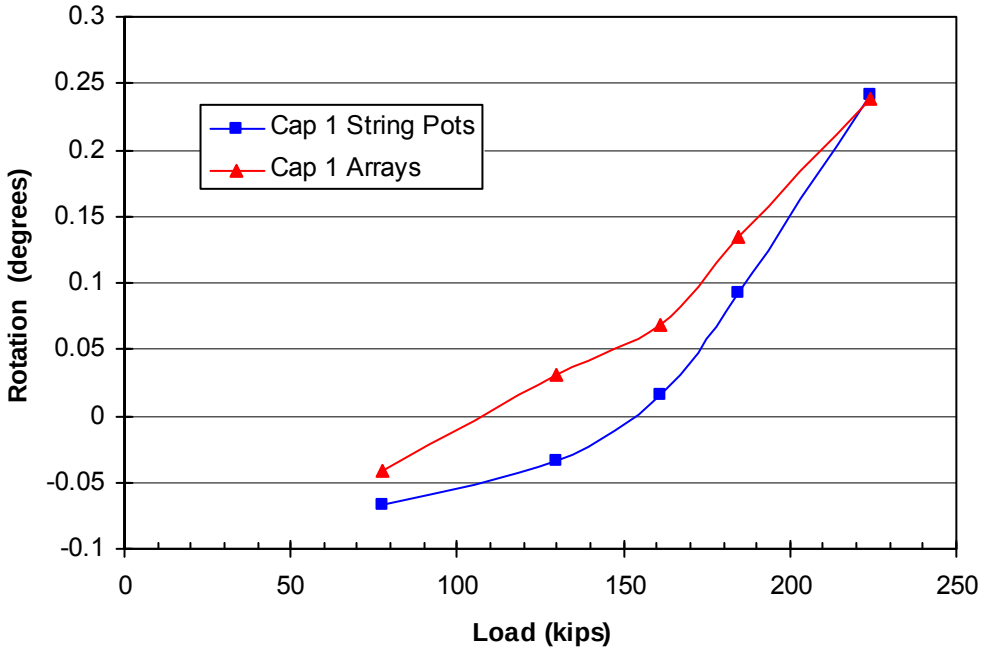

Figure 5-25 - Peak pile cap load versus pile head rotation for cap 1 during test 2 obtained from string potentiometer and shape array measurements.

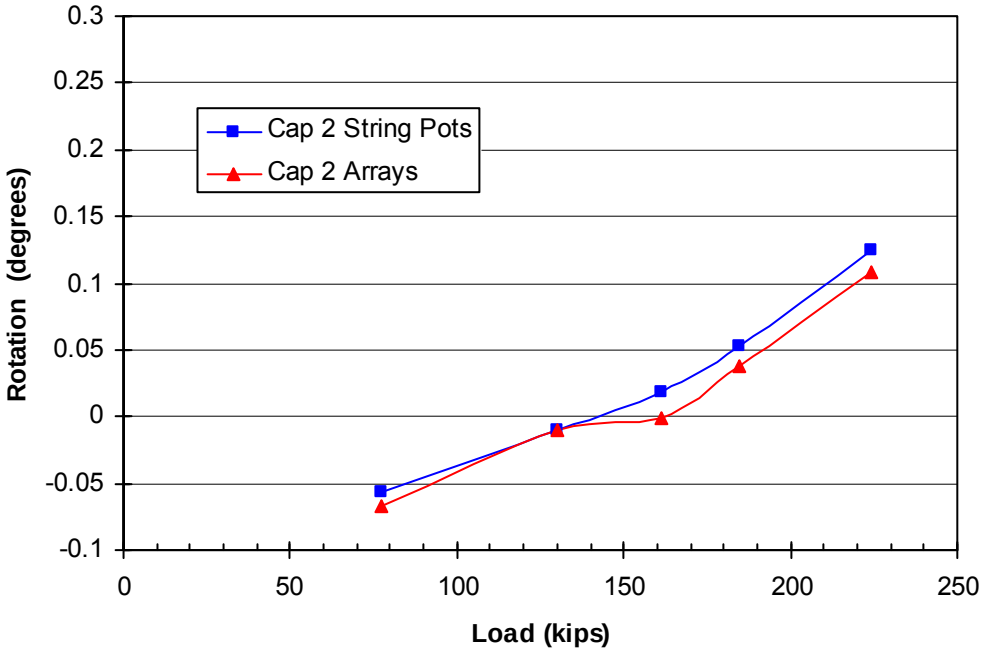

Figure 5-26 - Peak pile cap load versus pile head rotation for cap 2 during test 2 obtained from string potentiometer and shape array measurements.

5.2.3 Depth versus Displacement Results

Since cap 1 had the passive force on the pile cap removed, the remaining sections in this chapter will focus on the results from cap 1. It is sufficient to note that the load-displacement curves for cap 2 were plotting consistently with that seen in test 1 as shown in Figure 5-23 and therefore, had it displaced to the same levels, similar results would be apparent.

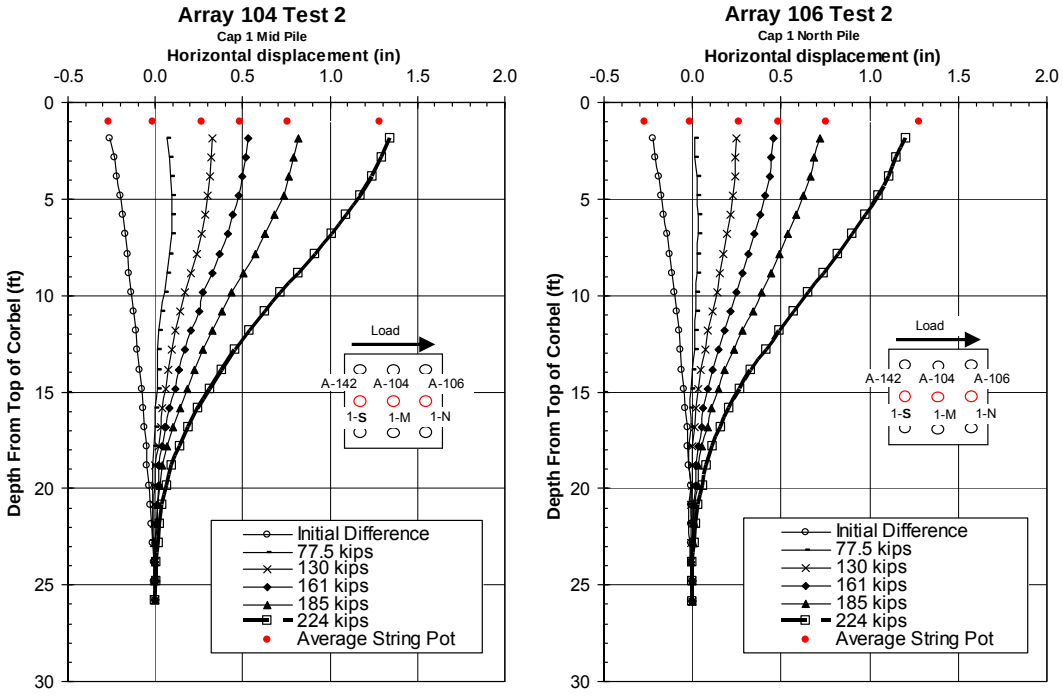

Figure 5-27 - Displacement versus depth curves obtained from shape arrays at several deflection increments for pile cap 1 during test 2. Pile head displacement from string potentiometers are shown for comparison.

Test 2 depth versus displacement profiles for cap 1 are shown in Figure 5-27. As mentioned before, there is no array data from the south pile due to the defective array 142. Displacements at the elevation of the applied load at 1 foot below the top of the corbel are also shown to provide an indication of the relative accuracy of the

measurements. Because of the initial offset, the displacement versus depth curves start with a negative displacement and slope. As load increases, the displacement increases and the slope becomes positive. The agreement between the shape arrays and the string potentiometers is reasonable for cap 1. Using the trendline extrapolation method described in section 5.1.3, the pile cap displacement from the center pile array (A-104) varied 0.1 inch from the measurements made with the string potentiometers in the worst case, while the pile cap displacements from the north array (A-106) varied by 0.03 inches or less from string potentiometer measurements. Typically, the pile cap displacements from the shape arrays were within about 1% to 3% of those obtained from the string potentiometer. This is essentially the same level of agreement noted in test 1 for cap 1.

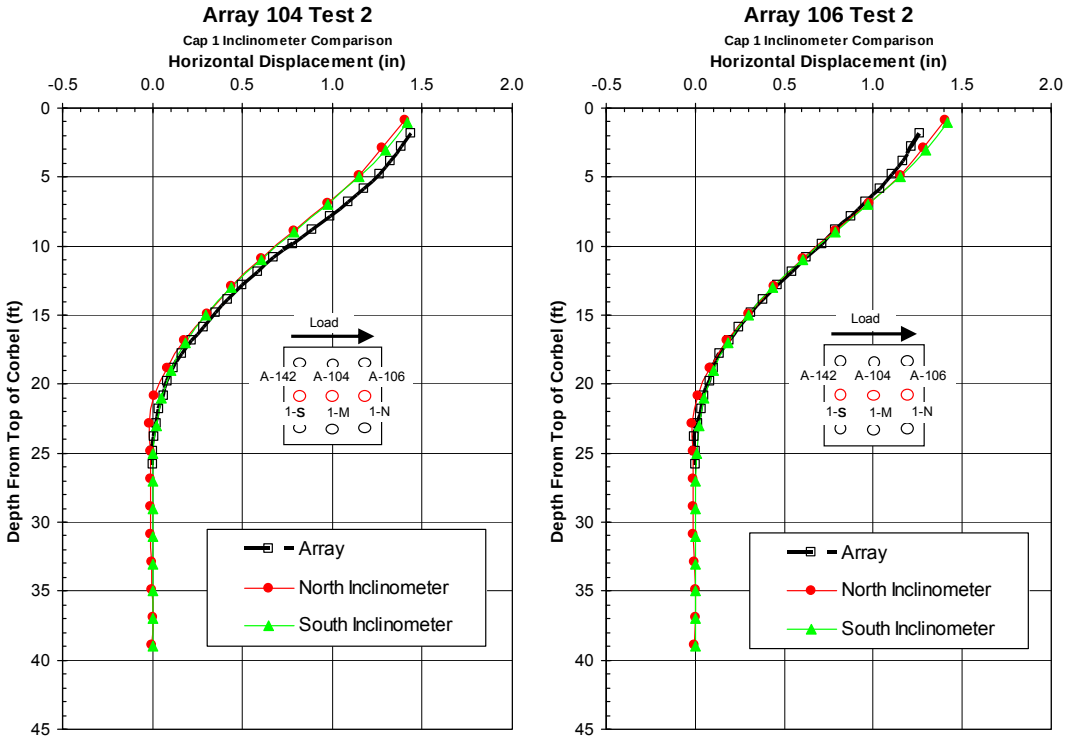

Figure 5-28 - Displacement versus depth profiles measured by shape arrays and inclinometers for the center and north piles in cap 1 during test 2 at maximum displacement.

Figure 5-28 shows the depth versus displacement profiles of the arrays and inclinometer readings on cap 1 at the maximum displacement during test 2. There is good agreement in the north pile even though there is a slight discrepancy starting at about 6 feet below the top of the corbel. The instrumentation in the center pile experiences a little more variance with the greatest discrepancy being about 0.1 inches or less. This discrepancy is also noted in the string potentiometer comparison in Figure 5-27. In spite of the minor discrepancies, the general trend and slope of the depth versus displacement profiles are consistent and provide an accurate representation of the deflections the piles are experiencing.

5.2.4 Bending Moment versus Depth Results

Bending moments were estimated from the depth versus displacement profiles from the center and north piles on cap 1 using the method described in Section 5.1.4. Figure 5-29 and Figure 5-30 provide bending moment versus depth curves at the five target displacement levels during test 2. The curves were obtained from the shape arrays while the individual points represent moments computed from the strain gages. The datum for the depth on the figures has been moved to the bottom of the cap. The maximum load at each target displacement is also listed in the legend for each figure.

The maximum positive bending moments from the center pile array in Figure 5-29 tend to occur from about 11.5 feet to 13.5 feet below the bottom of the cap. The positive moments measured from the strain gages are within 7 kip-ft (10% to 15%) or less of the moments from the array, with the only exception of the 185 kip

load or 1 inch test increment. The positive moments from the north pile in Figure 5-30 seem to be a little more consistent as the depths of the maximum moments occur at about 13.5 feet below the bottom of the cap. The moments from the strain gages are within 7 kip-ft (10% to 15%) or less of array moments at all test increments. Also, with the exception of the 77.5 kip load or 0.25 inch test increment, the positive moments from the arrays are within 2 kip-ft or less when comparing the two piles at the corresponding load.

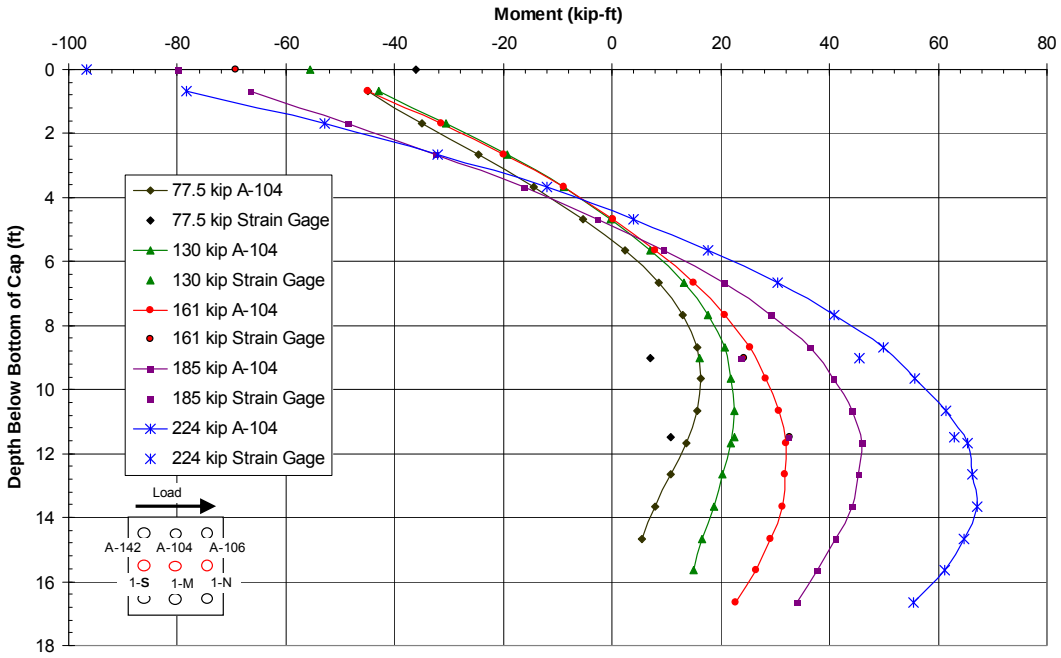

Figure 5-29 - Test 2 bending moment versus depth profiles from array data and strain gages on the center pile of cap 1.

The trends for the negative moments from the array in the center pile are in close agreement with the moments from the strain gages. If the array trends were to continue to the base of the cap only the 0.25 inch (77.5 kips) and 0.75 inch (161 kips) test increments would vary by more than 5 kip-ft. On the other hand, the array

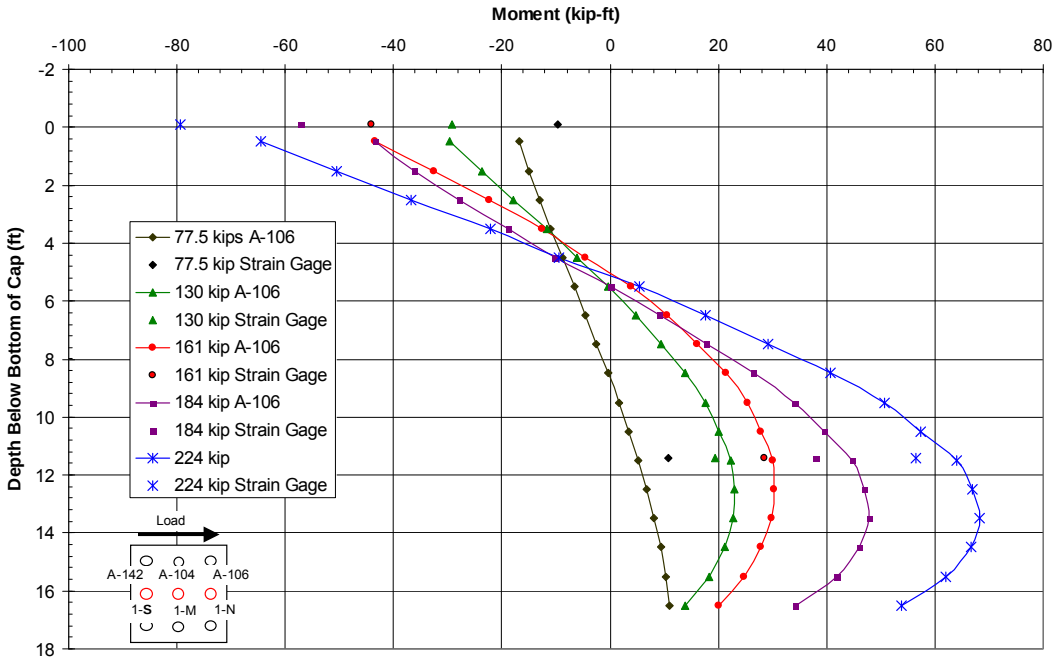

Figure 5-30 – Test 2 bending moment versus depth profiles from array data and strain gages on the north pile of cap 1.

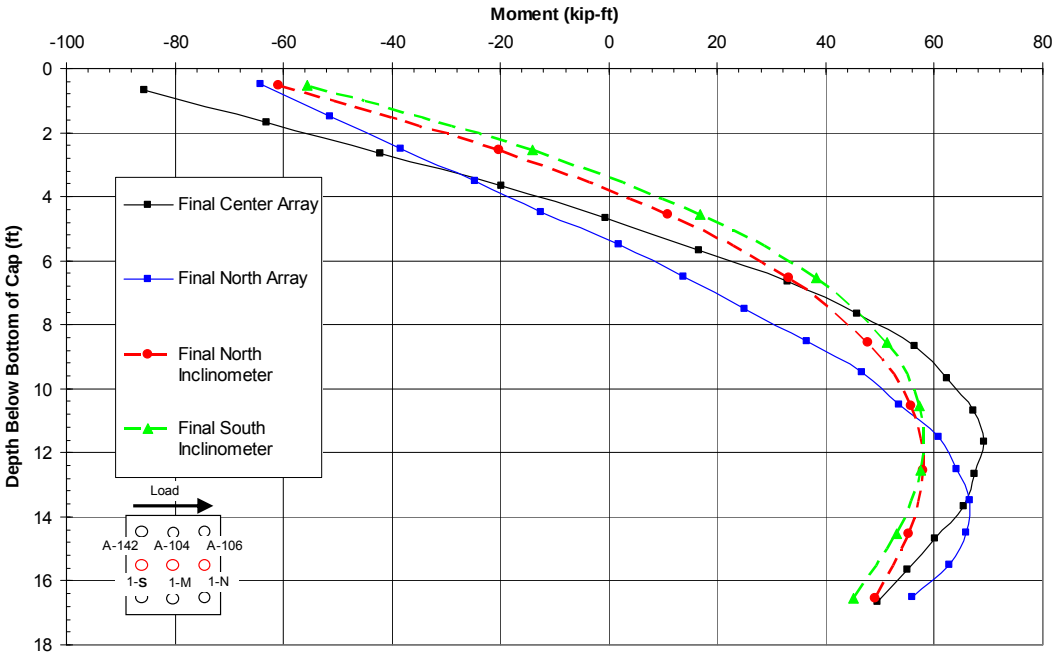

Figure 5-31 – Test 2 moment versus depth profiles from the arrays and inclinometers taken at the maximum displacement.

trends for the negative moments from the north pile are more inconsistent when compared to the strain gages. Most test increments are off by 8 kip-ft (12% to 17%) if the array trends were to continue to the bottom of the cap. The 1.5 inch or 224 kip load is the only one that appears to be in agreement. In addition the magnitude of the maximum negative moment at each test increment is about 13 kip-ft higher on the center pile than on north pile.

A comparison of the moments derived from the arrays and inclinometers at the maximum displacement is shown in Figure 5-31. There is good agreement with the inclinometers; however the trends from the arrays vary somewhat. The inclinometers and the center array place the maximum positive bending moment at about 11.5 feet, but the north array places it lower at 12.5 feet. When looking at the magnitude of the maximum positive moment, the inclinometers measure about 58 kip-ft, the north array 66.5 kip-ft, and the center array 69 kip-ft. The north array and the inclinometers are in fair agreement at the maximum negative moment measuring around -60 kip-ft, while the center array measures a higher value at about -95 kip-ft. The discrepancy in the negative moments for the center array is due to the fact that it recorded greater displacements at depths closer to the cap than the inclinometers as shown in Figure 5-28.

When comparing these results to that of test 1, the location of the maximum positive moment on the center pile was about one foot lower without the passive force behind the cap, but the magnitude stayed relatively similar at the same displacement increment. On the north pile the location of the maximum positive moment stayed within one foot or closer, but decreased about 5 kip-ft on average

without the passive force. The maximum negative moments on the center pile remained at the bottom of the cap, but increased 10 to 15 kip-ft on average from test 1. The maximum negative moments on the north pile also remained at the bottom of the cap, but decreased about 10 kip-ft on average without the passive force. The inconsistency in the magnitudes of the negative moments recorded by the strain gages and arrays makes it difficult to determine a difference in the trend between tests 1 and 2. However, it appears that the magnitudes of the negative moments for test 2 stayed within a range of plus or minus 10 kip-ft of the moments for test 1 compared at the same displacement increment, which would imply there was minimal change between test 1 and 2.

In summary, without the passive force behind the cap, the magnitudes of the positive bending moments decreased slightly, while the negative moments remained about the same being consistently in a range of plus or minus 10 kip-ft. The depth to the maximum positive moment typically increased about one foot, while the location of the maximum negative moments remained at the bottom of the cap. It is difficult to conclude at this point if the one foot increase in depth to the location of the maximum positive moment was due to the inaccuracies in the numerical method used to compute moment or indeed a reality.

5.2.5 Moment versus Load Results

Figure 5-32 and Figure 5-33 provide plots of the maximum positive and negative bending moments versus applied pile cap load respectively for cap 1 during test 2. Similarly, Figure 5-34 and Figure 5-35 provide plots of the maximum

positive and negative bending moments versus applied pile cap load, respectively for cap 2 during test 2. Moment data come from both shape array and strain gauge data when available. Initially, the curves are relatively linear; however, the bending moment tends to increase more rapidly with load at the higher load levels as the soil resistance is overcome. The curves from the strain gauges provide relatively consistent moment versus load curves with little evidence of strong group interaction effects for the displacement levels involved. The agreement between the curves computed by the strain gauges and shape arrays is generally reasonable. The results appear to be somewhat more consistent for the positive moments than for the negative moments.

Figure 5-36 illustrates the combined trends of the maximum positive moment versus load curves for test 1 and 2 on pile cap 1. Plots that experienced a wide range of values were eliminated to allow for comparisons of the general trend. The curves from test 1 are denoted with a square mark (blue) while those of test 2 are denoted with a triangle mark (red). At a given load, the curves from test 2 show a greater moment which is expected since test 2 had no passive resistance behind the pile cap and thus experienced greater displacement or bending at the same load. Figure 5-37 shows similar plots for the maximum negative moment versus load comparisons for test 1 and 2 on pile cap 1. Likewise, using the same marking convention, the curves for test 2 also plot greater bending moments at the same loading than test 1 curves. This is also what would be expected as test 2 experienced greater displacements at the same load.

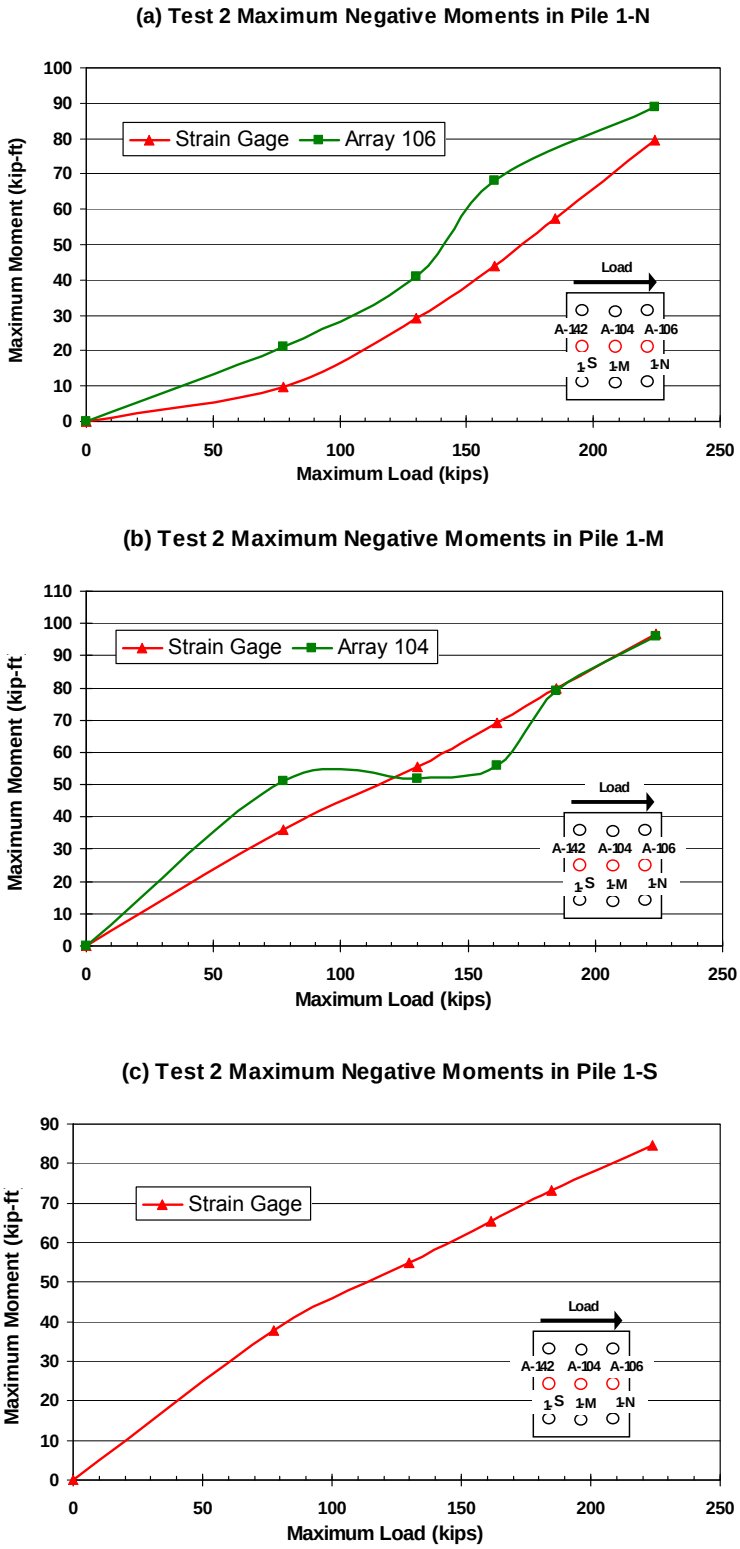

Figure 5-32 - Maximum negative moment (base of cap) versus total pile cap load for piles (a) 1-N, (b) 1-M, and (c) 1-S in cap 1 during test 2.

(a) Test 2 Maximum Positive Moments in Pile 1-N

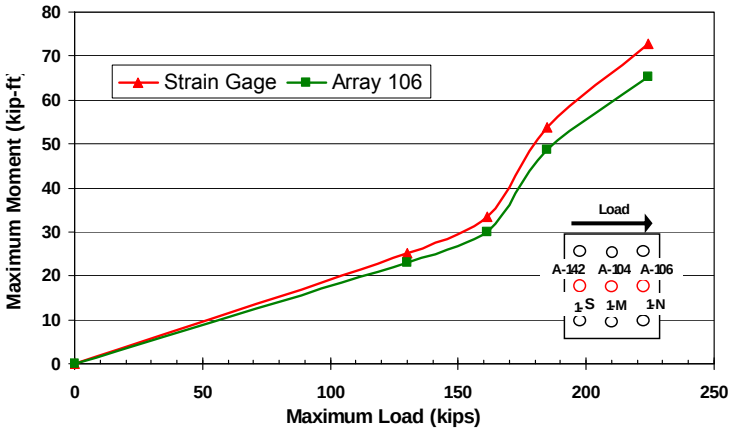

(b) Test 2 Maximum Positive Moments in Pile 1-M

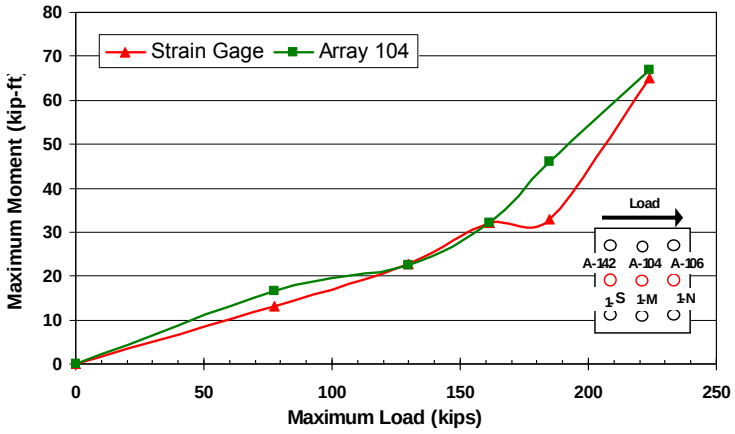

(c) Test 2 Maximum Positive Moments in Pile 1-S

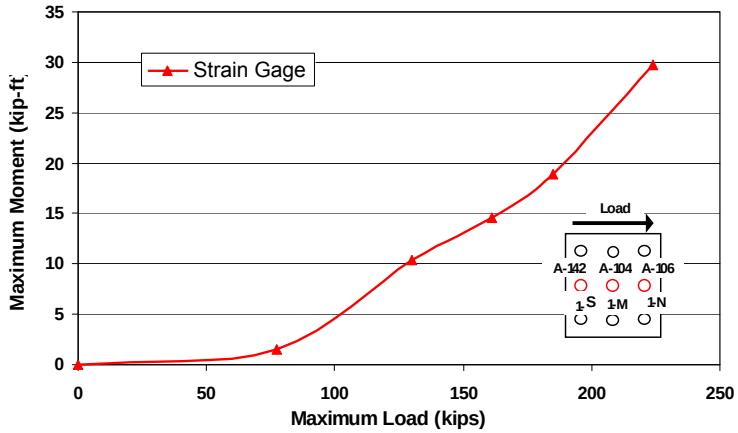

Figure 5-33 - Maximum positive moment versus total pile cap load for piles (a) 1-N, (b) 1-M, and (c) 1-S in cap 1 during test 2.

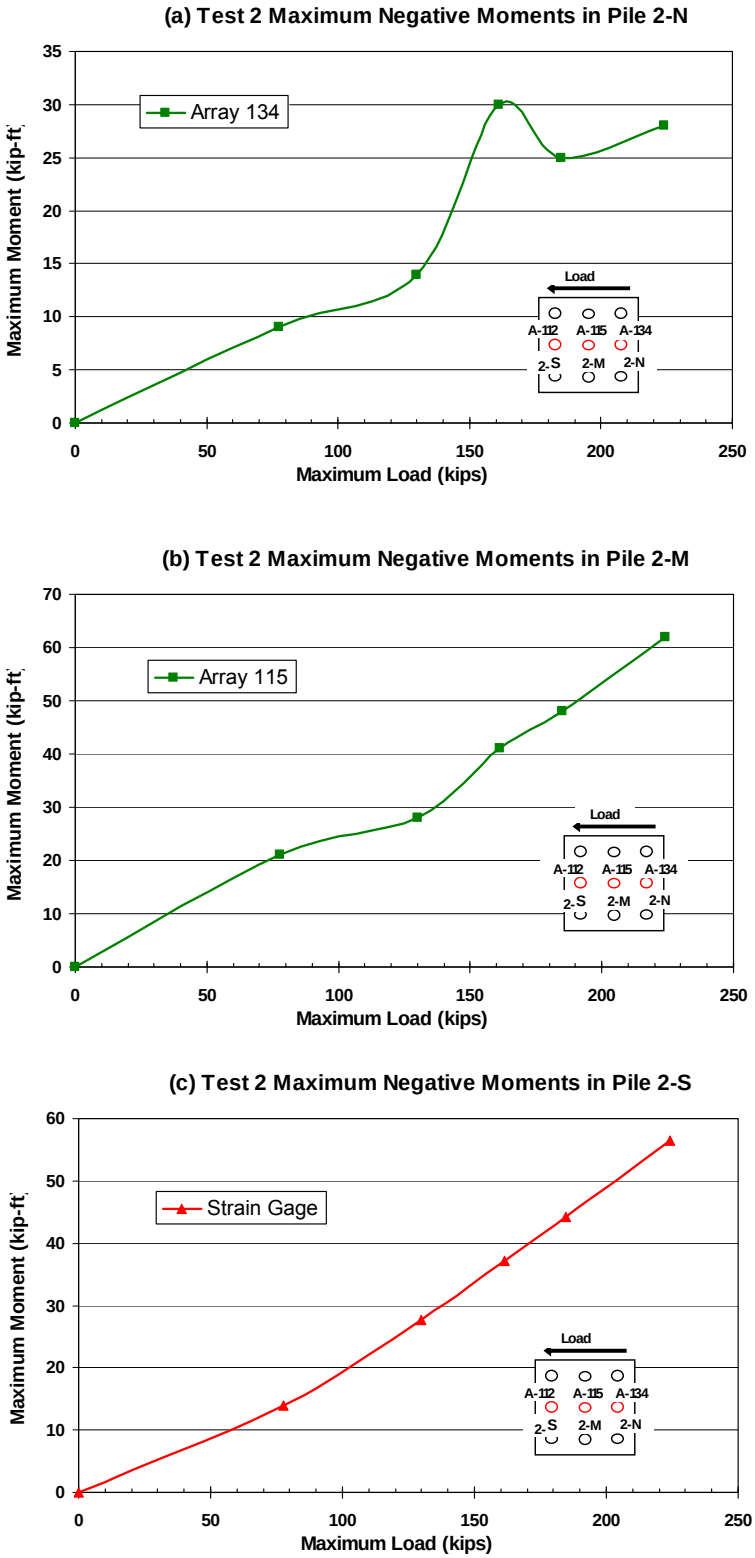

Figure 5-34 - Maximum negative moment versus total pile cap load for piles (a) 2-N, (b) 2-M, and (c) 2-S in cap 2 during test 2.

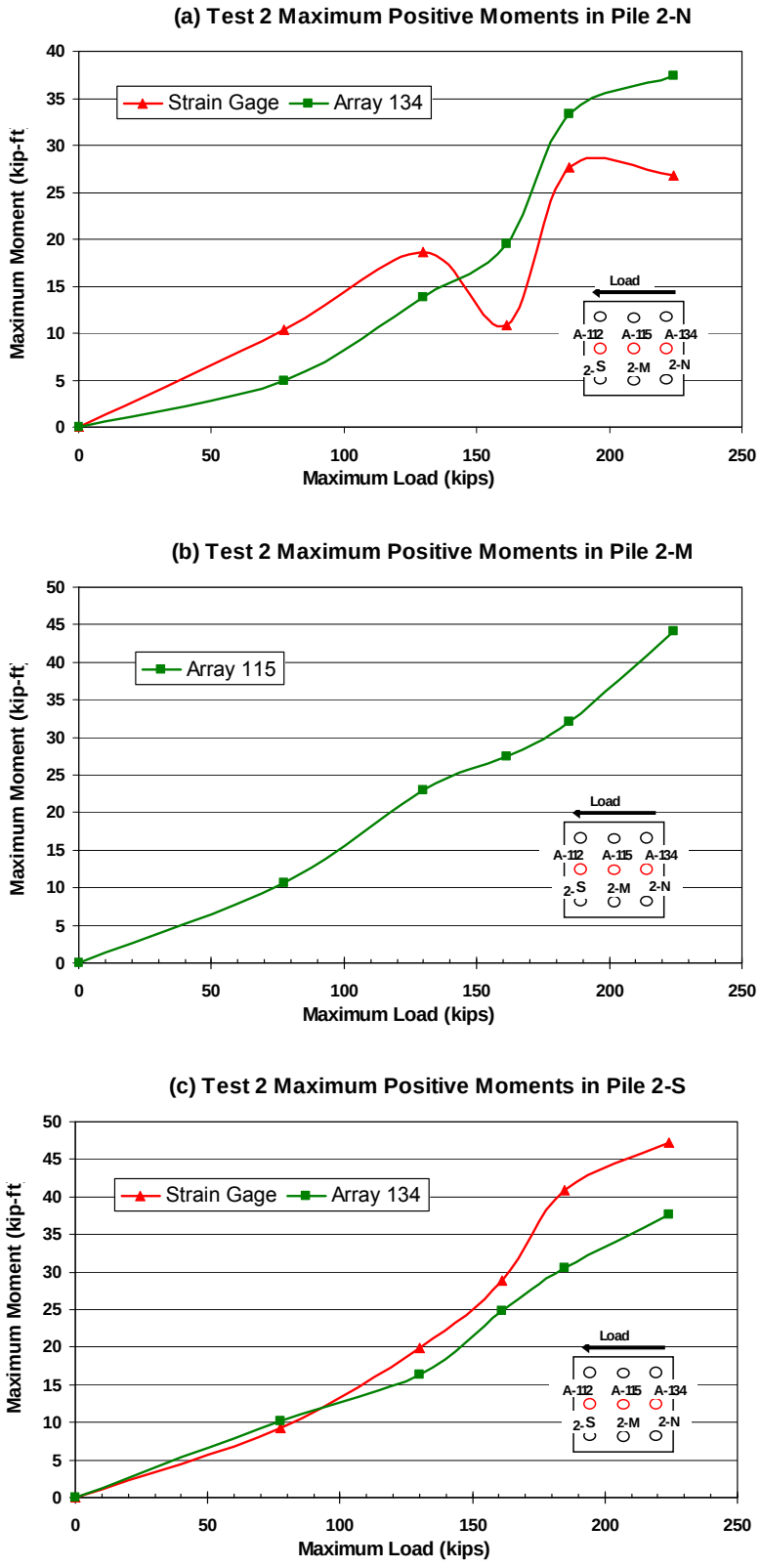

Figure 5-35 - Maximum positive moment versus total pile cap load for piles (a) 2-N, (b) 2-M, and (c) 2-S in cap 2 during test 2.

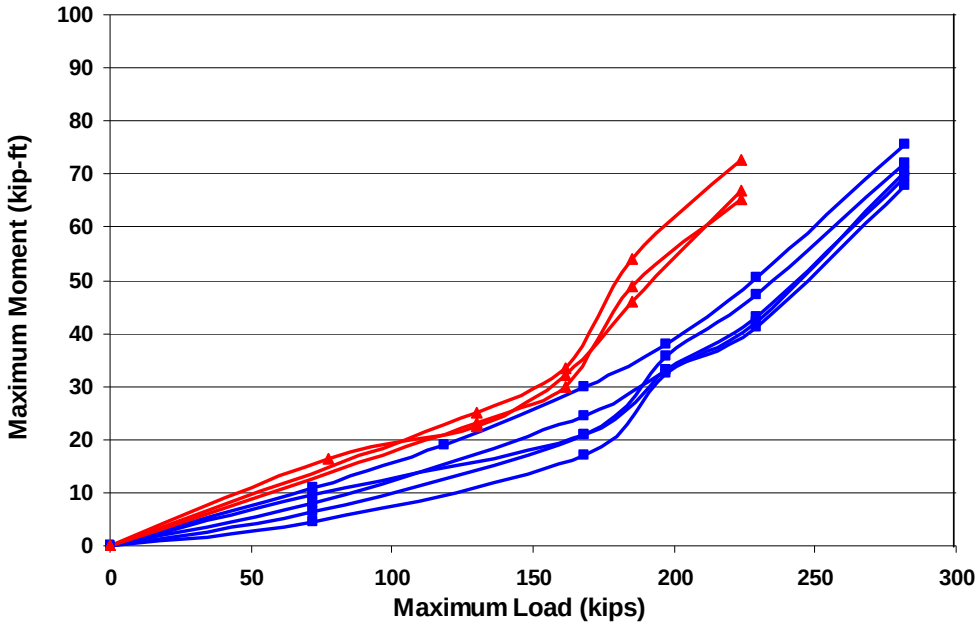

Figure 5-36 – Maximum positive moment versus load plots from test 1 and 2 illustrating general trends experienced by pile cap 1. (Test 1 plots are marked with a square (blue) while Test 2 plots are marked with a triangle.)

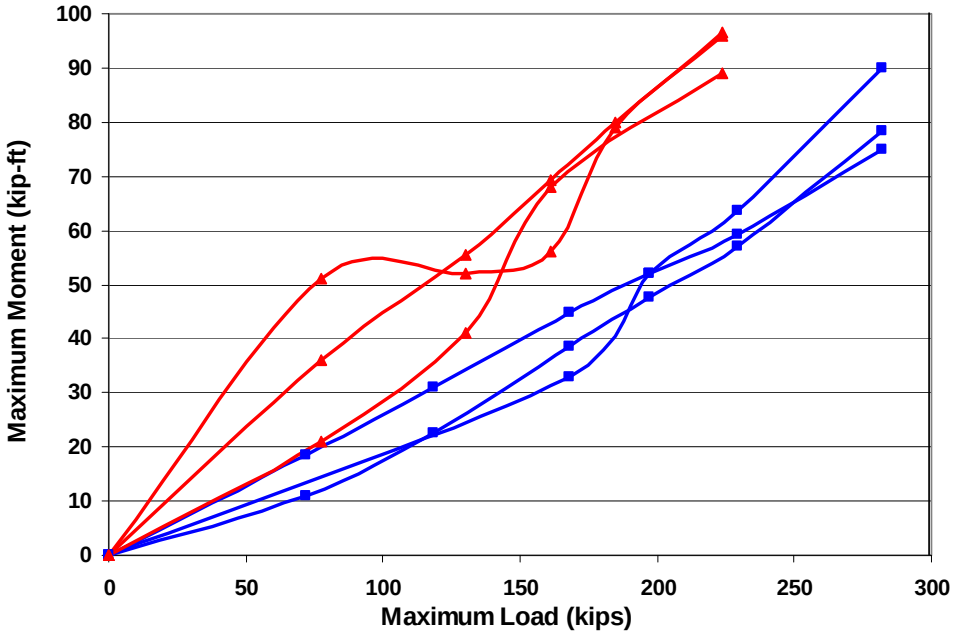

Figure 5-37 – Maximum negative moment versus load plots from test 1 and 2 illustrating general trends experienced by pile cap 1. (Test 1 plots are marked with a square (blue) while Test 2 plots are marked with a triangle.)

5.3 Mass Mix Test

The lateral load test involving the mass mix soil treated zone was test 9 in the series of 16 tests. The test commenced on August 22, 2008 after the mass mix improvement had cured for about 22 to 25 days. As indicated previously, a mass mixed wall was created on the south side of the cap which was ten ft deep, 4 ft wide in the direction of loading and 11 ft long transverse to loading. A simple schematic illustration of the test layout is found in Figure 4-16 and scaled plan and profile drawings are provided in Figure 4-18 and Figure 4-19. Cap 1 in this test was also treated with jet grout zone on the opposite side of the cap. As shown in Figure 4-19, the soil directly below the soil was not treated and the soil on the sides of the cap was not treated. In fact, a small gap was present along the sides of the cap during testing to eliminate the any contribution from side shear on the cap.

On August 17, 2008, after the jet grout and mass mix had cured for about 17 to 20 days, the increased resistance provided by jet grout was tested (test 8) by pushing pile cap 1 to the north in the opposite direction from the mass mixed wall. During test 8, the actuator extensions yielded and the test load was rapidly released. This caused the pile cap to rebound in the direction of the mass mixed wall In fact, at the end of test 8 cap 1 was left with 0.058 inch residual displacement into the mass mix. Therefore, the mass mix test begins with a small initial displacement of 0.058 inch. All instrumentation of string pots, shape arrays, inclinometers, actuator pressure transducer, strain gages, and surface grids were in place and initial measurements taken prior to the test. Except for the surface grids all instrumentation was zero set to the initial values of test 8. The string potentiometers were located one

foot from the top of the corbel at the load point of the cap. Shape arrays were placed in the south pile (closest to the load point) and the middle pile of cap 1. Strain gages on cap 1 were located on the three middle piles within each row. The test followed the standard procedure with no variations.

5.3.1 Load-Displacement Results

Figure 5-38 shows the complete load-displacement curve for test 8 including the cyclic loading cycles at each load increment and full load, unload, and reload curves. Data for Figure 5-38 was obtained from the actuator pressure transducer and the string pots attached to the cap. As shown, the test started at zero load and with the initial displacement of 0.058 inch displacement. The actuator pushed the cap to target the prescribed increments of 0.125, 0.25, 0.5, 0.75, 1.0, 1.5 inches, but because of variations in the lateral resistance of cap 2, the actual pile cap displacements were 0.14, 0.32, 0.62, 0.81, 1.08, and 1.75 inches respectively.

Figure 5-39 shows the load-displacement curve obtained by connecting the points defining the maximum load applied at each of the displacement increments. It also shows that the maximum applied load during the last push was 465.5 kips and resulted in a displacement of 1.75 inches. For comparison purposes the load of 448 kips at 1.5 inch displacement will be used for mass mixing.

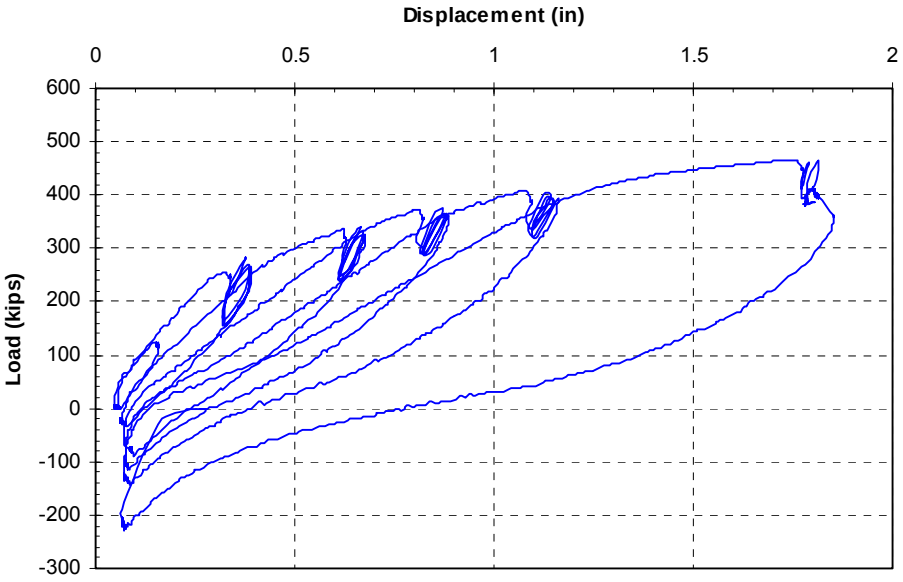

Figure 5-38 –Test 9 load-displacement curves for complete test.

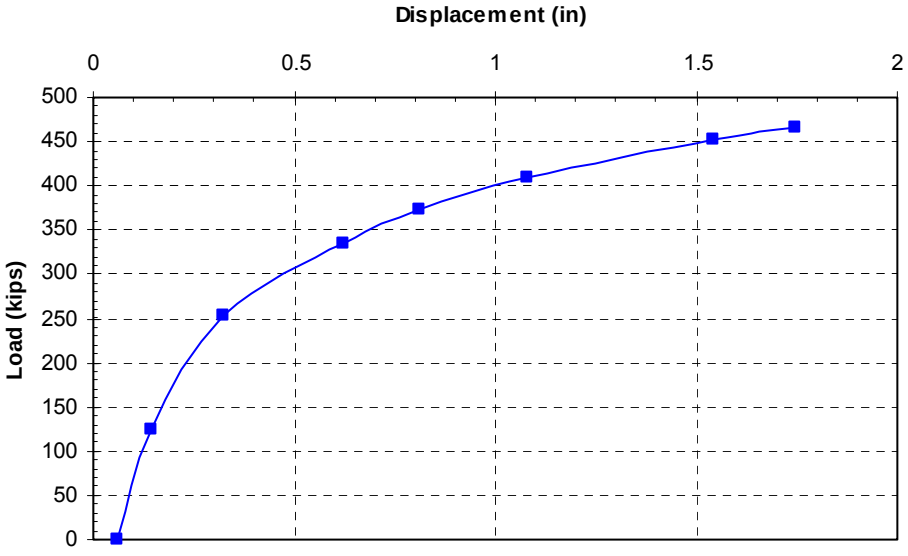

Figure 5-39 – Test 9 maximum load-displacement of each displacement increment.

5.3.2 Rotation versus Load Results

Pile cap rotation versus load curves based on the string potentiometer and shape array measurements for cap 1 during test 9 are provided in Figure 5-40. Due to the initial displacement offset into the mass mixed zone at the beginning of the test 9, the pile cap began with initial rotations from 0.02 to 0.04 degrees. The rotations from the shape arrays and the string potentiometers differ by 0.05 to 0.15 degrees with the string potentiometers measuring smaller rotations. However, both curves portray similar trends. The curves are relatively linear and flat up to a load of about 390 kips after which the rotation begins to increase more rapidly with load. Comparing the rotations on pile cap 1 of test 9 to test 1 shows that at the same rotation of about 0.35 degrees test 9 experienced about 460 kips while test 1 only 280 kips. This illustrates that mass mixing increased the stiffness of the foundation system.

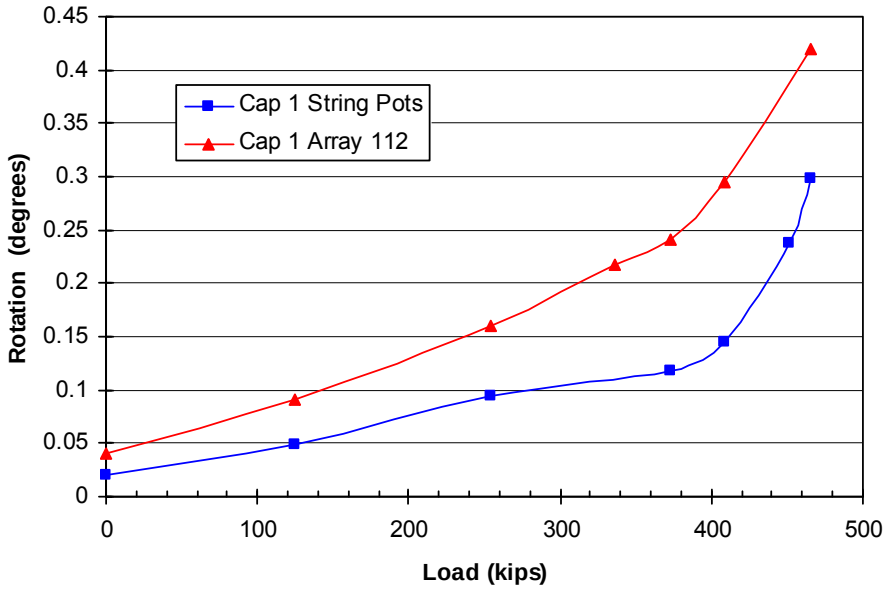

Figure 5-40 - Peak pile cap load versus pile head rotation for cap 1 during test 9 obtained from string potentiometer and shape array measurements.

5.3.3 Surface Failure Observations

Figure 5-41 and Figure 5-42 are photographs of the surface failure when the mass mixed zone was experiencing the greatest load and displacement in test 9. The painted grid in the figures is spaced every two feet in both directions. The greatest significance observed in the figures is a depression or failure plane that formed at about 5 to 5.5 feet from the face of the pile cap. This observed surface failure plane provides some evidence that the mass mixed zone behaved as a rigid body as it pushed against the weaker soil behind it. Other minor surface cracks are also marked in the figures; however, they appear to be shallow and do not denote a failure to any significant depth.

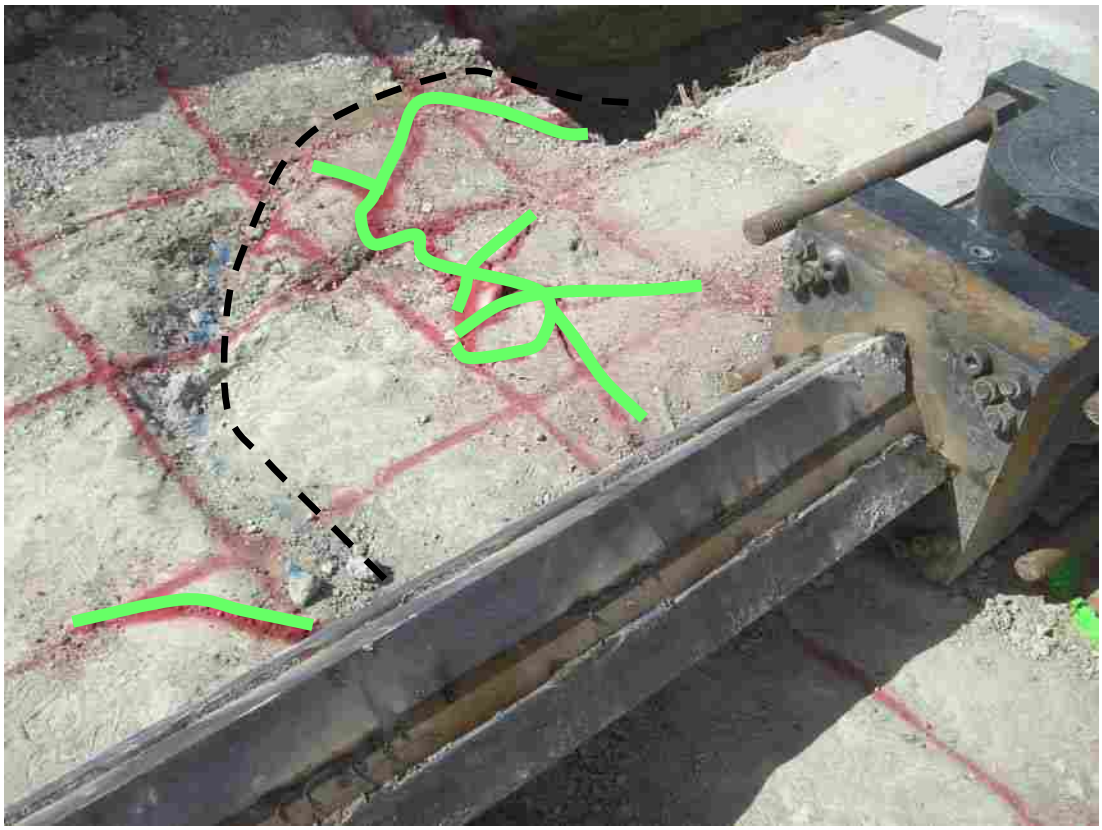

Figure 5-41– Photograph showing the west side of the mass mixed zone's surface condition taken at the greatest displacement and load for test 9. Green curves are cracks and dashed curve is boundary of observed failure block.

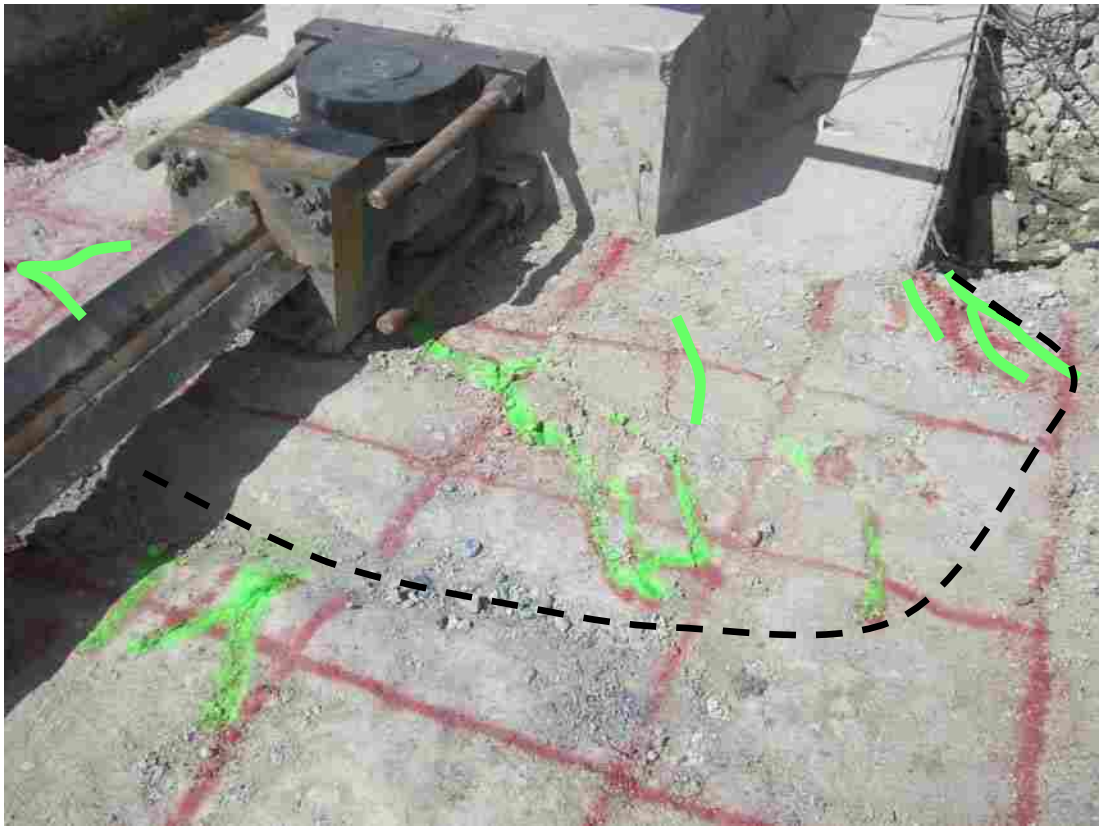

Figure 5-42 – Photograph showing the east side of the mass mixed zone's surface condition taken at the greatest displacement and load for test 9. Green curves are cracks and dashed curve is boundary of observed failure block.

5.3.4 Depth versus Deflection Results

The datum for depth was the top of the corbel, thus the load point for cap 1 was 11 inches or 0.92 ft down from the top of the corbel. Due to unknown reasons, shape array A-134 in the south pile gave erroneous data and results from this array will not be presented. Therefore all results from the mass mixing tests will be from the center pile shape array A-112. The data from center pile shape array A-112 was adjusted using the method discussed in Section 4.3 due to the rotation of accelerometer nodes that occurred during installation.

It is important to note that the final inclinometer measurement was taken after the maximum load was reached. Due to the time to take all the inclinometer measurements, the string potentiometers stopped recording once the maximum load was reached. As a result, Figure 5-43(a) contains no string potentiometer measurement at the final inclinometer reading. Additionally, a comparison between the string potentiometers at maximum load and the inclinometer could not be made as the cap tended to experience slight drift in displacements during the load hold for the inclinometer measurements. Therefore, the array was the only instrumentation taken at the same time as all the other instrumentation.

As is evident in Figure 5-43(a), there is some significant discrepancy between the slopes of the array and the inclinometer. The greatest difference in the displacements occurs at the depth of 15 feet below the top of the corbel. At this depth the measurements differ by about 0.15 inches. The displacements and slope continue to differ, but to a lesser extent at other depths.

These discrepancies could have resulted from a number of reasons. Both inclinometer tubes and the three array tubes where previously buried for the jet grouting procedure on the cap. Upon the excavation of the cap, some of the tubes extending above the cap were damaged. For example, the north inclinometer and array tubes were completely filled with grout and were no longer operational. As a result, no profiles could be obtained for this pile. Damage was also done to the South inclinometer tube although grout was kept out of it; the portion of the tube extending above the cap was slightly cracked. However, the damage seemed minor and the inclinometer was still able to travel down the tube.

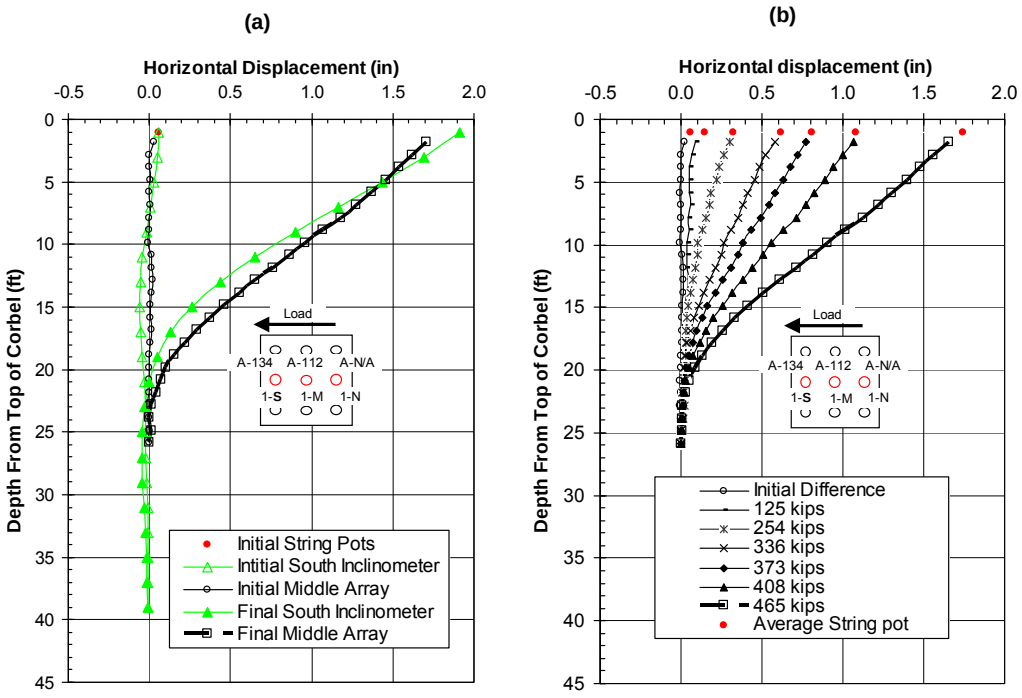

Figure 5-43 – (a) Test 9 depth vs. displacement profiles comparing the initial and final inclinometer measurements to that of the center array. (b) Depth vs. displacement curves obtained from shape array 112 at several displacement increments for pile cap 1 during test 9. Pile head displacement from string potentiometers are shown for comparison.

Two shape arrays were used; however, the array in the south pile (paired with the south inclinometer tube) gave values substantially lower and was dismissed as erroneous. Therefore, the only array data used was from the middle pile which could explain the slope difference when comparing the South pile inclinometer readings to that of the array. The middle array was placed at the top of the cap where the corbel ended. Therefore, its first measurement was at 1.83 feet. A trendline was created using the array's measurements at depths of 1.83 and 2.83 feet below the top of the corbel at the same time and maximum load. At these depths, it can be assumed that the array would behave linearly as the majority of that portion of the array was enclosed in the concrete pile cap. From the equation of that trendline, a displacement of 1.78 inches could be extrapolated for a 1 foot depth which is the

depth of the first inclinometer measurement. The inclinometer at that depth measured 1.91 inches, varying from that of the array by 7%.

Figure 5-43 (b) above shows the depth versus displacement curves at the maximum displacement of each test increment as measured by the array and string potentiometers. The array measured the pile cap displacements for each of the six test increments as 0.9, 0.30, 0.58, 0.77, 1.07, and 1.65 inches, respectively. When extrapolating the array to the same depth as the string potentiometers, by using the trendline method mentioned before, the 1 inch test increment showed the greatest difference between the array and the string potentiometers and yet only varied by 2% throughout the test. The rest of the test increments varied less than that and were closer to 1%. These slight errors are most likely due to the initial displacements of each measuring device. The string potentiometers measured the initial displacement at 0.058 inches, while the array's initial displacement was 0.026 inches when comparing the initial measurements of test 9 to that of test 8.

However, since all measurement devices had points fixed in or on the cap they should be consistent and there is still some uncertainty as to why that was not the case. In summary, the inclinometer's maximum deflection varied from the array by 7%, while the string potentiometers only varied by 2% or less.

5.3.5 Bending Moment versus Depth

By using the method described in section 5.1.4 the following bending moments in Figure 5-44 were obtained from the array displacements and strain gage measurements. The array measurements show that the location of the maximum

positive bending moments increased slightly with load and displacement. However, the depths of the maximum positive bending moments appear to be extremely low compared to the other tests. The 336, 408, and 465 kip test increments show that the array and strain gages measure fairly constant in magnitude, however, there maybe some discrepancy in the depth of where the moment occurred. The arrays measure the location closer to 15 feet, while the strain gages tend to suggest that it would be closer to 11 feet below the bottom of the cap.

A greater discrepancy is in the maximum negative moments. The numerical method used to derive the bending moments in some instances is prone to error. This is the case with the negative moments at shallow depths for test 9 as the moments derived at those depths were erroneous. In these events a piecewise polynomial fit analysis would be more appropriate. However, that analysis is beyond the scope of this thesis.

Since the data reduced from the array between depths 0 to 5 feet below the bottom of the cap were unreliable, a straight line was drawn from the last reasonable data point from the array to the moment computed from the strain gage at the bottom of the pile cap. This approach appears to give a somewhat reasonable shape for the moment versus depth curves. This also suggests that the moments obtained from the strain gages are reasonably accurate and consistent with those from the array.

Figure 5-45 provides a comparison of the bending moment versus depth curves obtained from the shape array and the inclinometer at the maximum load. Due to the different slopes measured by the array and the inclinometer, the bending moments

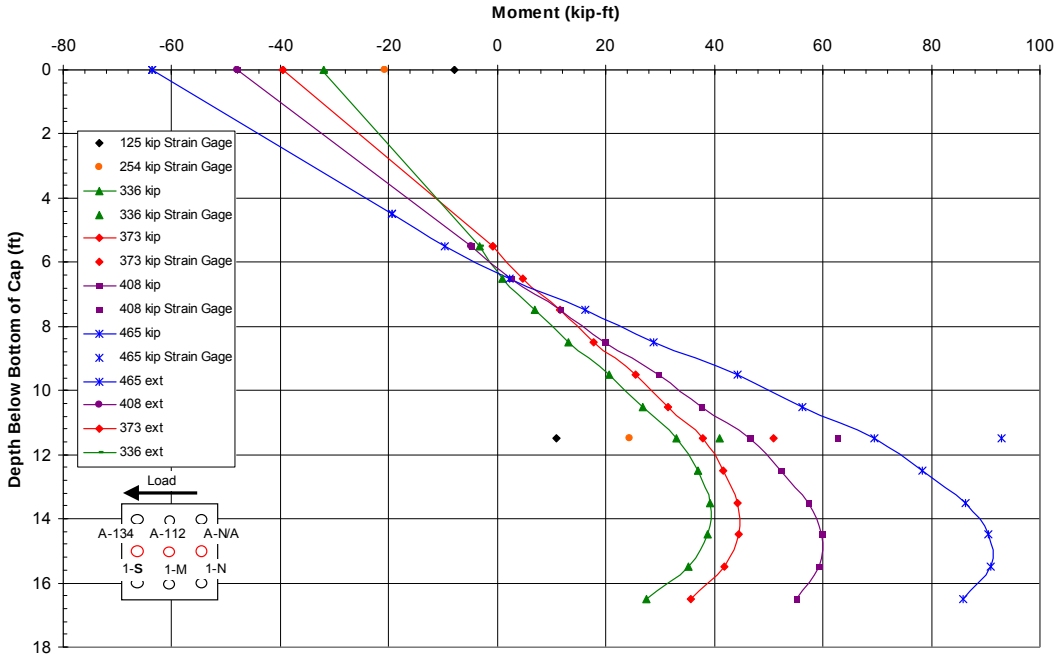

Figure 5-44 – Test 9 Bending Moment vs. Depth profiles obtained from array 112 and strain gage data as instrumented on the center pile.

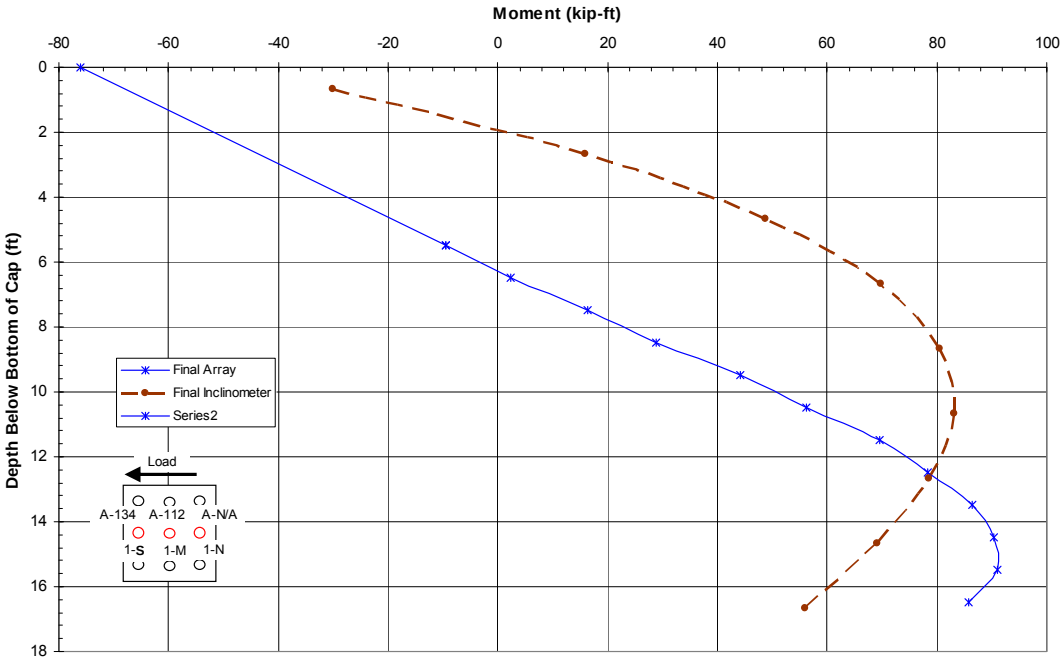

Figure 5-45 –Test 9 Bending Moment vs. Depth comparison of the array 112 and the inclinometer at maximum load.

profiles derived by the numerical method are significantly different as illustrated in Figure 5-45. For example, there is a significant difference between the maximum negative moment from the array curve (76 kip-ft) and that from the inclinometer (≈ 44 kip-ft) at the base of the cap. Nevertheless, the maximum positive moments are within about 10% of each other. The arrays place the maximum positive bending moment for the maximum displacement around the magnitude of 93 to 95 kip-ft at the depth of approximately 15 feet below the cap. The bending moment trend from the inclinometer places the maximum moment for the same test increment at about 83 to 85 kips at a depth of 11 feet. The strain gages would tend to agree with the arrays in the magnitude of the moments, but agree more with the inclinometer as to the depth of the moments. In summary, the magnitudes of the moments derived from that array appear to be somewhat accurate; however the array may be reporting the location of the maximum positive moment deeper than it is.

5.4 Lateral Load Test into Mass Mix Zone without Soil behind the Pile Cap

When considering the results of increased lateral strength due to mass mixing it is also important to know how much of that increased strength is due to the passive force directly behind the pile cap. To obtain the increased resistance due to passive force, a test was performed on the same cap (cap1) and the same mass mix wall. Only this time a one foot wide excavation of the mass mix wall was made along the south face of the cap to the depth of the cap to eliminate contact between the wall and the cap. An illustration of the test is found in Figure 4-17 and Figure 4-20. This test was number 15 in the series of 16 soil improvement tests.

Since this test was performed significantly later than the original mass mix test, some instrumentation had changed along with the relative position of the cap. The shape arrays were pulled from the cap for use in other tests, but put back into the cap prior to test 14. All other instrumentation remained intact. Since there was little anticipated load transferred to the near surface soil, no surface grid was painted.

All instrumentation was zero set to the initial values of test 8 with the exception of the shape array which was zero set to the beginning of test 14. Since the shape arrays had been moved between test 8 and 15, it was necessary to zero set them to when they were placed back into the cap at the beginning of test 14. This is primarily due to the fact that the arrays could not be inserted back into the cap and guarantee that all the nodes were in the exact location as before and that no rotation of the array had occurred. To make any reasonable comparison of slope and displacement, the lateral displacement measured by the inclinometer between test 8 and the beginning of test 14 were used to adjust the array data. To do this, a fifth order polynomial was fit to the inclinometer measurements at the beginning of test 14, with depths as the independent variable. Then using the equation of the trendline, the appropriate depth of the array nodes was inserted as the independent values and corresponding displacements were calculated. These nodal displacements were then added to the displacements measured by the array at each node. In short, the initial displacements from the inclinometers between test 8 and 14, were added to the array measurements for test 15 since it was zero set at the beginning of test 14. This essentially allowed all the data of test 15 to use the beginning of test 8, which was initial position of the cap after soil improvements prior to any testing.

In addition to the instrumentation changes, the testing procedure varied from the standard in regards to the test increments. The test increments were 0.5, 0.75, 1.0, 1.5, 2.0 inches. The main goal of the increased test increments was to make sure that a failure state of the soil was reached and to minimize error that might occur through the reloading of the soil. Also, without the passive resistance, much less force would be needed to pull the cap and therefore, we could obtain greater deflections. Other than the change in displacement increments, the standard testing procedure was followed.

5.4.1 Load-Displacement Results

The plot in Figure 5-46 provides the complete load-displacement curve for cap 1 during test 9 and defines the load path taken during loading, cyclic loading, unloading and reloading for each displacement increment. Figure 5-46 was obtained from the actuator pressure transducer and the string potentiometers attached to the cap. As shown, test 15 started with an initial displacement of 1.25 inches with a load of 117 kips into the mass mix. The load of 117 kips is down from 152 at the end of test 14. Test 14 ended at the 1.25 inch displacement and was held for instrumentation preparation and synchronization for test 15. During that displacement hold, the piles relaxed and thus the load dropped to 117 kips before test 15 was able to begin. Test 15 then commenced from that initial displacement of 1.25 inches and targeted the prescribed increments of an additional 0.5, 0.75, 1.0, 1.5, 2.0 inches, and actually displaced the cap 1.79, 2.1, 2.5, 2.83, and 3.15 inches, respectively.

Figure 5-47 provides plots of the peak load-displacement curve for test 15, after eliminating load and reload cycles, along with a comparable curve from test 9, which was the test involving a lateral pull into the mass mix with soil adjacent to the pile cap. The load-displacement curve defined during pull-back at the end of test 14 has been appended to the curve from the start of test 15 to provide the complete load-displacement curve. The portion of the data between test 14 and 15 where the piles relaxed at the initial displacement of 1.25 inches was removed for clarity. The maximum applied load during test 15 was 312 kips and resulted in a displacement of 3.15 inches. For comparison purposes, the displacement offset of 0.1 inches between test 15 and test 9 at zero load in Figure 5-47 was removed by subtracting the offset from test 15's data. By doing this, Figure 5-48 was obtained which makes it possible to get an accurate estimate of the strength increase due to the passive pressure behind the cap.

For test 9, at a displacement of 1.75 inches, which was the maximum displacement, the applied load was 465.5 kips. At this same displacement of 1.75 inches during test 15 the load was only 235 kips. This suggests that of the total lateral resistance of 465.5 kips in test 9, as much as 230.5 kips or about 49.5% was due do having the pile cap in connection with the mass mixed wall behind the pile cap. However, due to the reloading effects, this estimate is optimistic. As discussed previously, during reloading the peak load is typically only about 90% of the peak load during virgin loading. In addition, at displacements less than the previous peak displacement the load during reloading could be even less. To illustrate this point, the load-displacement curve during reloading up to the final displacement increment

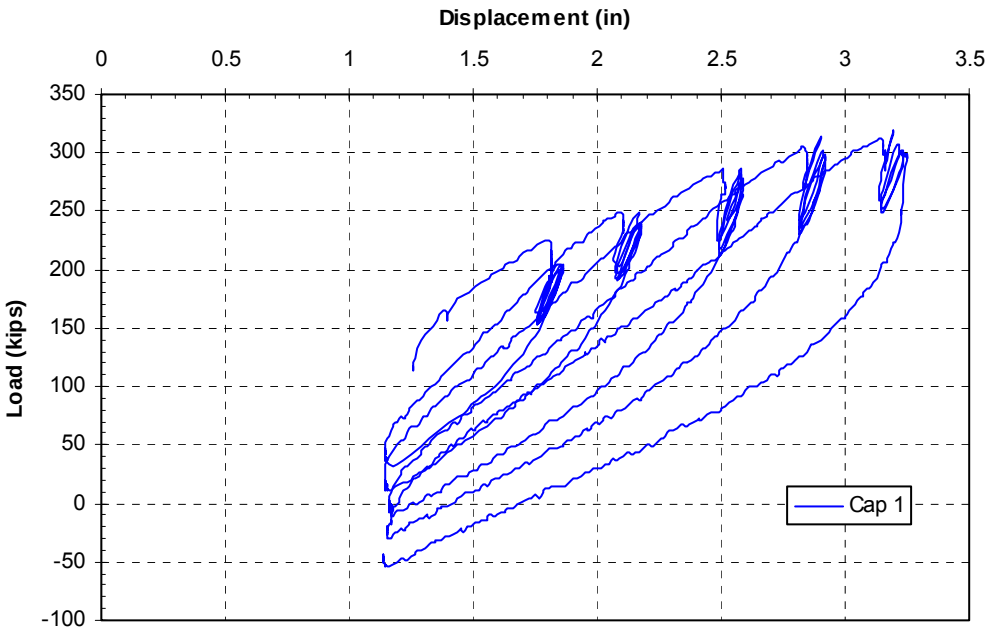

Figure 5-46 – Complete load-displacement curve for cap 1 during load test 15.

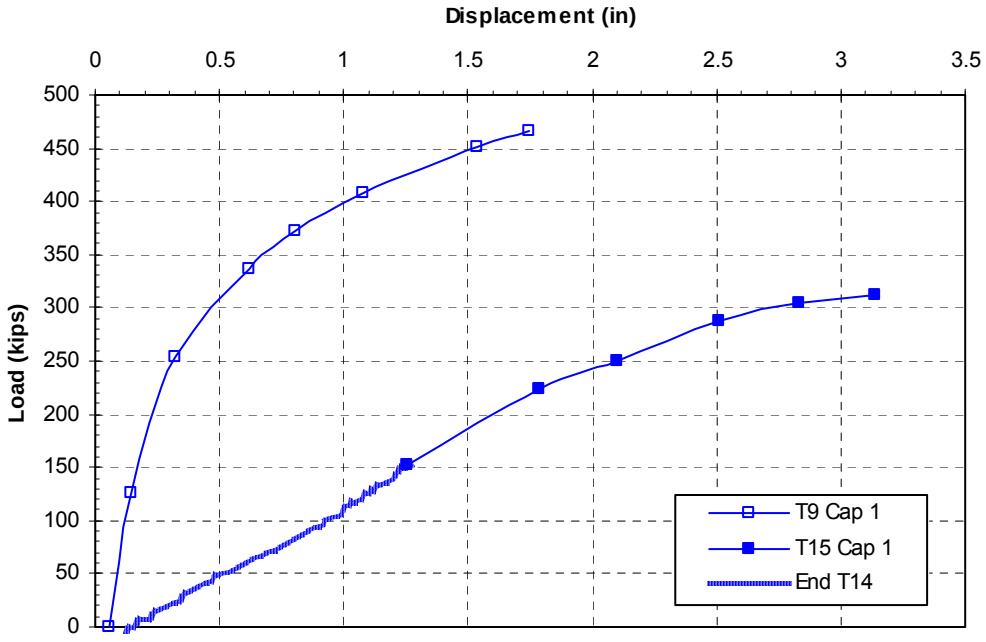

Figure 5-47 - Peak load-displacement curves for cap 1 during Test 9 and Test 15.

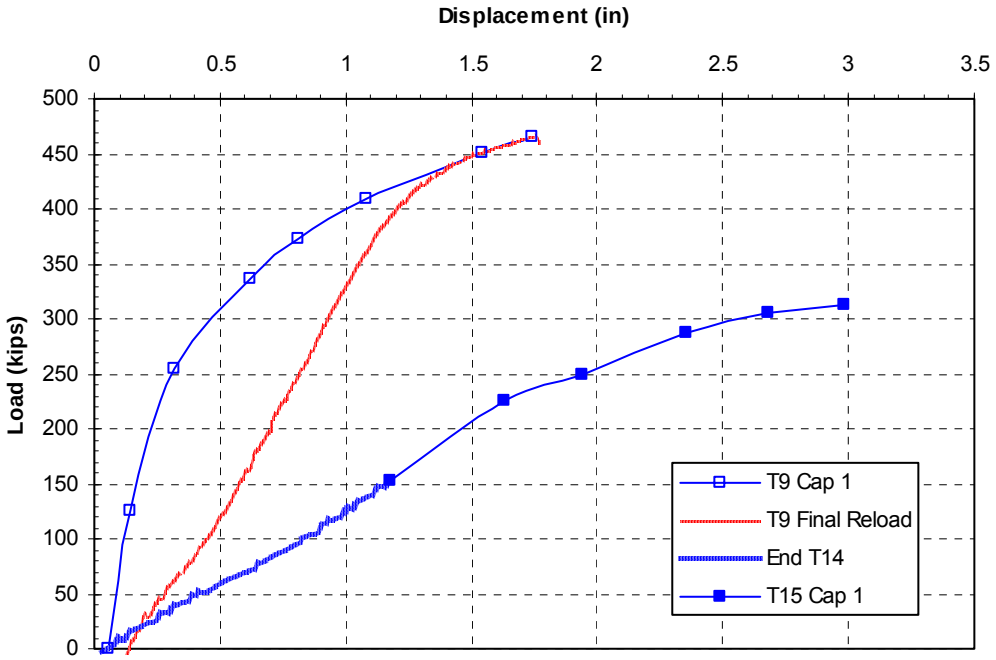

Figure 5-48 – Peak load-displacement curves for pile cap 1 during tests 1 and 15 along with complete reload-displacement curve for the last displacement increment during test 1.

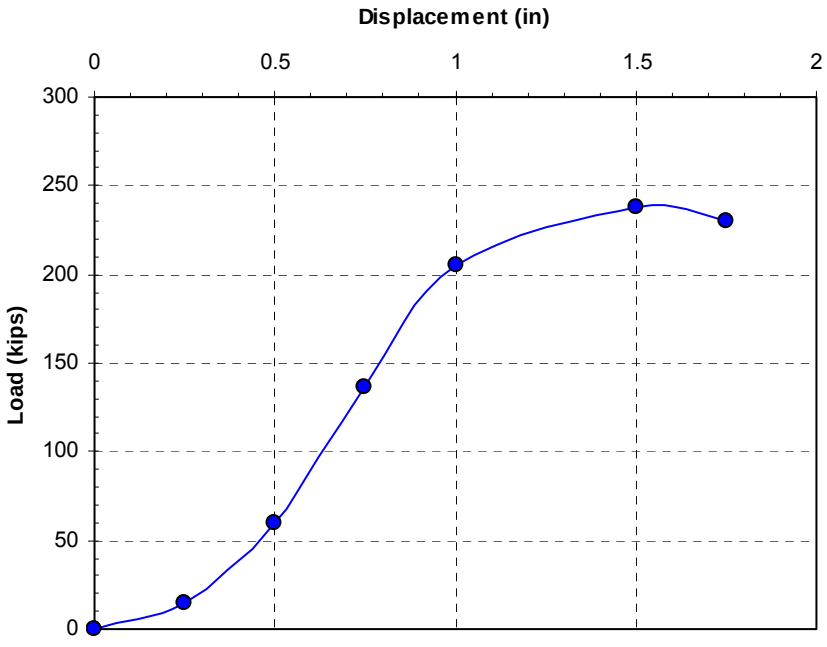

Figure 5-49 – The comparative difference of the final reload from test 9 and the maximum load and displacement of test 15.

for test 9 is shown in Figure 5-48 in comparison with the peak load-displacement curve during virgin loading. The decreased resistance during reloading is substantial and can be attributed to remolding of the soil and the formation of gaps during virgin loading.

Considering the reloading that occurred prior to test 15, a better indication of the development of increased resistance with displacement produced by the soil mix wall might be obtained by comparing the load-displacement curve from test 15 with the final reload-displacement curve for test 9. This approach would likely account for changes in soil strength due remolding but might not account for differences in gapping. Figure 5-49 shows the load-displacement curve obtained by subtracting the load from the load-displacement curve for test 15 from the load from the last reload curve for test 15.the. Because the one inch displacement was the previous test increment prior to the 1.5 inch as shown, the passive force at that one inch displacement will account for the greatest reloading effect. Thus, the difference in resistance at one inch displacement is about 210 kips or 45% of the total strength. Depending on how one interprets the data from tests 9 and 15, the lateral resistance provided by the having the pile cap in contact with the soil mixed wall would fall in the range between 49% and 45% of the total 465.5 kips of resistance.

5.4.2 Rotation versus Load Results

A pile cap rotation versus load curve based on measurements from the shape array (A-112) in the center pile for cap 1 during test 15 is provided in Figure 5-50. The rotation measurements from the string potentiometers are not provided due to

erroneous data. Additionally, a slight crack formed at the interface of the corbel and pile cap. The crack was minor and the only data affected was the rotation versus load, which may allow for slightly higher measurements of rotation. The rotation appears to be fairly linear for test 15 with almost double the total rotation of that measured for test 9 despite the fact that the applied load is only about half as great. A portion of this can be attributed to the minor crack, however, this increase in rotation is expected because of the decreased resistance and rotational stiffness which accompanied the removal of the soil mix wall adjacent to the pile cap and the fact that the pile cap was displaced twice as much as test 9. Also, cap 1 in test 15 experienced about 0.2 degrees more rotation than test 2 for similar loadings, although this is most likely due to the minor crack.

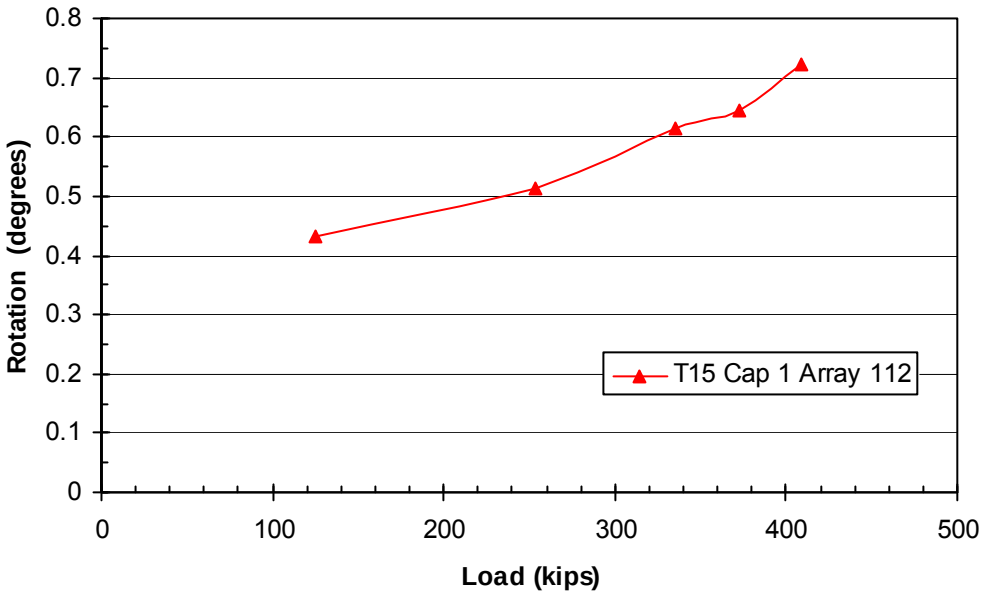

Figure 5-50 - Peak pile cap load versus pile head rotation for cap 1 during test 9 obtained from center pile shape array measurements.

5.4.3 Depth versus Displacement Results

As mentioned earlier in the introduction to Section 5.4, the array data were zero set to the beginning of test 14 and offset by the initial displacement of the inclinometer. This allowed all instrumentation to be zero set to the original displacement datum prior to test 8. The datum for depth was measured from the top of the corbel, thus the load point for cap 1 was 11 inches or 0.92 feet below the top of corbel. The south shape array (A-134) data was erroneous, so only the middle shape array (A-112) is shown in the depth versus displacement graphs. Furthermore, the data from center pile shape array (A-112) was adjusted using the method discussed in Section 4.3 due to the rotation of is nodes that occurred during installation. As is evident in Figure 5-51 (a), the initial displacements of the inclinometer and string potentiometers at the load point vary by only 0.07 inches. With the shape arrays using the initial offset of the inclinometer, they recorded 0.06 to 0.07 inches off of the string potentiometers at the load point as shown in Figure 5-51 (b). When all the data was zero set to the beginning of test 14, all instrumentation measured less than 1% off when comparing displacements at the load point. With the instrumentation zero set to test 8, that percent error increased slightly to about 2% due to the 0.07 inch initial discrepancy. Therefore, any error in test 15 results is most likely due to the discrepancies in the initial position of the cap prior to the test.

Figure 5-51 (a) shows a slight variation in slope especially at about the depth of 5 feet below the top of the corbel. This variation could be due to the fact that the array and inclinometer are in different piles. The inclinometer was located at the

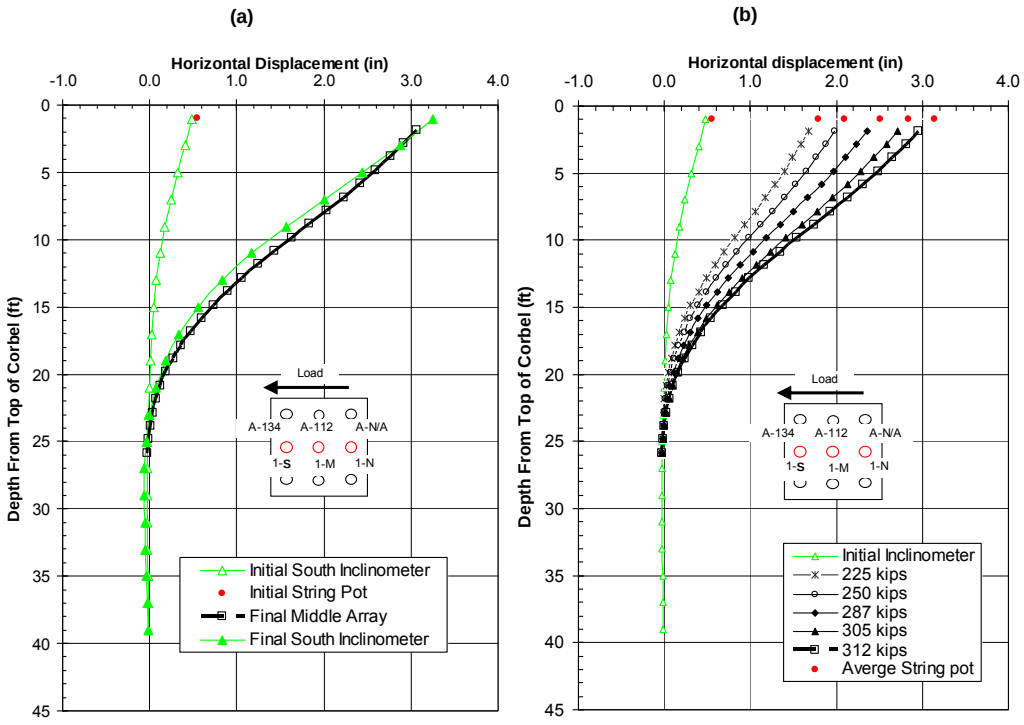

Figure 5-51 – (a) Test 15 depth vs. displacement profile of the initial inclinometer that was added to the array data. Also shown is the final comparison of the adjusted shape array to the south inclinometer. (b) Depth vs. displacement curves obtained from shape array 112 at several displacement increments for pile cap 1 during test 15. Pile head displacement from string potentiometers are shown for comparison.

middle pile of the front row, while the array was located in the middle pile of the middle row. The greatest difference in measured deflections occurs around the depth of 12 feet below the top of the corbel with measurements varying by up to 0.15 inches or 13%. However, at depths between 1 through 5 feet and 20 through 24 feet the difference in displacement is only 6% or less with 0.07 inch being the greatest discrepancy. The discrepancies could result from many reasons as mentioned in Section 5.3.3 or 5.1.4.

Figure 5-51 (b) above shows the depth versus displacement curves at the maximum displacement of each test increment as measured by the array. The array measured the pile caps displacements for each of the five test increments as 1.67,

1.98, 2.36, 2.71, and 2.95 inches respectively. These measurements include the initial displacement of 1.25 inches for test 15 and thus, represent the total displacement the cap has experienced since soil treatment. Using the same trendline method described in Section 5.3.3, the array deflections were extrapolated to the same depth as the string potentiometers. When compared at the same depth as the load point, the displacements measured by the array vary by about 2% or less with the greatest discrepancy occurring at the 312 kip load where displacements differed by only 0.07 inches.

5.4.4 Bending Moment versus Depth

Bending moments were calculated from the array deflection data using the method mentioned in Section 5.1.4. Also, the array displacements that were used to derive the bending moments were adjusted using the initial displacements of the inclinometer as mentioned earlier in this section. Since the strain gages were zero set at the beginning of test 14, the moments derived from the initial inclinometer displacements were added to the moments measured by the stain gages. The strain gages at the bottom of the cap were reduced by the 15.5 kip-ft positive moment as denoted by the initial moment derived from the inclinometer at that depth. Similarly the values of the strain gages at 11.5 feet below the bottom of the cap were increased by 16.67 kip-ft. Thus, all moments shown in Figure 5-52 and Figure 5-53 are relative to the beginning of test 8 before any testing took place on the improved soil.

It was observed in test 15 that as the load increased the maximum positive moment increased, but the location of the maximum positive moment remained

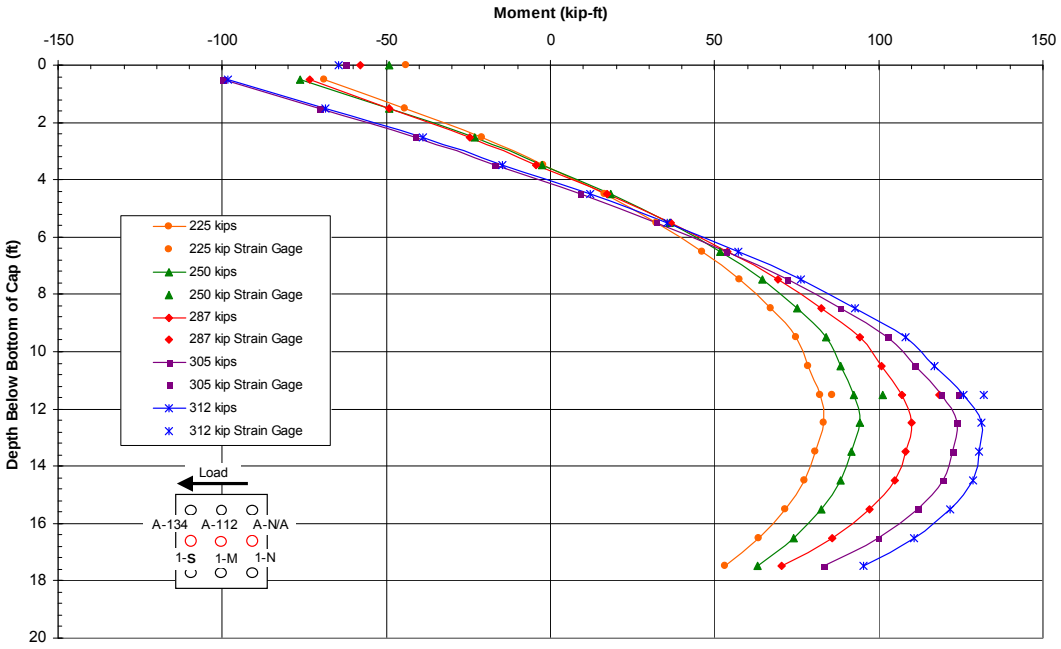

Figure 5-52 – Test 15 bending moments based on array measurements taken at each test increments maximum load using the initial inclinometer displacement adjustment.

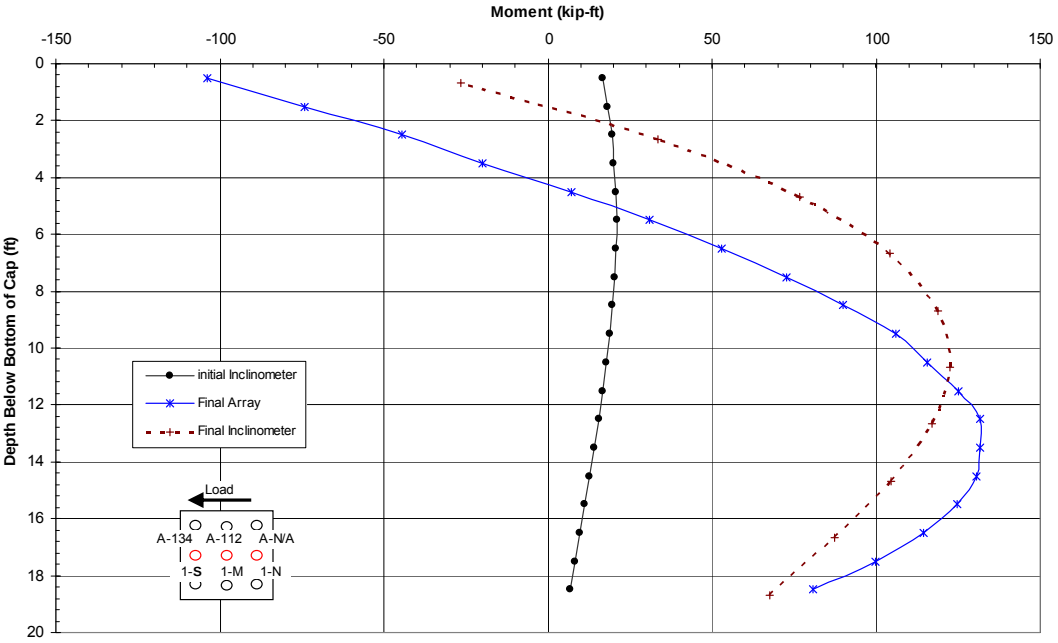

Figure 5-53 – Comparison of array and inclinometer bending moments vs. depth for test 15. The final measurements were taken during the inclinometer measurement hold at maximum displacement.

relatively constant at a depth of 12.5 below the bottom of the cap. The magnitude of the moments from the strain gages and the shape arrays are reasonably consistent for the positive moments, but are significantly different for the maximum negative momenta. The negative moments from the strain gages are about 50% lower than those interpreted from the shape arrays.

The bending moment versus depth profiles obtained from shape arrays and the inclinometer at the final displacement increment are provided in Figure 5-53. The difference between the bending moments derived from the inclinometer compared to the trends derived from the arrays appears to be mostly due to the slight differences seen in the depth versus displacement measurements. Despite these minor discrepancies, it appears that the maximum positive moments occurred in the relative vicinity of the measured strain gages. Moments derived from the strain gages at 11.5 feet below the bottom of the cap measure within 5 to 10 kip-ft (4% to 10%) of the shape array at that depth. The maximum negative moments, however, differ by a factor of about 1.7 to 2 for the shape arrays compared to the strain gages. The maximum negative moment derived from the inclinometer profile provides better agreement with the maximum moment obtained from the strain gages than does that from the arrays.

In interpreting this test data, it can be said that the maximum positive bending moment likely occurred between 11 and 13 feet below the cap and measured between 130 and 133 kip-ft at the greatest displacement. It is also important to note that the depth of the maximum bending moment occurred at relatively the same depth (about 12.5 feet for the arrays) for each test increment. This trend differs from

what was observed from the virgin soil tests, however this variation could be due to inconsistencies in the numerical method.

6 Discussion of Results

Based on the results from the previously discussed tests, conclusions can be drawn with regards to the strength increase produced by mass mixing adjacent to a pile group soft clay. To do this, the results from test 1 on the pile cap in virgin clay are compared to the results from test 9 on the pile cap after mass mixing for soil improvement. Additionally, the results for test 2 involving the pile cap in virgin clay without soil adjacent to the cap are compared to the results in test 15, which involved the pile cap with the mass mix soil improvement with the soil excavated adjacent to the cap. With conclusions from these tests comparisons failure mechanisms of the mass mix will be explored, the ultimate passive resistance from the mass mixed zone will be calculated, an analysis of the computed lateral force will be discussed, general trends of displacement versus depth and bending moment versus depth plots will be outlined, and finally a basic cost and effectiveness of the mass mixing soil improvement will be evaluated.

6.1 Load-Displacement Discussion

Figure 6-1 shows the load-displacement curves for cap 1 during test 1 (virgin clay) and test 9 after the mass mix soil improvement. The mass mix curve originally had an initial displacement of 0.05 inches. For an accurate plot comparison of the

total displacement starting at zero load, the mass mix curve was shifted to the left 0.05 inches. Comparing the loads at the 1.5 inch displacement, the pile cap after mass mixing resisted 453 kips compared to the 282 kips resisted by the pile cap in the virgin clay. This is a lateral resistance increase of 171 kips or 62.5%. It is also interesting to evaluate the increase in initial stiffness due to the mass mixing. Prior to treatment, the initial slope of the load-displacement curve to the one-eighth inch test increment was 800 kips/in, while after soil mixing the stiffness increased to 1300 kips/in. This represents an increase in stiffness of about 65%. Thus, mass mixing improved the lateral resistance of the weak clay by a factor of 1.6 and increased the stiffness of the soil by a factor of 1.65.

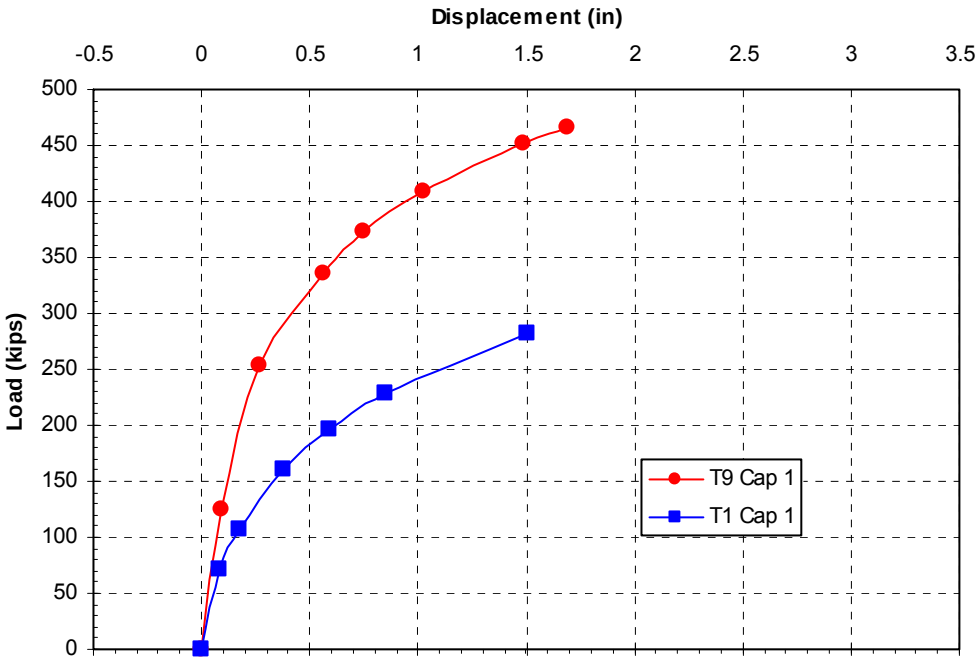

Figure 6-1 – Comparison of virgin clay (test 1) and the mass mix soil improvement (test 9) load-displacement curves.

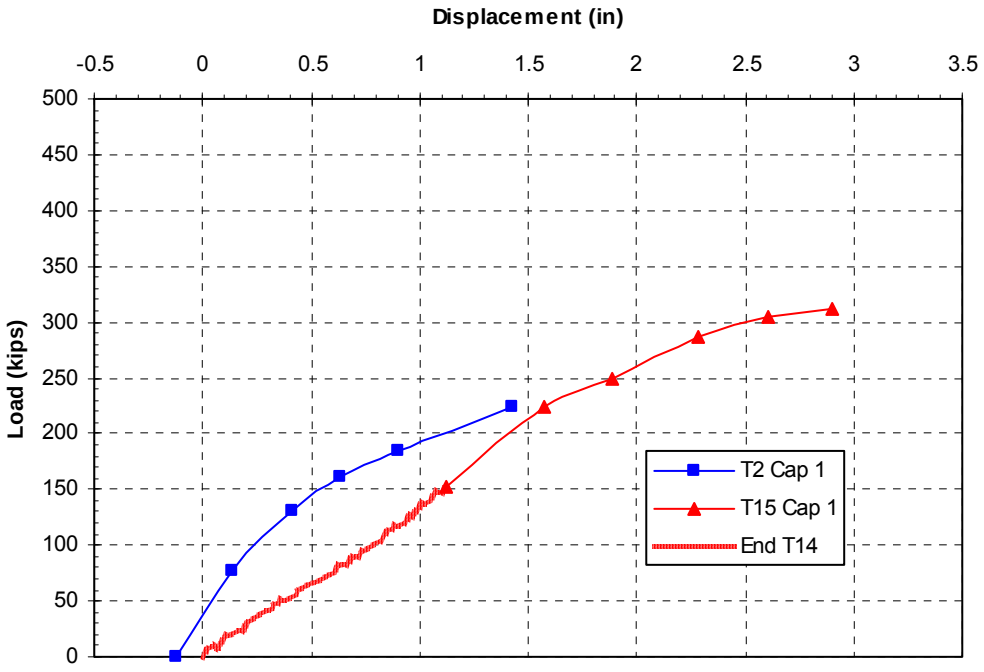

Figure 6-2 – Comparison load-displacement curves for the no passive cases of the virgin clay (test 2) and mass mix soil improvement (test 15).

Figure 6-2 provides a comparison of the load-displacement curves for pile cap 1 in test 2 in the virgin clay and test 15 after mass mixing. In both cases the soil adjacent to the pile cap has been excavated. The curve for test 2 was plotted with its initial offset and adjustment of 0.15 inches due to the gap effect mentioned in section 5.2.1. Additionally, the mass mix curve with no passive (test 15) was shifted to the left 0.05 inches to measure the total displacement from zero load. Although the load-displacement curve for test 15 was much lower than that for test 2 during re-loading, for virgin loading, at displacements greater than 1.5 inches, the curve for test 15 appears to be a very natural extension of the curve for test 2. This observation suggests that the mass mixing had little impact on the soil strength below the cap. The agreement in the slopes of the two curves for the no passive case

would also imply that the majority of the strength increase from the mass mixing was due to the passive strength increase in the soil directly behind the pile cap.

It could be argued that the test 2 load-displacement curve could decrease rapidly after 1.5 inches, but this would be highly unlikely considering that the slope of the curve approaching 1.5 inches is still increasing and is identical to the slope of the test 15 load-displacement curve from 1.75 to 2.5 inches. Considering the minor adjustments to the displacements noted previously, it is possible that there would be a 10 to 20 kip discrepancy between the load-displacement curves for tests 2 and 15. This difference in lateral resistance could be easily attributed to a slight increase in the soil-pile interaction below the pile cap. Therefore, 90% to 100% of the increased lateral resistance is likely attributable to the passive resistance of the mass mix directly behind the pile cap along with side and bottom friction on the mass mixed wall. Additionally, up to 10% of the increased lateral resistance could be due to the increased resistance from the soil-pile interaction.

Further support for the source of increased lateral resistance is also provided by a comparison of the maximum positive moment versus load curves for tests 1, 2, and 9 on cap 1 are provided in Figure 6-3. The moment versus load curves obtained from each pile during tests 1 and 2 are shown in Figure 6-3 to account for potential variations from the average. For a given load, the moment developed in the cap during test 2 is higher than that for test 1 because the passive resistance on the pile cap had been eliminated and the piles had to carry a greater load. In addition, pile head restraint could have been reduced somewhat.

If it is assumed that the mass mixed wall is providing nearly all of the increased lateral resistance observed in test 9, then the moment versus load curve for test 9 would be expected to be very similar to that observed for test 1. In contrast, if the mass mixing is increasing the resistance provided by soil pile interaction, then greater moments would be expected for a given load. To make an accurate comparison, the increase in load observed in test 9 was removed from the total load when plotting the load versus moment curve shown in Figure 6-3 under the assumption that all increased resistance came from the mass mixed wall. When this was done, the moment versus load curve for test 9 plotted near the high end of curves obtained from test 1 thus illustrating that the resistance from pile-soil interaction was essentially the same and that mass mixing indeed did little to improve the soil-pile interaction.

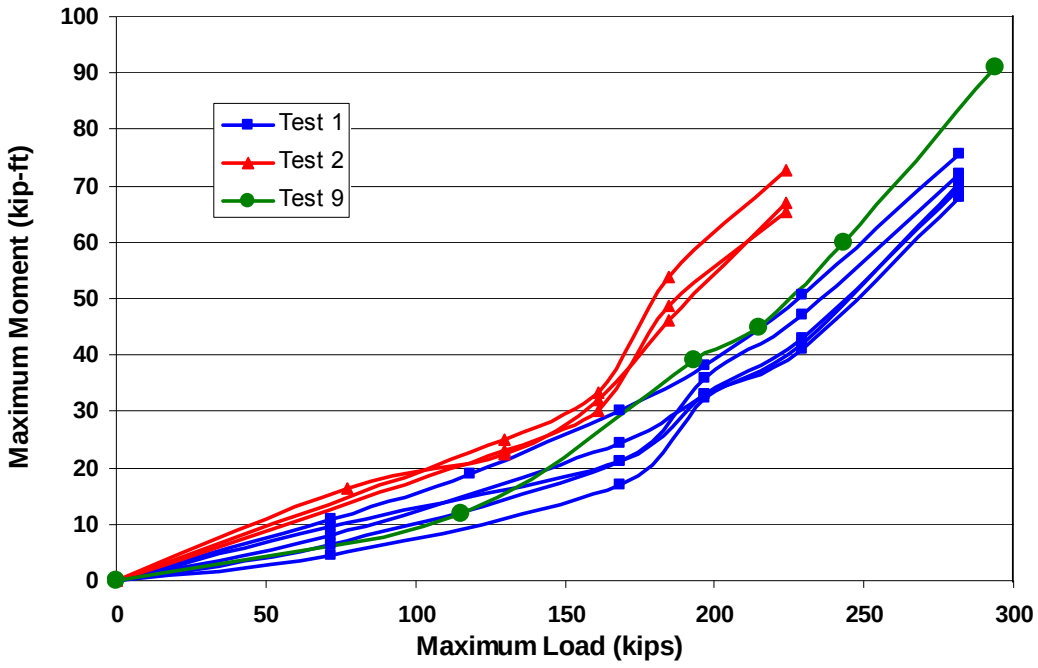

Figure 6-3 – Maximum positive bending moment versus load comparisons of tests 1, 2 and 9 for pile cap 1.

Although it does appear that bending moments at greater loads for test 9 plot slightly higher than for test 1, this is most likely due to reloading effects. As piles experience cyclic loading such as occurred in pile cap 1 during these tests, the stiffness of the soil around the piles is reduced and gaps are formed due to the shear stresses induced by the lateral loads. This reduction in resistance causes more of the stress to be transferred to the pile thus generating slightly larger bending moments for a given load. For example, during tests on piles in similar clays, Snyder (2004) observed an increase in maximum moment for a given load of about 15% after 15 cycles of loading. Overall, the adjusted bending moment versus load curve for test 9 after mass mixing is in close agreement to the bending moment versus load plot of the virgin clay test 1, thus supporting the contention that 90% to 100% of the increase lateral resistance observed through mass mixing can be attributed to passive and side shear resistance on the wall and that minimal improvement was from soil-pile interaction.

The sources of the increased lateral resistance are also consistent with the geometry involved. When the mass mixed wall was in contact with the pile cap, lateral movement of the pile cap would push the wall laterally so that passive force on the back of the wall and shear on the base and side of the wall would develop increased lateral resistance. When the connection between the soil mixed wall and the pile cap was eliminated in test 15, this lateral resistance would not develop unless the piles impinged on the wall. Unfortunately, a 1.5-ft wide zone of soft clay remained between the piles and the wall which could not be treated by mass mixing due to the presence of the pile cap. Therefore, lateral movement of the piles would

result in deformation in the soft clay, but would not likely lead to any significant deformation of the wall. The clay soil between the front row of piles merely displaced around the piles and the mass mix treated soil, thus never engaging the strengthened soil. Without the direct connection between the cap and the mass mixed wall, this zone of weak clay would not transfer the load applied from the piles to the strengthened mass mix zone. This explains why increases in lateral resistance from soil-pile interaction would likely be relatively small while no increase in lateral resistance would be expected from movement of the mass mixed wall.

6.2 Potential Failure Mechanisms

Although the 60% increase in lateral resistance appears to result from the movement of the mass mixed zone, it is not immediately apparent how this resistance was generated and what failure mechanisms were involved. To answer this question a few scenarios need to be considered. One scenario is that the mass mixed zone could have sheared and thus only a portion of it really contributed as shown in Figure 6-4 . Another scenario is that the whole zone of mass mix acted as a rigid block of soil against the weak clay behind it as shown in Figure 6-5.

To consider the first scenario that the mass mix sheared, the shear strength of the mass mix along a potential shear plane would need to be estimated. Assuming that the mass mix did indeed have a consistent unconfined compressive strength of 140 psi, its shear strength, τ, would be one-half of the unconfined compressive strength or 70 psi, which is equal to 10,080 psf. By multiplying that shear strength by the shear area of 11 feet by 4 feet, the shear capacity of the mass mix would be

about 440 kips. The maximum load applied to cap 1 in test 9 was about 465 kips at the caps greatest displacement of 1.75 inches. However, not all of that 465 kips would have been transferred to the mass mix zone, as some load would be taken by

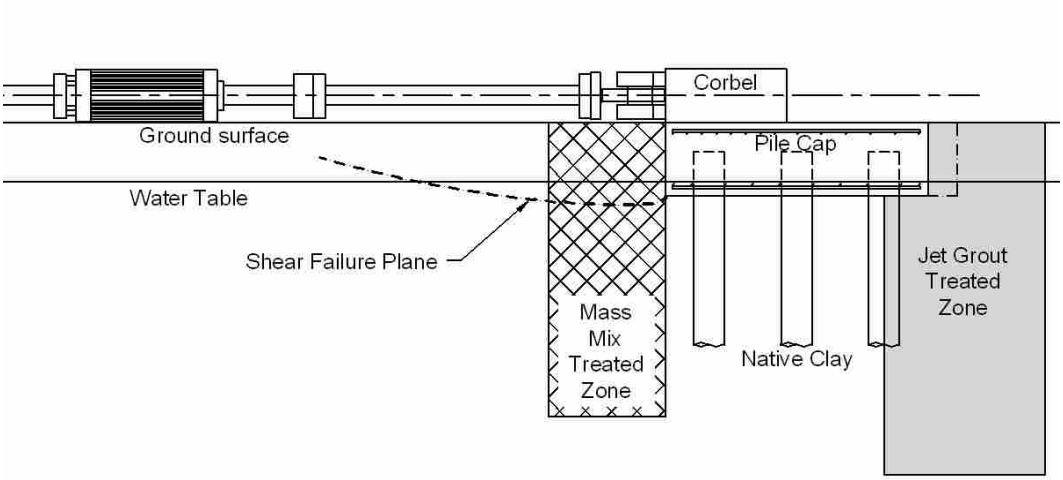

Figure 6-4 – Profile view of a shear failure scenario for the mass mixed soil improvement.

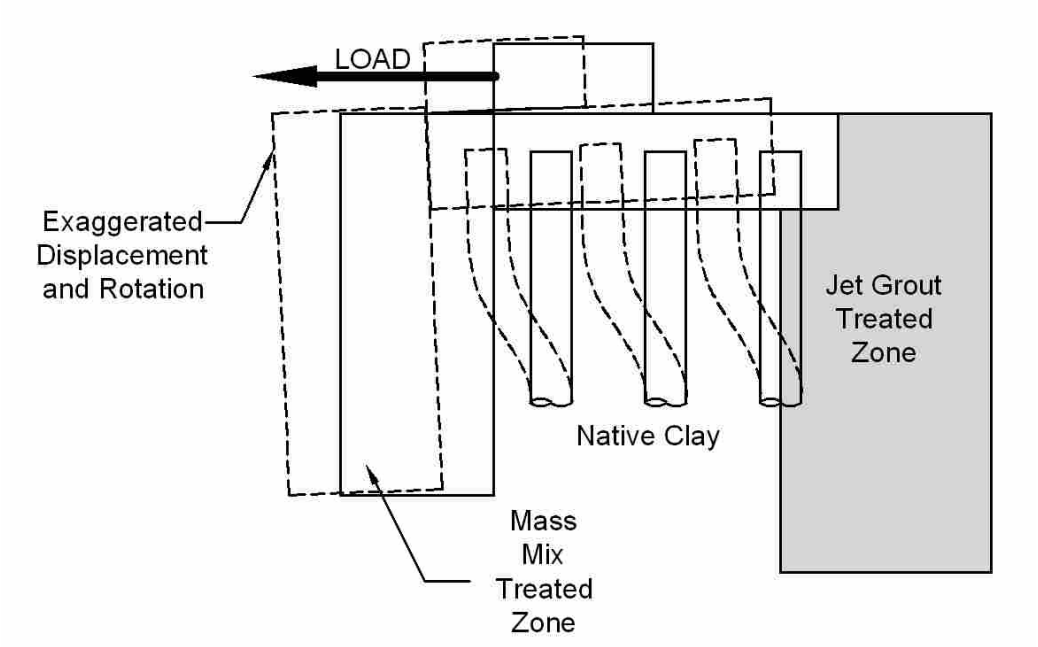

Figure 6-5 – Profile view of the mass mixed zone acting as a rigid block as it was displaced.

the piles. When examining the load-displacement results from test 15, only 235 kips was applied at the 1.75 inch displacement. Since it has been established prior that the increase in lateral resistance is primarily due to passive and side frictional forces acting on the mass mixed zone, the ultimate load the mass mixed zone would have experienced directly from the pile cap would have been the difference of the 465 and 235 kips which is 230 kips. Thus, only about 230 kips would be transferred to the mass mix, which is substantially less than the shear capacity of the mass mix wall making it highly unlikely that a shear failure occurred.

Additionally, because a shear failure is likely to be a brittle failure in soil-crete there should be some discontinuity in the load-displacement curves followed by a decrease in strength if a shear failure occurred. When examining the load-displacement curve for test 9 in Figure 6-1 and Figure 5-38, no such discontinuity occurred. Instead the slope of the curve seems to be smooth and although decreasing, still never reaches a minimum which would denote a failure.

6.3 Calculation of the Ultimate Lateral Force Provided by the Mass Mixed Zone

A better understanding of the forces acting on the mass mixed zone would be helpful in understanding the behavior of the zone and in analyzing potential failure mechanisms from shear and bending. This analysis would also be useful in determining if the increased lateral resistance produced by the mass mixed wall can be adequately accounted for using basic geotechnical design concepts.

Figure 6-6 (a) shows a free body diagram with all the forces acting on the mass mixed zone. (Hand calculations for the forces shown in the free body diagram

are provided in Appendix B). The passive resistance consisted of 61 kips from the ground surface to a depth of 2.5 feet and 105 kips between a depth 2.5 and 10 feet. The passive force of 61 kips was calculated based on an average undrained shear strength of 1040 psf and a unit weight of 117 pcf for the clay from the ground surface to a depth of 2.5 ft acting over the 11 ft length of the mass mixed wall. This 1040 psf shear strength was back-calculated based on Rankine theory from the results of test 2 which showed that approximately 50 kips of passive force was provided by the virgin clay acting on the pile cap which was 9 ft wide and 2.5 ft deep. The Rankine theory applies the passive force equation

$$\frac{1}{2}(\gamma)(H^2)(W)(K_p) + 2(C_u)(H)(W)(\sqrt{K_p}) \qquad \textbf{(6-1)}$$

where γ is the unit weight of soil, H is the height of the wall or pile cap, B is the base width, c_u is the undrained cohesion or undrained shear strength of the soil, and K_p is the passive earth pressure coefficient. For undrained conditions which are assumed for this situation, K_p is equal to 1.0. This strength value is reasonably consistent with the strength estimated by the CPT testing at the site (see Figure 3-3), but somewhat higher than would be expected based on the torvane tests and unconfined compression test. The higher strength in this zone could be attributed to the partially saturated condition of the soil in this depth range during the testing.

Further analysis, that will be presented later, found that the average shear strength of the first 10 feet of the soil profile was about 475 psf. To be consistent with that average shear strength and since the first 2.5 feet was 1040 psf, then the

average shear strength for the clay between 2.5 to 10 feet below the ground surface would have to be around 287 psf which is consistent with the findings of the geotechnical site investigation (see Figure 3-3). The lower portion of the passive resistance in Figure 6-6 (a) was calculated using Rankine theory assuming this shear strength of 287 psf and a unit weight of 112 pcf.

The shaded portion in Figure 6-6 (a) represents the mass mixed zone and the arrows in that portion represent the side and bottom shear resistance due to skin friction or cohesion. Each of the components of the side resistance was based on the corresponding soil shear strength described previously and the bottom resistance was based on the shear strength of 350 psf as denoted in the geotechnical site investigation for 10 feet below the ground surface. In all calculations the width of the mass mixed wall was taken as 4 ft. The total resistance due to skin friction was calculated to be 54 kips and combined with the 166 kips of passive resistance they produced the overall soil resistance of 220 kips. Since the additional lateral resistance of the pile cap produced by installation of the mass mixed wall was between 220 and 230 kips, this analysis further bolsters the conclusion that nearly all of the increased lateral resistance was due to passive force and shear resistance on the mass mixed wall. The small difference between computed and measured resistance may be attributed to a slight increase in the soil-pile interaction or uncertainties in the soil strength parameters and geometry of the mass mixed zone.

After taking into account all the sources of resistance on the mass mixed zone, a more accurate estimate of the shear forces within the mass mix zone can be obtained. The shear diagram in Figure 6-6 (b) shows that the maximum shear the

mass mixed zone would experience is about 140 kips, which is significantly lower than the shear capacity of 440 kips, further supporting the contention that the mass mixed zone did not fail in shear.

Another failure mechanism to consider in conjunction with shear is failure due to bending. Figure 6-6 (c) shows the bending moment diagram derived from the shear diagram. From the diagram, the maximum moment applied to the mass mixed zone would be about 170 kip-ft. Typical tensile strength for concrete occurs on order of about 8% to 15% the unconfined compressive strength (MacGregor 2005). If it is assumed that the mass mix would crack at about 15% of its unconfined compressive strength of 140 psi, then its theoretical bending moment to initiate cracking would be about 89 kip-ft. (Hand calculations for this procedure are found in Appendix B.) Since the maximum moment was about 170 kip-ft, this would imply that the mass mixed zone would likely have cracked along its tensile face closest to the pile cap. To have adequate capacity in bending, the mass mix would have to have an initial tensile capacity of about 30% of its unconfined compression strength. It is a possibility that the soil-crete nature of the mass mix might allow for a higher tensile stress, however, further testing would need to be done to quantify this assumption. Although no load-displacement data from the unconfined compression tests was recorded, it was observed that the mass mix cored samples failed in a slightly more ductile manner compared to samples of jet grout and pile cap concrete. This small degree of ductility could make it possible for the mass mixed zone to slightly crack and not completely sever into two separate components.

Another consideration in evaluation the bending moment capacity of the mass mix zone, is to consider the bottom boundary condition of the mixed zone. Since it is a likely possibility that the mass mixed zone experience some degree of horizontal translation at the bottom zone, due to the large displacements at the load point and minimal measured rotation on the pile cap, this would not model a typical fixed boundary condition and as a result actually lower the bending moment applied to the mass mixed zone. However, additional testing would have to be done to quantify this possibly.

Even though the tensile face of the mass mixed zone could have cracked, it is likely that the side in compression would have remained intact and allowed the native soil in contact with the mass mixed zone to develop the passive resistance along the entire mass mixed zone. A complete failure in bending simply could not explain the fact that the passive resistance and side shear from the soil around the entire mass mixed zone was equal to the observed increase in lateral resistance. The mass mixed zone may have cracked along the tensile face, but there is no evidence that it cracked into two separate components denoting a failure in bending during testing. Ultimately, further testing and analysis needs to be done to accurately quantify the bending capacity of a mass mixed zone.

Since there was no evidence of a shear failure and a failure in bending seems unlikely, it is believed that the mass mix acted as a rigid zone of soil against the weaker clay behind it. This conclusion would suggest that 90% to 100% of the strength increase observed by the mass mix was due to the passive force behind the cap in conjunction with the skin friction on the bottom and sides.

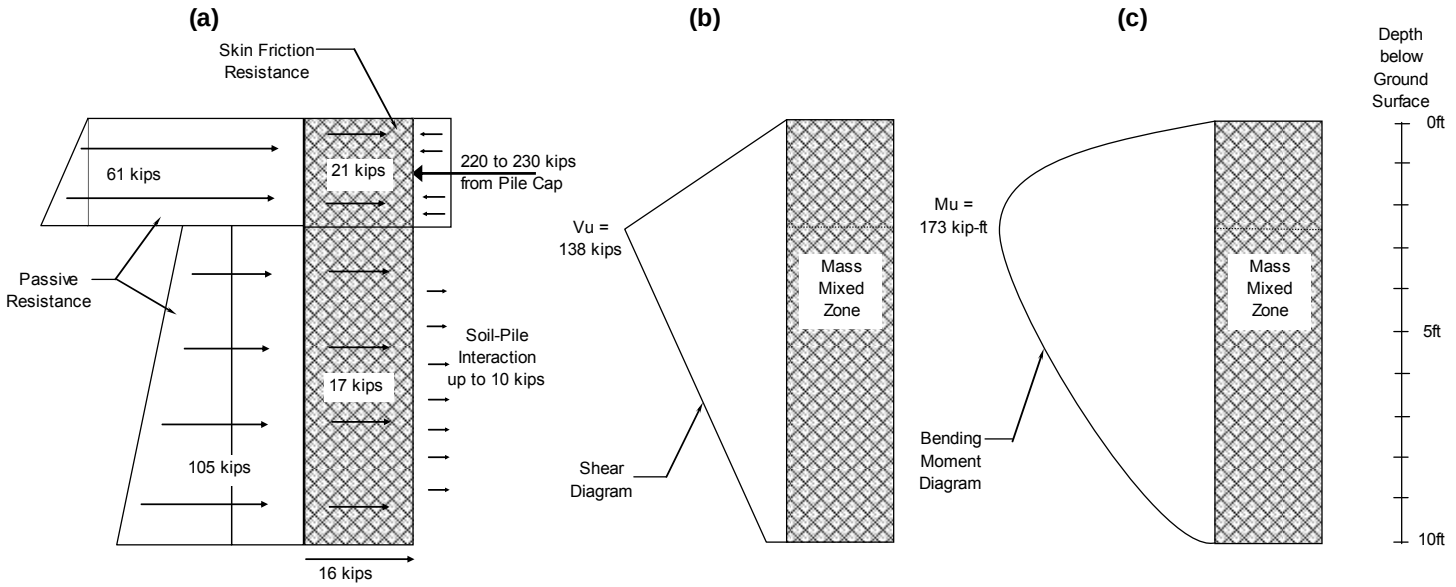

Figure 6-6 – (a) The free body diagram defining all the forces on the mass mixed zone as passive resistance, skin friction resistance, soil pile interaction, and the load transferred from the pile cap. (b) The shear diagram of the mass mixed zone defining the maximum shear as 138 kips at a depth of 2.5 feet below the ground surface. (c) The bending moment diagram of the mass mixed zone defining the maximum bending moment as 173 kip-ft at a depth of 2.5 feet below the ground surface.

The total strength increase was measured by subtracting the load-displacement results of test 2 from that of test 9 at 1.5 inches of displacement, which is about 220 kips. This is also consistent with taking the overall strength increase of 170 kips obtained by subtracting the load-displacement results of test 1 from test 9 and adding the 50 kips of passive resistance obtained from subtracting the load-displacement results of test 1 from test 2. If the entire mass mix zone did indeed contribute to the increase in lateral resistance, this 220 kips should be equal to the passive resistance of the clay directly behind the mass mix zone along with side and bottom skin friction or cohesion.

6.4 Computed Lateral Force-Displacement Relationships

The total lateral force-displacement curve for the mass mixed wall is the resultant of the passive force-displacement curve and the shear force-displacement curve. Typically, the shear resistance on the side of a wall or a pile has been found to develop with relatively small movements while passive force develops after larger movements. Therefore, the lateral force-displacement curves for each component of force were developed separately and then combined to compute the total lateral force-displacement curve for the mass mixed wall.

The force-displacement behavior of the soft clay against the mass mix wall was computed using the spreadsheet PYCAP developed by R.L. Mokwa and J.M. Duncan (2001). The spreadsheet computes the ultimate passive force and then uses a hyperbolic curve to compute the development of passive force with displacement. For the undrained loading case, with ϕ=0, PYCAP computes the ultimate passive

force using the Rankine theory and shear zones at the end of the wall are assumed to form parallel to the direction of loading so that 3-D effects need not be considered. PYCAP develops the hyperbolic force-displacement curve using the initial soil modulus to define the initial stiffness and the ultimate passive force as an asymptote as shown in Figure 6-7.

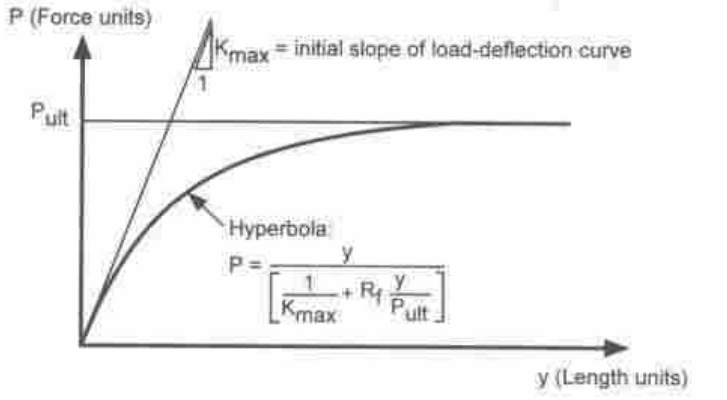

Figure 6-7 – Graphic of the hyperbolic model (Duncan 2001).

Using the hyperbolic model in PYCAP, a hyperbolic curve was computed to define the passive force-displacement curve using the input values in Table 6-1. To do this the mass mix was treated as a pile cap being 11 feet wide and 10 feet deep. The initial soil modulus, E_i in kips/ft^2 was estimated using the equation

$$E_i \approx \frac{15 \cdot C_u}{PI(\%)} \qquad \textbf{Equation 6-2}$$

where c_u is the undrained shear strength of the soil in kips/ft^2 and PI is the plasticity index in percent which was developed by (Termaat, 1985). For this analysis the plasticity index was taken as 25% based on the geotechnical investigation. It was

also assumed that the ultimate resistance would be developed for a wall movement of equal to about 1.5% of the wall height based on findings by Brandenberg (2005) for naturally occurring cohesive soils. Table 6-1 shows an ultimate force which is the horizontal component combined with the vertical. Since this analysis is measuring lateral resistance, only the horizontal component of the passive force was considered. To do this, the vertical component which is the shear strength time the pile cap area was subtracted from the ultimate force.

In a first analysis, just the passive resistance of the soil behind the wall was considered, however, the average undrained shear strength for the soil needed to be around 725 psf to obtain the total resistance measured shown in Figure 6-10. This value is high compared with the results in the Geotechnical Site Characterization section found in chapter 3 which suggests that an average shear strength for the first 10 feet of the soil profile would be around 450 to 500 psf. If the mass mix zone was acting as a rigid block then it would be necessary to consider the cohesion on the sides and bottom of the mass mixed wall in computing the total passive resistance.

As indicated in the previous section, about 166 kips of force can be attributed to passive force on the mass mixed wall while an additional 54 kips would be due to shearing on the side and base of the mass mixed wall. Based on a Rankine analysis, an ultimate passive force of 166 kips would be predicted for an average undrained shear strength or undrained cohesion of 475 psf in the upper 10 ft of the soil profile. This overall average is consistent with an average undrained shear strength of 1040 psf in the upper 2.5 ft of the profile and an average undrained shear strength of about 285 psf in the range from 2.5 ft to 10 ft below the ground surface. To simplify the

PYCAP analysis the passive force-displacement curve for the native clay was computed using 475 psf for the average undrained shear strength from the ground surface to the base of the wall at a depth of 10 ft. The computed passive force-displacement curve using this approach is presented in Figure 6-8.

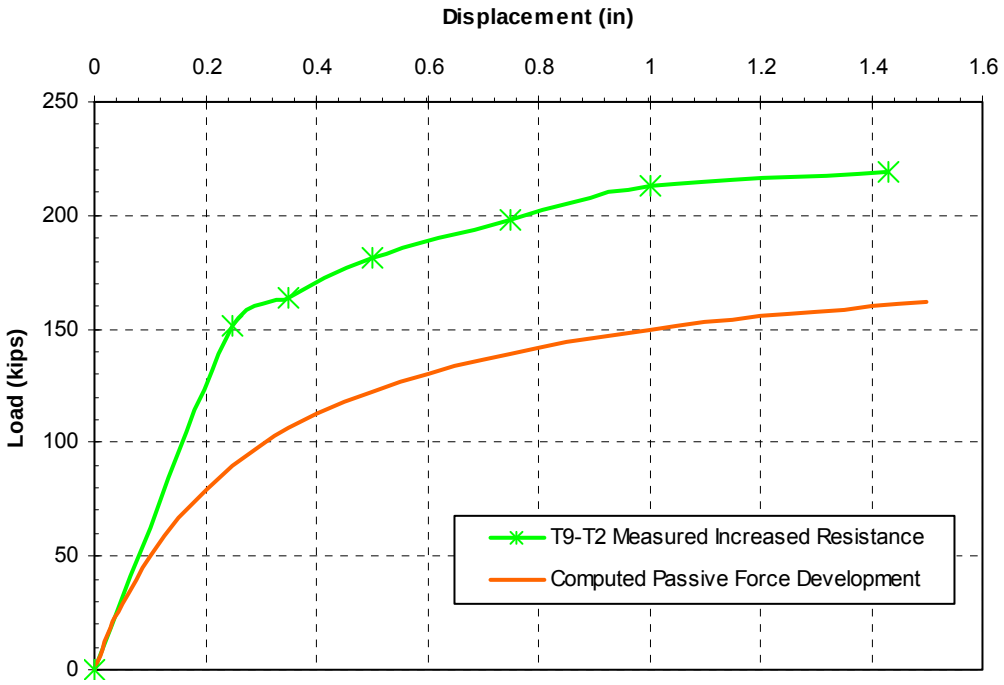

Figure 6-8 - The portion of the measured increased total resistance due to passive force behind the mass mixed zone as computed by PYCAP.

To compute the development of the force due to side shear and base shear, it was necessary to estimate the movement required to develop full skin friction resistance. Evaluation of current literature suggests that maximum skin resistance based on load tests for both piles and drilled shafts is on the order of 0.12 to 0.4 inches (Bowles 1996). Another source suggests that skin friction is mobilized at about one-tenth of the displacement required to mobilize the end bearing resistance

(Budha 2007). In the PYCAP analysis, a displacement equal to 1.5% of the mass mixed zone height was used as the displacement necessary to develop full passive resistance. Using the method suggested by Budah, considering the passive resistance behind the mass mixed zone as end bearing, a displacement equal to one-tenth of 1.5% times the height of 10 feet (0.18 inch) would be necessary to mobilize full skin friction. This value is consistent with the range suggested by Bowles and for simplicity was rounded up to 0.2 for use in these simplified analysis. Therefore, the development of side shear and base shear was assumed to be linear up to a displacement of 0.2 inch and then remain constant. Figure 6-9 provides a plot the development of the skin friction reaching the full resistance of 55 kips by 0.2 inch and then remaining constant.

Finally, the computed passive force-displacement curve and the computed side and base shear curves shown in Figure 6-8 and Figure 6-9 were combined by superposition to produce the computed lateral force-displacement curve shown in Figure 6-10. For comparison purposes the measured force-displacement curve representing the total increased resistance for the mass mixed wall is also shown in these three figures. The measured lateral force-displacement curve was obtained by subtracting the load-displacement curve for test 2 involving the pile cap 1 in the virgin clay with no soil adjacent to the pile cap from the load-displacement curve for pile cap 1 in test 9 where the mass mixed wall was in place. The computed lateral force-displacement curve is almost a perfect fit to the measured lateral force-displacement curve from the mass mix test, which supports the contention that essentially all of the increased lateral resistance from the mass mix soil improvement

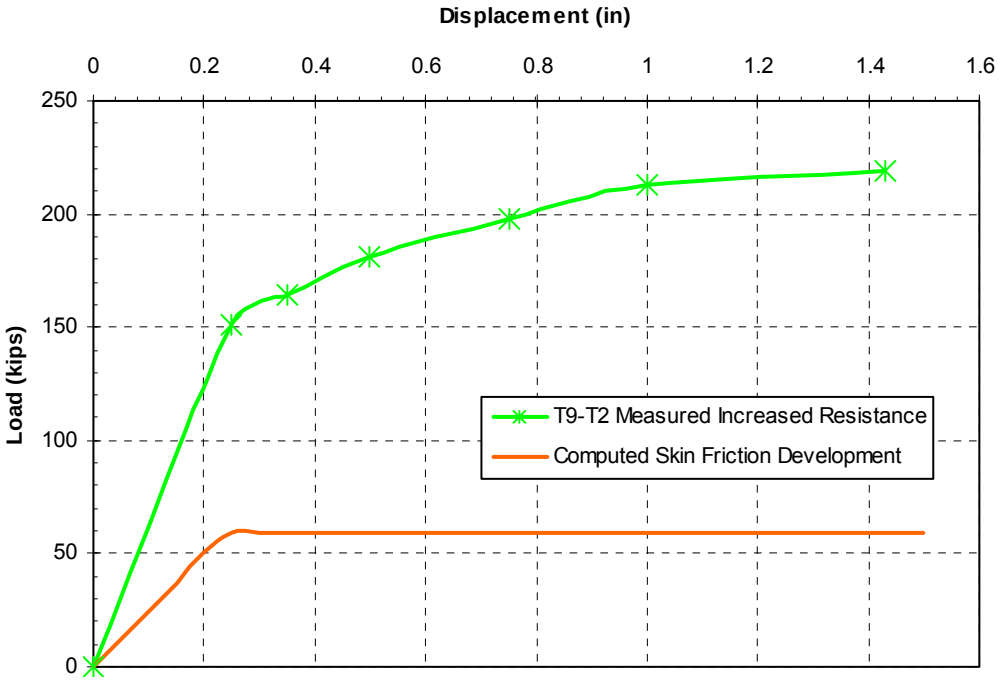

Figure 6-9 – The portion of the measured increased total resistance due to side and bottom skin friction of the massed mixed zone as computed by PYCAP.

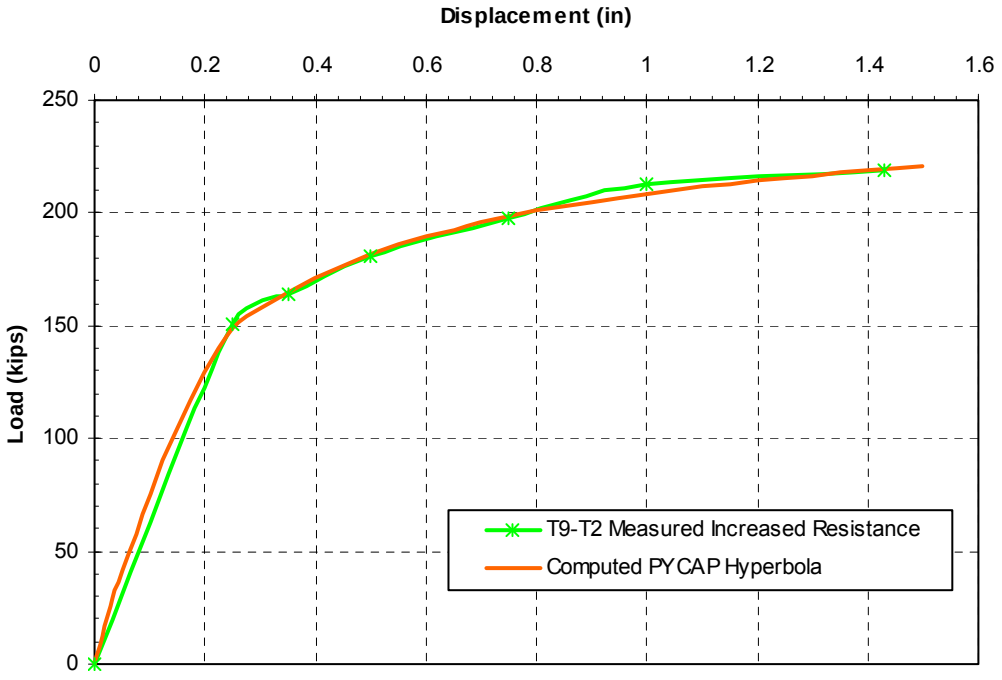

Figure 6-10 – Comparison of the computed PYCAP hyperbolic method to the measured increased resistance obtained by subtracting the load-displacement curve of test 2 from test 9.

Table 6-1 – Input and output values from the PYCAP analysis treating the mass mix as a rigid body 11 feet wide and 10 feet deep.

Input Values (red)		
cap width,	b (ft) =	**11.00**
cap height,	H (ft) =	**10.00**
embedment depth,	z (ft) =	**0.00**
surharge,	q_s (psf) =	**0.0**
cohesion,	c (psf) =	**475.0**
soil friction angle,	ϕ (deg.) =	**0.0**
wall friction,	δ (deg.) =	**0**
initial soil modulus,	E_i (kip/ft^2) =	**285**
poisson's ratio,	ν =	**0.50**
soil unit weight,	γ_m (pcf) =	**112.0**
adhesion factor,	α =	**1.00**
Δ_{max}/H, (0.04 suggested, see notes) =		**0.015**
Calculated Values (blue)		
K_a (Rankine) =		**1.00**
K_p (Rankine) =		**1.00**
K_p (Coulomb) =		**1.00**
$K_{p\phi}$ (Log Spiral, soil weight) =		**Rankine Kp**
K_{pq} (Log Spiral, surcharge) =		**Rankine Kp**
K_{pc} (Log Spiral, cohesion) =		**Rankine Kp**
E_p (kip/ft) =		**15.10**
Ovesen's 3-D factor, R =		**1.000**
k_{max}, elastic stiffness (kip/in) =		**677.3**
		phi = 0 Solution
$P_{ult\ (horz+vert)}$ (kips) =		**224.3**
Horizontal values using the Log Spiral theory		
Phorz 2-D (kips) =		166.1

was due to passive resistance or side/base shear against the soil mixed wall as the pile cap pushed the wall laterally.

Additionally, to verify the results of the PYCAP analysis, a hyperbolic curve was also fit to the measured passive force-displacement curve obtained from the tests on the pile caps in virgin clay. This was done by subtracting the load-displacement curve for pile cap 1 in test 2 from the load-displacement curve for pile cap 1 in test 1 as shown in Figure 6-11, then varying the inputs slightly so that the PYCAP model would equal the ultimate horizontal passive force of 50 kips as observed in the field

tests. The input values remained fairly consistent with the soil profile from chapter 3 Geotechnical Site Characterization and are shown in Table 6-2. The cap dimensions were updated to that of the actual pile cap being 9 feet wide and 2.5 feet deep. The shear strength used in this comparison needed to be around 1040 psf which is high, but in the range of the CPT tests for the first 2.5 feet below the ground surface. In addition, displacement necessary to mobilize full passive, (Δmax) was increased to 2% of wall height (H) as it provided a somewhat better fit than the 1.5% value used previously.

The computed passive force-displacement curve is plotted along with the measured curve in Figure 6-11. Overall, the hyperbolic method fit the virgin soil passive curve reasonably well. However, there appears to be a discrepancy with the initial soil modulus. The slope of the initial soil modulus from the hyperbolic model appears to be too steep compared to the virgin clay passive curve. This discrepancy may in part be due to difficulties in making direct comparisons with the measured field test results at these small displacement levels. Due to the initial offset and gap effects, there is no accurate data for the passive force-displacement curve between 0 and 0.25 inch, which could account for the discrepancy in the slope.

In summary, the computed force-displacement curves indicate that the increase in the lateral resistance recorded in the mass mix soil improvement tests, did come as a result of the mass mix zone acting as a rigid body 11 feet wide and 10 feet deep against the weaker clay behind it. This in turn increased the surface area that the clay could react against and also allowed for additional resistance to develop through skin friction along the sides and bottom, thus increasing the overall lateral resistance

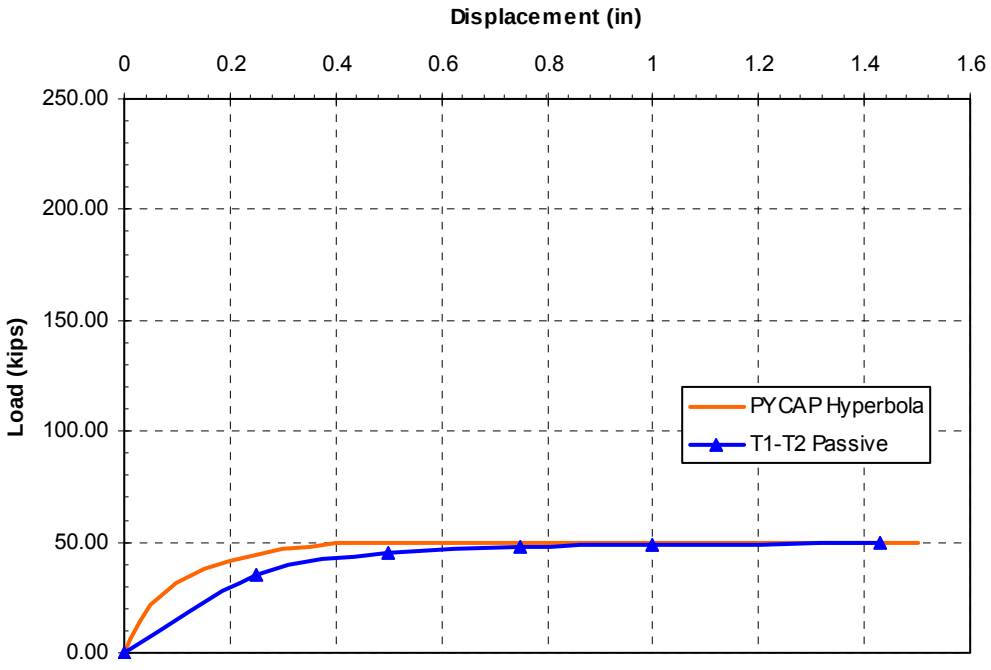

Figure 6-11 - Comparison of the PYCAP hyperbola method to the passive force obtained by subtracting the load-displacement curve from test 2 from test 1.

of the native clay by a factor of 1.6. The results of these analyses also suggest that the increased resistance from installing a mass mixed wall can be reasonably well predicted using well-established geotechnical design concepts associated with the development of passive force and side/base shear in clays.

It needs to be noted that the conclusion of this analysis was based on the likelihood that a small amount of horizontal translation on the order of 0.12 inches or greater (Bowles 1996) occurred at the base of the mass mixed zone sufficient to develop a resistance due to base shear. Considering the maximum top surface displacement of 1.75 inches of the mass mixed zone, the small rotation of 0.35 degrees measured on the pile cap at that displacement, and the relative shear or rigid strength of the mass mixed zone it does seem highly likely that the bottom surface

Table 6-2 - Input data for the PYCAP analysis for the virgin soil directly behind the pile cap.

Input Values (red)		
cap width,	b (ft) =	**9.00**
cap height,	H (ft) =	**2.50**
embedment depth,	z (ft) =	**0.00**
surharge,	q_s (psf) =	**0.0**
cohesion,	c (psf) =	**1040.0**
soil friction angle,	ϕ (deg.) =	**0.0**
wall friction,	δ (deg.) =	**0**
initial soil modulus,	E_i (kip/ft^2) =	**624**
poisson's ratio,	ν =	**0.50**
soil unit weight,	γ_m (pcf) =	**117.0**
adhesion factor,	α =	**1.00**
Δ_{max}/H, (0.04 suggested, see notes) =		**0.020**
Calculated Values (blue)		
K_a (Rankine) =		**1.00**
K_p (Rankine) =		**1.00**
K_p (Coulomb) =		**1.00**
$K_{p\phi}$ (Log Spiral, soil weight) =		**Rankine Kp**
K_{pq} (Log Spiral, surcharge) =		**Rankine Kp**
K_{pc} (Log Spiral, cohesion) =		**Rankine Kp**
E_p (kip/ft) =		**5.57**
Ovesen's 3-D factor, R =		**1.000**
k_{max}, elastic stiffness (kip/in) =		**717.8**
		phi = 0 Solution
$P_{ult\ (horz+vert)}$ (kips) =		**74.3**
Horizontal values using the Log Spiral theory (Brinch Hansen)		
Phorz 2-D (kips) =		50.1

would at least translate horizontally a minimum of 0.12 to 0.2 inches to develop a shear force along the bottom surface. However, it is still a possibility that the bottom surface of the mass mixed zone did not translate horizontally and instead the mass mixed zone merely rotated. If this were the case, very similar ultimate loads and load-displacement curves would be obtained if it was assumed that the average shear strength between 2.5 and 10 feet below the ground surface was 340 psf instead of the

285 psf used in the analysis considering base shear. This higher average shear strength would still be in reasonable agreement with the measured strength profile. To completely validate either approach, further testing or numerical model analysis would need to be done to better establish the actual behavior at the interface between the bottom of the mass mixed zone and the underlying clay.

6.5 Displacement versus Depth Discussion

The primary instrumentation used to measure the displacements and moments at various depths were the shape arrays. Despite some minor incongruities, the shape arrays proved to be fairly reliable when compared to the secondary instrumentation of string potentiometers, inclinometers, and strain gages.

The displacement versus depth profiles for all tests showed that the majority of displacement first occurred between 23 to 25 feet below the top of the corbel, with maximum curvature occurring between 15 and 19 feet. Then in most cases a fairly linear trend of displacement occurred from 15 feet to the load point around 1 foot below the top of corbel. These displacement versus depth profiles were then used to derive the bending moments for each test.

6.6 Bending Moment versus Depth Discussion

When comparing the bending moments from the virgin clay test (test 1) to the mass mix soil improvement test (test 9), the locations of the maximum bending moments appeared to increase in depth as the lateral load applied to the piles increased. Although, at greater displacements and loads the location of the

maximum bending moment tended to consistently range between 11 and 12 feet below the bottom of the pile cap. Since the height from the top of corbel to the bottom of cap is 4.33 feet, this is consistent with the trend of maximum curvature seen in the displacement versus depth profiles that the datum taken from the top of corbel. The magnitude of the positive bending moments were slightly higher for the mass mix test, which is mainly due to the fact that the displacements were higher than the virgin clay test. Overall, the location of the maximum positive bending moment remained relatively the same.

The magnitudes of the negative bending moments were difficult to measure and estimate as was evident to the inconsistencies between the arrays and strain gages, especially in the mass mix tests. If the trends of the negative bending moments for test 9 in Figure 5-44 were to continue to the vicinity of the strain gages at the bottom of the cap the magnitude would be about 15 to 20 kip-ft lower than those observed from test 1. There is no reasonable explanation for this other than the general discrepancies brought about by the disagreement in the instrumentation as the material properties, especially EI, change as the piles begin to enter the pile cap.

When comparing the bending moments from the no passive case tests 2 and 15, the locations of the positive bending moments for test 2 occurred between 11.5 and 13.5 feet, while the depth remained fairly constant in test 15 around 12.5 feet. When test 1 and 2 were compared at the end of 5.2.4 it was thought that the location of the maximum positive bending moment actually lowered in the no passive case, but when looking at the results comparing the two no passive cases it merely appears that the locations recorded in test 2 might just be lower than it actually was. The

magnitudes of the positive moments in test 15 are significantly higher due to the almost double displacements than that of test 2.

There were a few discrepancies between the instrumentation measuring the magnitudes of the maximum negative moments occurring at the bottom of the cap for the no passive cases. However, the middle pile in test 2 appears to have good agreement with the strain gages and is a good comparison for test 15. The moments derived from the array during test 15 measure 20 to 30 kip-ft higher than test 2 which would be expected since test 15 almost doubled the displacement of test 2.

Finally, when looking at the trends between the test 1 and 2 the virgin clay test, the magnitudes of the positive bending moments decreased slightly, while the negative moments remained within a range of plus or minus 10 kip-ft. The location of the positive moments appeared to have dropped about 1 foot, but this is most likely due to an inconsistency with moment locations derived by test 2. The location of the maximum negative moments remained at the bottom of the cap.

Due to the different test increments between test 9 and 15, the mass mix tests, few direct comparisons can be made in regards to the locations for the maximum bending moments. The virgin clay tests might give the most insight as the behavior of the moments in regards to a passive and no passive case. It can be observed though, based on the inclinometer and stain gage readings for test 9 and the arrays for test 15, that the location of the maximum positive moments tended to stay the same for the mass mix tests especially at the greater load and displacement increments.

6.7 Basic Cost and Effectiveness Considerations

It was observed that mass mixing improved the lateral resistance of the pile group by 170 kips. The cost of producing this increased lateral resistance due to soil improvement also needs to be quantified to determine if it can be considered as not only a viable solution, but as a cost-effective solution as well. To do this a rough estimate of the cost incurred to produce the soil mixed wall will be compared to the alternative of adding more piles and a larger pile cap.

The basic approach for mass mixing taken in this experiment consisted merely of three elements: a grout slurry, an excavator or track hoe, and an operator. A grout slurry with an unconfined compression strength of 140 psi can be ordered from any concrete supplier. One local supplier in Salt Lake City, Utah charges about $50 per cubic yard. The volume needed for this application of mass mixing was about 9 cubic yards and would result in a cost of about $450. The track hoe rented for the project cost about $1000/day with a $200/hr charge for an operator. The whole mass mixing process took less than 8 hours to complete which would cost about $2600. As a minimum, the total cost of the mass mixing soil improvement was around $3000.

One alternative to mass mixing would be to simply add more piles and increase the size of the pile cap. According to the test results for cap 1 during test 2, the maximum load taken by the piles was about 230 kips. If this load is distributed evenly, each pile would have carried about 26 kips. To obtain the same lateral resistance of 170 kips that the mass mix achieved, about 7 piles would have to be added, thus making a new 4x4 pile configuration. Steel pipe pile costs during the

project were on the order of $30/ft. Assuming typical pile lengths of 80 feet, 7 additional piles would cost $16,800. Mobilization and driving costs were about $15,000 plus $8/ft of driving. Therefore, the 7 additional piles would cost $20,120 to drive into place. Assuming the same pile spacing of 3 feet on center, the new pile cap would have dimensions 12'x12'x2.5' and would have a volume of 360 cubic feet. If the volume of the existing pile cap is subtracted from the 360 cubic feet the net additional volume of concrete needed for the additional pile cap would be 157.5 cubic feet or about 6 cubic yards. The average cost for concrete and reinforcement on the project was about $300 per cubic yard. That would amount to $1,800 for the additional pile cap. The volume of concrete needed to fill the additional 7 piles would be about 16 cubic yards and would amount to an additional $4800 of concrete and steel. The total estimated cost to obtain the same improvement in lateral resistance as the mass mix by adding additional piles and increasing the pile cap would be about $44,000. In conjunction with the increased costs is also the increased time to add the 7 new piles and construct a new pile cap. The amount of time to construct the additional pile foundation would vary depending on number workers and experience. Considering the crane mobilization time and driving rate of the crew on the project, the seven new piles could be placed in about 1 day, with an additional 2 days to tie rebar and pour concrete, resulting in about an additional 3 days.

The cost difference between $3,000 for the mass mix improvement and the $44,000 for additional piles appears to be significant. Therefore, a value engineering assessment would probably recommend soil improvement, if other factors were

equal. Of course, this analysis is rough and the cost difference may be somewhat closer, nevertheless, this example clearly illustrates how mass mixing can be a viable and cost-effective solution to increasing the lateral resistance of driven pile foundations.

7 Conclusions

In light of the findings in this thesis the following conclusions can be made in regards to using mass mixing as a soil improvement method to increase the lateral resistance of deep foundations in cohesive soils.

- Mass mixing with a cement content of approximately 13 lbs/ft^3 was able to increase the average compressive strength of a soft, plastic clay from an average of 6 to 8 psi to an average of 140 psi. This result is consistent with past performance.
- Construction of a mass mixed wall (10 ft deep, 4 ft wide, and 11 ft long) adjacent to an existing pile cap (9 ft square and 2.5 ft deep) increased the lateral resistance from about 280 kips to 450 kips at a displacement of 1.5 inches. This increase of 170 kips represents a 60% increase in lateral resistance.
- Subsequent testing, after excavation of the mass mixed wall to the base of the pile cap, indicates that essentially all of the 170 kip increase was due to passive resistance and side/base shear against the soil mixed wall as the pile cap pushed the wall laterally.

- No appreciable increase in lateral resistance could be attributed to soil-pile interaction. This is likely due to the fact that back of the mass mixed wall was about 1.5 feet away from the first row of piles.
- Analyses suggest that the shear strength of the mass mixed wall was sufficient to allow the wall to behave as a rigid block. Since the mass mixed zone extended 7.5 feet below the base of the cap, it essentially increased the surface area that the native soil could react against. Reasonable estimates of the lateral resistance for the wall can be obtained by considering passive force on the face of the wall and shear on the sides and base of the wall.
- Analyses of passive force versus deflection response indicate that passive force in the soft clay was likely developed with lateral displacements between 1.5% and 2% of the wall height.
- Mass mixing provides the opportunity to significantly increase the lateral resistance of existing pile group foundations with relatively little investment of time, effort, and expense.

REFERENCES

ALLU (2007). "ALLU Stabilisation System." http://www.allu.net/index.php/en_en/allu-one-step-ahead, accessed April, 2007.

Bowles, J. E., (1996). Foundation Analysis and Design; McGraw Hill Incorporated, USA. pp. 1066.

Brandenberg, S. J., Boulanger, R. W., Kutter, B. L., Chang, D., (2005). "Behavior of Pile Foundations in Laterally Spreading Ground during Centriufuge Tests." Journal of Geotechnical and Geoenvironmental Engineering, 131(11), 1389.

Bruce, D.A., Bruce, M.E. and DiMillio, A.F., (1998), "Deep Mixing Method: A Global Perspective," Soil Improvements for Big Digs, ASCE Geotechnical Special Publication No. 81, pp. 1-26.

Budha, M., (2007). Soil Mechanics and Foundations; John Wiley and Sons Inc. 111 River St, Hobokan, NJ 07030-5774. pp. 407.

Duncan, J. M., (2001). "Passive Earth Pressures: Theories and Test." Journal of Geotechnical and Geoenvironmental Engineering, 127(3), 248-257.

MacGregor, J.G., Wright, J.K., (2005) Reinforced Concrete Mechanics and Design; Prentice Hall, Upper Saddle River, New Jersey 07458. pp. 60.

Porbaha, A., K. Zen & M. Kobayashi, (1999), "Deep Mixing Technology for Liquefaction Mitigation," Journal of Infrastructure Systems, ASCE, March 21-34.

Snyder, J. L., (2004) "Full-Scale Lateral-Load Tests of a 3x5 pile group in Soft Clays and Silts." Thesis. Brigham Young University.

Terashi, M. and Juran I., (2000), "Ground Improvement – State of the Art," In: *GeoEng2000: An International Conference on Geotechnical and Geological Engineering*, held 19-24 November, 2000, Melbourne, Vol. 1, pp. 461-519.

Terashi, M., (2003), "The State of Practice in Deep Mixing Methods," In: *Grouting and Ground Treatment, proceedings of the 3rd Intl. Conference*, L.F. Johnsen, D.A. Bruce and M.J. Byle, eds., ASCE Geotechnical Special Publication No. 120, Vol. 2, pp. 25-49.

Yang, D., (2003), President, Raito, San Leandro, California, personnal communication.

Appendix A. Design of Corbel

A.1 Corbel Specifications and Design Values

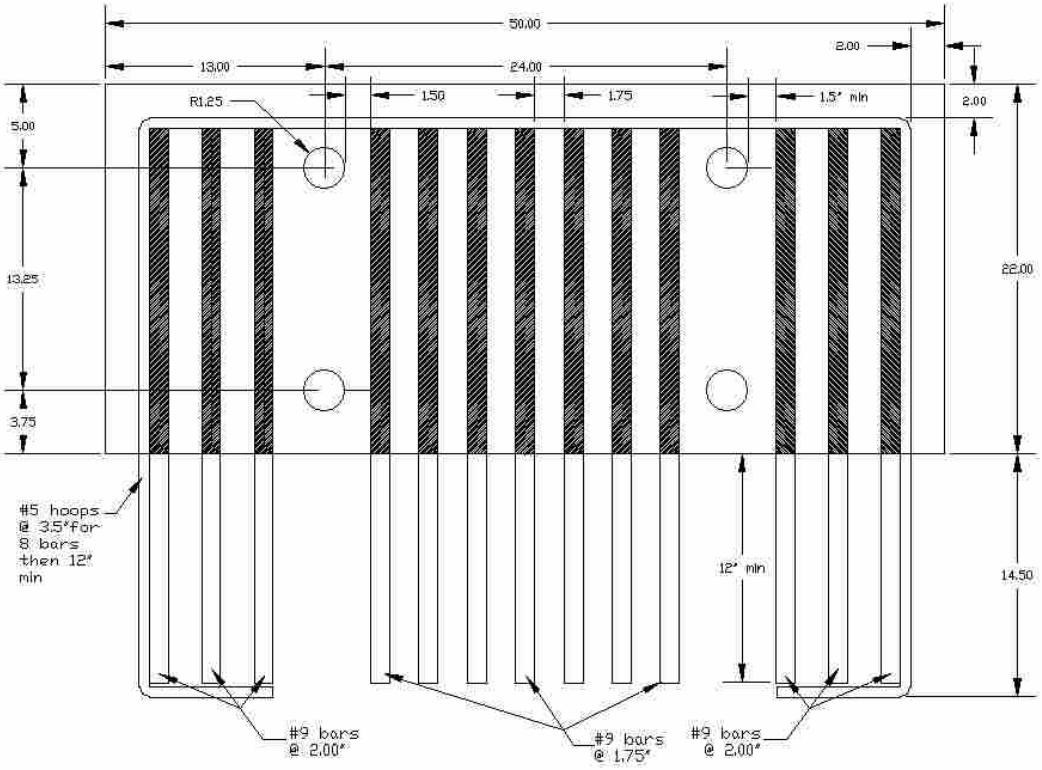

Figure A-1– Front view of the corbel steel where the actuator would connect to the corbel.

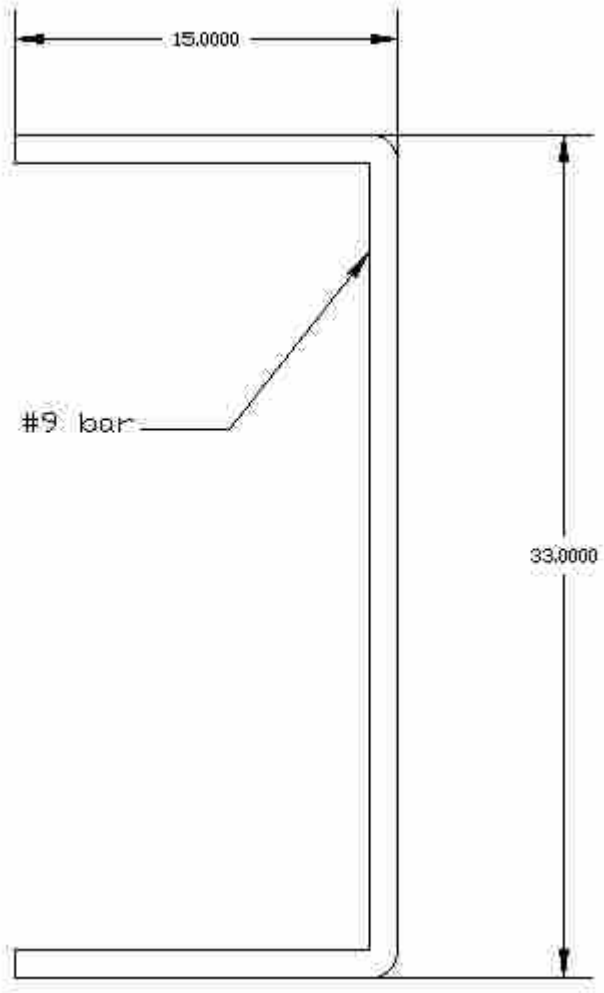

Figure A-2 – The #9 bar main reinforcement for the corbel.

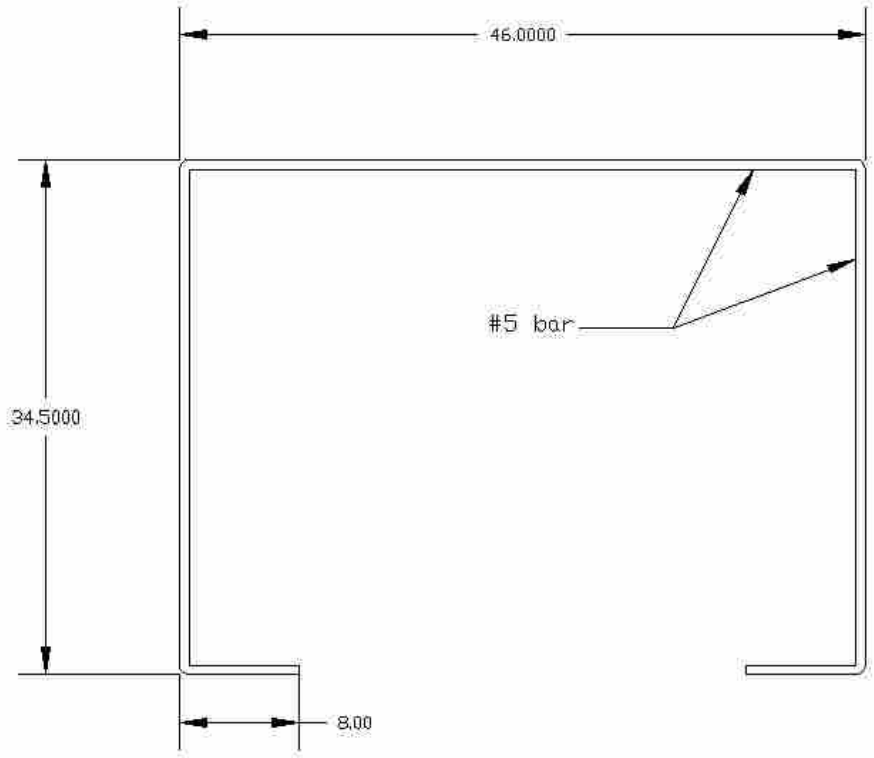

Figure A-3 – The transverse or hoop reinforcement for the corbel.

Mark Herbst
Corbel Design

Enter Value
Guess or Over Ride
Calculated Value

Parameters		
F'c	5000	psi
Vu (factored)	840	kips
Fy	60000	psi
Bw (guess)	50	inches

Bearing Plate Calcs			
b dim of plate	30		
Φ	0.65		
Bstress	2.7625	ksi	
Plate width	10.13574661	inches	try
L dim of plate	20	in min	30 x20x1.5 OK
L	22		

Depth of Corbel			
Vn(d)	50		
Vn(d)	40		
Used Vn(d)	40		Say
d min	28	inches	48 in
Φ	0.75		

Forces		
Nuc	168	kips
Av	10.5	in
h	50	in
d	48	
Mu	9156	kip-in
Φ	0.75	

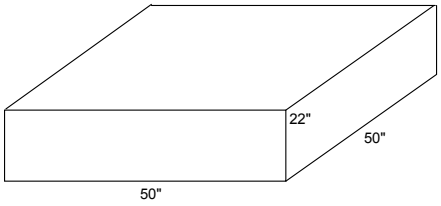

Shear Friction Steel		
λ	1	
Avf	13.33	in^2

Flexural Reinforcement		
Assume	d-a/2 = .9d	
Af	4.71	in^2
recompute a	1.33	
recompute Af	4.30	
An	3.733333333	in^2

Tension Tie Reinforcment	
Asc1	8.03
Asc2	12.62222222
Ascmin	8
	12.62

Bar Sizes	Area in^2	Diameter in	# Bars	Area	Total DofA w/#4 stirup	Spacing Cl	1 row clearance
3	0.11	0.378	115	12.6500	44.47	117	-111.47
4	0.2	0.5	64	12.8000	33	66	-49
5	0.31	0.625	41	12.7100	26.625	43	-19.625
6	0.44	0.75	29	12.7600	22.75	31	-3.75
7	0.6	0.875	22	13.2000	20.25	24	5.75
8	0.79	1	16	12.6400	17	18	15
9	1	1.128	13	13.0000	15.664	16.536	17.8
10	1.27	1.27	10	12.7000	13.7	14.43	21.87
11	1.56	1.41	9	14.0400	13.69	14.28	22.03
14	2.25	1.693	6	13.5000	11.158	11.465	27.377
18	4	2.257	4	16.0000	10.028	9.771	30.201

Size	#Bars	As	Enough Steel
9	13	13	YEP!

Area of Horizontal Stirrups		
Ah	4.44	in^2

Bar Sizes	Area in^2	Diameter in	# Bars	Area	Total DofA w/#4 stirup	Spacing Cl	1 row clearance
3	0.11	0.378	41	4.5100	16.498	43	-9.498
4	0.2	0.5	23	4.6000	12.5	25	12.5
5	0.31	0.625	15	4.6500	10.375	17	22.625

Size	#Bars	As	Enough Steel
5	8 Double leg	4.96	YEP!

Development Length			
Ldh	10.72	in	say 12
Db	1.128	in	
Reg Ld	62.21	in	5.1845069 ft
α	1.3		
β	1		
γ	1		
λ	1		
12*d	13.536		say 14

Figure A-4 – Corbel design calculated values using ACI section 11.9.

Appendix B. Mass Mix Analysis of Applied Forces

The following calculations were done and the computational computer program MathCad version 13. Due to the difficulty of importing the MathCad data into the word processing program the data was saved as screen shot and imported at a picture, thus the text styles and format will vary from the rest of this document.

B.1 Hand Calculations

Mark Herbst
Mass Mix Thesis Calculations
Soil Passive Resistance and Side Friction
Mcr Analysis

Solving for Mcr

$$\sigma := \frac{M \cdot Y}{I} \rightarrow M := \frac{\sigma \cdot I}{Y} \rightarrow Mcr := \frac{Fr \cdot I}{Y}$$

As a rough estimate we will assume Fr equals 15% of unconfined compression strength.

$Fr := 0.15 \cdot 140psi$ $\quad Fr = 21\ psi$

Sloving for I

$b := 11ft$ $\quad h := 4ft$

$$I := \frac{b \cdot h^3}{12} \quad I = 1.217 \times 10^6\ in^4$$

$Y := 24in$

$$Mcr := \frac{Fr \cdot I}{Y} \quad Mcr = 88.704\ kip \cdot ft$$

Mark Herbst
Mass Mix Thesis Calculations
Soil Passive Resistance and Side Friction
Shear Analysis

Basic Equation

$$\frac{1}{2}\cdot\gamma\cdot H^2\cdot B\cdot Kp + 2\cdot Cu\cdot H\cdot B\cdot\sqrt{Kp} + 2\cdot Cu\cdot H\cdot W$$

Soil Profile for depths 0 to 2.5 ft below ground surface

$H1 := 2.5\,ft$ $\quad B := 11ft$

$W := 4ft$ $\quad \gamma 1 := .1175\cdot\frac{kip}{ft^3}$

$Cu1 := 1.040\frac{kip}{ft^2}$ $\quad Kp := 1$

$$P1 := \frac{1}{2}\cdot\gamma 1\cdot H1^2\cdot B\cdot Kp + 2\cdot Cu1\cdot H1\cdot B\cdot\sqrt{Kp} + 2\cdot Cu1\cdot H1\cdot W$$

$P1 = 82.039\,kip$

Soil Profile for depths 2.5 to 5 ft below ground surface

$H2 := 2.5\,ft$ $\quad B := 11ft$

$W := 4ft$ $\quad \gamma 2 := .112\cdot\frac{kip}{ft^3}$

$Cu2 := .287\frac{kip}{ft^2}$ $\quad Kp := 1$

$$P2 := \frac{1}{2}\cdot\gamma 2\cdot H2^2\cdot B\cdot Kp + (2\cdot Cu2\cdot B\cdot\sqrt{Kp} + \gamma 1\cdot H1\cdot B\cdot Kp)\cdot H2 + 2\cdot Cu2\cdot H2\cdot W$$

$P2 = 33.453\,kip$

Soil Profile for depths 5 to 7.5 ft below ground surface

$H3 := 2.5 \cdot ft$ $B := 11ft$

$W := 4ft$ $\gamma 2 := 112 \cdot \frac{kip}{ft^3}$

$Cu2 := .287 \frac{kip}{ft^2}$ $Kp := 1$

$$P3 := \frac{1}{2} \cdot \gamma 2 \cdot H3^2 \cdot B \cdot Kp + \left(2 \cdot Cu2 \cdot B \cdot \sqrt{Kp} + \gamma 1 \cdot H1 \cdot B \cdot Kp + \gamma 1 \cdot H2 \cdot B \cdot Kp\right) \cdot H3 + 2 \cdot Cu2 \cdot H3 \cdot W$$

$P3 = 41.531\,kip$

Soil Profile for depths 7.5 to 10 ft below ground surface

$H4 := 2.5 \cdot ft$

$W := 4ft$

$Cu2 := .287 \frac{kip}{ft^2}$

$$P4 := \frac{1}{2} \cdot \gamma 2 \cdot H4^2 \cdot B \cdot Kp + \left(2 \cdot Cu2 \cdot B \cdot \sqrt{Kp} + \gamma 1 \cdot H1 \cdot B \cdot Kp + \gamma 2 \cdot H2 \cdot B \cdot Kp + \gamma 2 \cdot H3 \cdot B \cdot Kp\right) \cdot H4 + 2 \cdot Cu2 \cdot H3 \cdot W$$

$P4 = 48.853\,kip$

Bottom Friction

$Cu3 := .350 \frac{kip}{ft^2}$ $P5 := W \cdot B \cdot Cu3$

$P5 = 15.4\,kip$

Total Resistance

$Ptotal = P1 + P2 + P3 + P4 + P5$

$Ptotal = 221.277\,kip$

Shear Forces $Force := 220 \cdot kip$

@ 0ft Depth

$V1 := 0$

@ 2.5ft Depth

$Vu := -Force + P1 \text{ float},4 \rightarrow (-138.0) \cdot kip$

@ 5ft Depth

$V3 := -Force + P1 + P2 \text{ float},4 \rightarrow (-104.5) \cdot kip$

@ 7.5ft Depth

$V4 := -Force + P1 + P2 + P3 \text{ float},4 \rightarrow (-62.98) \cdot kip$

@ 10ft Depth

$V5 := -Force + P1 + P2 + P3 + P4 + P5 \text{ float},4 \rightarrow 1.277 \cdot kip$

Moment Forces $Increment := 2.5ft$

@ 0ft Depth

$M1 := 0$

@ 2.5ft Depth

$$Mu := \frac{Increment \cdot Vu}{2} \text{ float},4 \rightarrow (-172.5) \cdot ft \cdot kip$$

@ 5ft Depth

$$M3 := \frac{Increment \cdot V3}{2} \text{ float},4 \rightarrow (-130.6) \cdot ft \cdot kip$$

@ 7.5ft Depth

$$M4 := \frac{Increment \cdot V4}{2} \text{ float},4 \rightarrow (-78.73) \cdot ft \cdot kip$$

@ 10ft Depth

$$M4 := \frac{Increment \cdot V5}{2} \text{ float},4 \rightarrow 1.596 \cdot ft \cdot kip$$